

**Assessment of Suspended Sediment Concentration in the Padma River Using Satellite
Remote Sensing**

A thesis by

Mashrekur Rahman

Submitted in partial fulfillment of the requirements for the degree of

MASTER OF SCIENCE IN WATER RESOURCES DEVELOPMENT



Institute of Water and Flood Management
BANGLADESH UNIVERSITY OF ENGINEERING AND TECHNOLOGY

October 2016

BANGLADESH UNIVERSITY OF ENGINEERING AND TECHNOLOGY
INSTITUTE OF WATER AND FLOOD MANAGEMENT

The thesis titled ‘Assessment of Suspended Sediment Concentration in the Padma River Using Satellite Remote Sensing’ submitted by Mashrekur Rahman, Roll No. 1014282014F, Session: October 2014, has been accepted as satisfactory in partial fulfillment of the requirements for the degree of Master of Science in Water Resources Development on 3rd of October, 2016.

BOARD OF EXAMINERS

1. 

Dr. G. M. Tarekul Islam
Professor
Institute of Water and Flood Management
Bangladesh University of Engineering and Technology, Dhaka
Chairman
(Supervisor)
2. 

Dr. Mashfiqus Salehin
Professor and Director
Institute of Water and Flood Management
Bangladesh University of Engineering and Technology, Dhaka
Member
(Ex-Officio)
3. 

Dr. Md. Munsur Rahman
Professor
Institute of Water and Flood Management
Bangladesh University of Engineering and Technology, Dhaka
Member
4. 

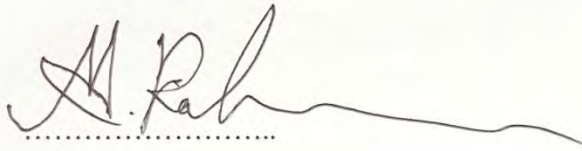
Dr. Mohammad Anisul Haque
Professor
Institute of Water and Flood Management
Bangladesh University of Engineering and Technology, Dhaka
Member
5. 

Dr. Md. Mafizur Rahman
Professor
Department of Civil Engineering
Bangladesh University of Engineering and Technology, Dhaka
Member
(External)

CANDIDATE'S DECLARATION

It is hereby declared that this thesis or any part of it has not been submitted elsewhere for the award of any degree.

Signature of the Candidate

A handwritten signature in black ink, appearing to read 'M. Rahman', written over a dotted horizontal line. The signature is stylized and extends to the right with a long, thin flourish.

Mashrekur Rahman

*Dedicated to
All the scientists who study Bangladesh and her incredible natural
mysteries*

Acknowledgement

Firstly, I would like to express my heartfelt gratitude and sincere appreciation towards my thesis supervisor, Dr. G M Tarekul Islam, Professor, IWFM, BUET, for his valuable advice, constant supervision and guidance throughout the duration of this research; it is a privilege for me to have worked with him. I will forever be grateful to him.

I would also like to dearly thank Dr. Md. Munsur Rahman, Professor, IWFM, BUET and Principal Investigator of the ‘Assessing Health, Livelihoods, Ecosystem Services and Poverty Alleviation in Populous Deltas (ESPA Deltas Project)’, for always supporting my endeavors and providing guidance during the course of this research.

My gratitude lies towards Dr. Mohammad Anisul Haque, Professor, IWFM, BUET, for supporting my personal academic development in a plethora of ways. I would also like to thank him for motivating me at different times.

I would like to thank the ESPA Deltas Project for funding this thesis.

During my thesis, I have received assistance from Rabeya Akter, M.Sc. student and Md. Sazzad Hossain, PhD candidate of IWFM, BUET. I am thankful to them as well.

In addition, I would like to thank all my friends, colleagues and mentors who have helped me at different stages of my thesis.

Finally, I want to thank my parents who have provided me personal and moral support throughout the duration of this research.

Abstract

Variation of Suspended Sediment Concentration (SSC) is an important parameter in the hydrologic, morphologic and ecosystem studies of large alluvial rivers; especially in the Ganges-Brahmaputra-Meghna (GBM) delta. Traditional in situ measurement of SSC in the large Padma River is challenging in terms of time, cost, skilled personnel and spatial coverage. Moreover, there are limitations in terms of spatial and temporal acquisition of reliable data. Satellite remote sensing offers convenient assessment and spatio-temporal mapping of suspended sediments in large alluvial rivers. This study investigated the applicability of open-access Landsat Enhanced Thematic Mapper (ETM+) images in estimating the SSC of the Padma. Multiple-temporal Landsat 7 ETM+ images were processed to extract Digital Numbers (DN) of pixels corresponding to Bangladesh Water Development Board (BWDB)'s river measurement station, Mawa (SW93.5L). The DNs were converted to radiance and ultimately to top-of-atmosphere (ToA) reflectance. Since mostly clear scenes were used, in situ atmospheric correction was ignored. The ToA values for Landsat-7 bands 1-4, which sense electromagnetic radiation of 0.45-0.52, 0.52-0.60, 0.63-0.69 and 0.76-0.90 μm respectively, were combined with corresponding measured values of SSC, procured from historical data archives of BWDB, between the years 2000 to 2010 for determination of statistical relationship between them. R^2 for bands 1, 2, 3 and 4 were 0.64, 0.51, 0.44 and 0.67 respectively. The results from analysis showed that Coefficient of Determination (R^2) value of band 4 (Near Infrared) presented the best relationship - therefore chosen as the best SSC indicator. Scatter plot of predicted SSC values from a polynomial equation based on band 4 against in situ values of SSC with 1:1 fit line generated strong positive coefficient of determination of 0.89 and Root Mean Square Error (RMSE) of 88.3 ppm.

Using a polynomial model based on the band 4 data, spatial distribution maps of SSC, between the years 2000 and 2010, for monsoon and post-monsoon seasons were demonstrated. SSC levels appeared to be generally higher in monsoon and flood seasons compared to post-monsoon season. However, there were exceptions in this observation too. Rise in discharge, water level and flow velocity increased the overall SSC. During cross-section analysis, it was generally observed that rise in bed level also caused small jumps in

SSC levels. Using statistical correlation analysis of measured values of SSC and corresponding in situ values of flow velocity, a logarithmic relationship model was derived. Using these models and SSC spatial distribution maps, spatial variation maps of water flow velocity were created.

Table of Content

| | |
|--------------------------------|--------------|
| <i>Certificate of Approval</i> | <i>ii</i> |
| <i>Declaration</i> | <i>iii</i> |
| <i>Acknowledgment</i> | <i>v</i> |
| <i>Abstract</i> | <i>vi</i> |
| <i>Table of Contents</i> | <i>viii</i> |
| <i>List of Figures</i> | <i>x</i> |
| <i>List of Tables</i> | <i>xv</i> |
| <i>Abbreviations</i> | <i>xvi</i> |
| <i>List of Symbols</i> | <i>xviii</i> |

Chapter 1. Introduction

| | |
|--|---|
| 1.1 Significance of Suspended Sediment Concentration | 1 |
| 1.2 Constraints in Acquisition of SSC Data | 2 |
| 1.3 Significance of SSC in the Ganges-Brahmaputra Rivers | 2 |
| 1.4 Remote Sensing using Landsat | 3 |
| 1.5 Scope of the Study | 4 |
| 1.6 Objectives of the Study | 4 |

Chapter 2. Literature Review

| | |
|---|----|
| 2.1 Application of Remote Sensing in Retrieval and Monitoring of SSC Values | 5 |
| 2.2 Constraints in the Estimation of SSC from Spectral Reflectance | 6 |
| 2.3 Methodologies of Estimating SSC using Remotely Sensed Satellite Data | 7 |
| 2.4 Satellite Remote Sensing of SSC in Large Alluvial Rivers | 16 |

Chapter 3. The Ganges-Brahmaputra Rivers System

| | |
|--|----|
| 3.1 Significance of Geographical Location | 24 |
| 3.2 Geologic History of the Ganges-Brahmaputra Basin | 25 |
| 3.3 Nature of Sediment Transport along the Ganges-Brahmaputra Rivers | 26 |

| | |
|---|-----|
| 3.4 Morphology of the Ganges-Brahmaputra System | 28 |
| 3.5 Location of In situ Data Point at The Padma River | 31 |
| Chapter 4. Data Collection | 32 |
| 4.1 In situ SSC Data Acquisition by BWDB | 32 |
| 4.2 Acquisition of Landsat Data | 38 |
| 4.3 Hydro-morphological Data Collection | 39 |
| Chapter 5. Satellite Image Processing | 40 |
| 5.1 Processing Landsat Data | 40 |
| 5.2 Conversion of DN into Radiance | 42 |
| 5.3 Conversion of Radiance into Top of Atmosphere Reflectance | 42 |
| Chapter 6. Development of SSC- Spectral Reflectance Relationships | 45 |
| 6.1 Investigating SSC-ToA Reflectance for Individual Bands | 46 |
| 6.2 Investigating Robust SSC- Spectral Reflectance Relationship | 53 |
| Chapter 7. Spatio-temporal Variation of SSC | 57 |
| 7.1 Retrieval of Spatial Distribution of SSC | 57 |
| 7.2 Spatial Distribution Maps of SSC in the Padma River | 59 |
| 7.3 Temporal Variation of SSC at Mawa | 77 |
| 7.3 Relationship between SSC and Cross-section of River | 77 |
| 7.4 Measured Average Discharge, Water Level and Flow Velocity | 82 |
| 7.6 Relationship between Measured SSC and Flow Velocity | 84 |
| Chapter 8. Conclusions and Recommendations | 85 |
| 8.1 Conclusions | 85 |
| 8.2 Recommendations | 86 |
| References | 87 |
| Appendix-A: Historical sediment data corresponding to Mawa SW 93.5L | 95 |
| Appendix-B: Water Level, discharge and flow velocity data sets | 102 |
| Appendix-C: DN values extracted from Landsat ETM+ images | 108 |
| Appendix-D: Earth-sun distance correction coefficient (d) table | 117 |
| Appendix-E: Values of $E_0\lambda$, the mean solar ToA Irradiance | 121 |
| Appendix-F: List of all Landsat ETM+ images acquired for this thesis | 122 |

List of Figures

| Figure No. | | Page No. |
|-------------------|---|-----------------|
| Figure 2.1 | Effect of SSC on the reflectance of red light tested in laboratory | 6 |
| Figure 2.2 | Correlation between ground-measured turbidity and satellite-observed red reflectance | 8 |
| Figure 2.3 | Scatterplots showing the natural logarithm (ln) of in situ SSC measurements and red reflectance (band 2) and total reflectance (band 1 + band 2 + band 3) | 9 |
| Figure 2.4 | Suspended Matter (TSM) concentration as a function of atmospherically corrected MODIS Terra 250 m band 1 reflectance | 10 |
| Figure 2.5 | Plot of the concentrations of suspended sediments with base pixel values for Landsat Multispectral Scanner (MSS) Band 1 data | 11 |
| Figure 2.6 | Plot of the concentrations of suspended sediments with base pixel values for Landsat Multispectral Scanner (MSS) Band 2 data | 12 |
| Figure 2.7 | Plot of the concentrations of suspended sediments with base pixel values for Landsat Multispectral Scanner (MSS) Band 3 data | 12 |
| Figure 2.8 | Plot of the concentrations of suspended sediments with base pixel values for Landsat Multispectral Scanner (MSS) Band 4 data | 13 |
| Figure 2.9 | Graph of MSS radiance in band 5 plotted against suspended solids | 14 |
| Figure 2.10 | Distribution of TSS over the study area in Istanbul on 04 June 2005 | 15 |
| Figure 2.11 | Relation between SSC and water reflectance at Bands 1–4 in | 17 |

| | | |
|-------------|--|----|
| | the Upper and Middle Yangtze River | |
| Figure 2.12 | SSC distribution map in the Upper Yangtze showing the spatial variations of SSC | 17 |
| Figure 2.13 | SSC distribution map in the Middle Yangtze showing the spatial variations of SSC | 18 |
| Figure 2.14 | SSC distribution map in the Lower Yangtze showing the spatial variations of SSC | 18 |
| Figure 2.15 | Regression relationship between SSC and water reflectance between band 2 and band 5 | 19 |
| Figure 2.16 | Scatter plot of observed SSC against estimated SSC of the Lower Yangtze River | 20 |
| Figure 2.17 | Residual of SSC versus estimated SSC | 20 |
| Figure 2.18 | Scatter plots and best-fit curves for the relationship between SSL and Exoatmospheric reflectance | 21 |
| Figure 2.19 | Scatter plot of predicted values by the polynomial model based on NIR band Exoatmospheric reflectance and measured values of SSL with 1:1 fit line | 22 |
| Figure 2.20 | Relationship between reflectance of TM band 3 and suspended sediment concentration (SSC) for Ganges-Brahmaputra Rivers | 23 |
| Figure 3.1 | Geologic map of the Bengal basin | 26 |
| Figure 3.2 | Predicted sediment budget of the GBM delta | 27 |
| Figure 3.3 | River channel patterns and typical cross-sections | 29 |
| Figure 3.4 | Geomorphic map of the Bengal basin and surroundings superimposed on the SRTM-90 m digital elevation model | 30 |
| Figure 3.5 | Location of in situ data collection point | 31 |
| Figure 4.1 | Bangladesh Water Development Board's water survey catamaran stationed at Mawa 93.5L gauge station | 32 |
| Figure 4.2 | An automatic pulley system used to lift and submerge gauging equipment | 33 |
| Figure 4.3 | Sediment gauging equipment being prepared for sample | 33 |

collection

| | | |
|-------------|--|----|
| Figure 4.4 | Sediment sampling equipment being lowered for water sample collection | 34 |
| Figure 4.5 | Sediment sampling equipment being lifted up after water sample collection | 34 |
| Figure 4.6 | Water sample being transferred to another container from sediment sampling equipment | 35 |
| Figure 4.7 | Sample being transferred from the container to the measurement tube using a funnel | 35 |
| Figure 4.8 | Measurement tubes being separated after collection of sample | 36 |
| Figure 4.9 | Samples in measurement tubes being stored to be transferred to laboratory for testing | 36 |
| Figure 4.10 | Example of True Color Landsat 7 ETM+ Product | 39 |
| Figure 5.1 | Screenshot of ILWIS while extraction of DN with pixel information | 41 |
| Figure 6.1 | Scatter plot of Measured SSC versus Reflectance Percentage of Band 1 | 45 |
| Figure 6.2 | Scatter plot of Measured SSC versus Reflectance Percentage of Band 2 | 46 |
| Figure 6.3 | Scatter plot of Measured SSC versus Reflectance Percentage of Band 3 | 46 |
| Figure 6.4 | Scatter plot of Measured SSC versus Reflectance Percentage of Band 4 | 47 |
| Figure 6.5 | Scatter plot of measured SSC versus ToA reflectance percentage of bands 1-4 with linear trend lines | 48 |
| Figure 6.6 | Scatter plot of measured SSC versus ToA reflectance percentage of bands 1-4 with exponential trend lines | 49 |
| Figure 6.7 | Scatter plot of measured SSC versus ToA reflectance percentage of bands 1-4 with logarithmic trend lines | 50 |

| | | |
|-------------|--|----|
| Figure 6.8 | Scatter plot of estimated SSC values by the polynomial model based on band 4 (Near Infrared) Exoatmospheric reflectance and measured SSC data with 1:1 fit line. | 51 |
| Figure 6.9 | Residue of SSC versus measured SSC | 52 |
| Figure 6.10 | Scatter plot of relative error percentage of estimated SSC from measured SSC | 52 |
| Figure 6.11 | Bands 1-4 ToA reflectance percentage Plot | 55 |
| Figure 7.1 | Spatial distribution map of SSC in the Padma River for Monsoon of 2000 | 59 |
| Figure 7.2 | Spatial distribution map of SSC in the Padma River for Post-Monsoon of 2000 | 60 |
| Figure 7.3 | Spatial distribution map of SSC in the Padma River for Monsoon of 2001 | 61 |
| Figure 7.4 | Spatial distribution map of SSC in the Padma River for Post Monsoon of 2001 | 62 |
| Figure 7.5 | Spatial distribution map of SSC in the Padma River for Monsoon of 2002 | 63 |
| Figure 7.6 | Spatial distribution map of SSC in the Padma River for Post Monsoon of 2002 | 64 |
| Figure 7.7 | Spatial distribution map of SSC in the Padma River for Post Monsoon of 2003 | 65 |
| Figure 7.8 | Spatial distribution map of SSC in the Padma River for Monsoon of 2004 | 66 |
| Figure 7.9 | Spatial distribution map of SSC in the Padma River for Post Monsoon of 2004 | 67 |
| Figure 7.10 | Spatial distribution map of SSC in the Padma River for Monsoon of 2005 | 68 |
| Figure 7.11 | Spatial distribution map of SSC in the Padma River for Post Monsoon of 2005 | 69 |
| Figure 7.12 | Spatial distribution map of SSC in the Padma River for Post Monsoon of 2006 | 70 |

| | | |
|-------------|---|----|
| Figure 7.13 | Spatial distribution map of SSC in the Padma River for Monsoon of 2007 | 71 |
| Figure 7.14 | Spatial distribution map of SSC in the Padma River for Post Monsoon of 2007 | 72 |
| Figure 7.15 | Spatial distribution map of SSC in the Padma River for Monsoon of 2008 | 73 |
| Figure 7.16 | Spatial distribution map of SSC in the Padma River for Post Monsoon of 2008 | 74 |
| Figure 7.17 | Spatial distribution map of SSC in the Padma River for Post Monsoon of 2009 | 75 |
| Figure 7.18 | Spatial distribution map of SSC in the Padma River for Post Monsoon of 2010 | 76 |
| Figure 7.19 | Temporal variation of SSC | 77 |
| Figure 7.20 | Variation of cross section and corresponding SSC for Post Monsoon of 2001 | 78 |
| Figure 7.21 | Variation of cross section and corresponding SSC for Monsoon of 2002 | 78 |
| Figure 7.22 | Variation of cross section and corresponding SSC for Post Monsoon of 2005 | 79 |
| Figure 7.23 | Variation of cross section and corresponding SSC for Post Monsoon of 2008 | 79 |
| Figure 7.24 | Measured average yearly discharge at Mawa 93.5L | 80 |
| Figure 7.25 | Measured average yearly water level at Mawa 93.5L | 81 |
| Figure 7.26 | Measured average yearly flow velocity at Mawa 93.5L | 81 |
| Figure 7.27 | Scatter plot of measured flow velocity and measured SSC | 82 |
| Figure 7.28 | Spatial variation of flow velocity for monsoon of year 2000 | 84 |
| Figure 7.29 | Spatial variation of flow velocity for post monsoon of year 2002 | 84 |

List of Tables

| Table No. | | Page No. |
|------------------|---|-----------------|
| Table 4.1 | An example of the Padma's sediment data set provided by the BWDB | 37 |
| Table 5.1 | Resultant ToA Reflectance (dimensionless) values | 44 |
| Table 6.1 | Data sets used for validation of polynomial model | 51 |
| Table 6.2 | Output table of regression analyses | 54 |
| Table 6.3 | Summary of outputs of regression analyses | 54 |
| Table 6.4 | Residual output of regression analyses | 54 |
| Table 7.1 | Relative error assessment of estimated flow velocity | 83 |

Abbreviations

| | |
|--------|---|
| IWFM | Institute of Water and Flood Management |
| BWDB | Bangladesh Water Development Board |
| BUET | Bangladesh University of Engineering and Technology |
| NASA | National Aeronautics and Space Administration |
| USGS | United States Geological Survey |
| EROS | Earth Resources Observation and Science |
| TM | Thematic Mapper |
| ETM+ | Enhanced Thematic Mapper + |
| MSS | Multi Spectral Scanner |
| MODIS | Moderate Resolution Imaging Spectroradiometer |
| CMODIS | Chinese Moderate Resolution Imaging Spectrometer |
| GBM | Ganges-Brahmaputra-Meghna |
| MRD | Mississippi River Delta |
| LP | Lake Pontchartrain |
| PAD | Peace Athabasca Delta |
| SSC | Suspended Sediment Concentration |
| AVHRR | Advanced Very High Resolution Radiometer |
| SWIR | Short Wave Infrared |
| TSM | Total Solid Matter |
| PPM | Parts Per Million |
| ARE | Absolute Relative Error |
| RMSE | Root Mean Square Error |
| RRMSE | Relative Root Mean Square Error |
| ToA | Top of Atmosphere |
| BCM | Billion Cubic Meters |
| WL | Water Level |
| SSL | Suspended Sediment Load |
| GPS | Global Positioning System |
| MSCD | Mirror Scan Correction Data |

| | |
|-------|--|
| SLC | Scan Line Corrector |
| ILWIS | Integrated Land and Water Information System |
| DN | Digital Number |
| TIF | Tagged Image File |
| QGIS | Quantum Geographic Information System |
| PToA% | Top of Atmosphere Reflectance Percentage |

List of Symbols

- $L\lambda$ = Spectral Radiance ($\text{m W cm}^{-2}\text{sr}^{-1}\mu\text{m}^{-1}$)
- L_{max} = Radiance measured at detector saturation ($\text{m W cm}^{-2}\text{sr}^{-1}\mu\text{m}^{-1}$)
- L_{min} = Lowest radiance measured by the sensor ($\text{m W cm}^{-2}\text{sr}^{-1}\mu\text{m}^{-1}$)
- $\rho\lambda$ = ToA or Exoatmospheric Reflectance as a function of the band width λ
- d = Correction factor for variation in solar irradiances due to varying earth-sun distance
- $E_o\lambda$ = Exoatmospheric Irradiance ($\text{W}\mu\text{m}^{-2}$)
- θ_s = Solar Zenith Angle (rad)
- Q = Flow discharge (m^3/s or cumec)

Chapter 1

Introduction

1.1 Significance of Suspended Sediment Concentration

Suspended Sediment Concentration (SSC) is a measure of the amount of sediment suspended in water bodies. The quantification of suspended sediments and their transport mechanism are essential in understanding riverine, estuarine and coastal processes. SSC is required to estimate and predict soil erosion and sediment transport caused by changes in land use patterns (Collins and Walling, 2004). Suspended sediments also play important role in water quality management because it is connected to total primary productivity, such as transport of nutrients, to fluxes of metals, radio-nuclides and organic micro-pollutants (Ouillon et al., 2004). Variations in SSC of rivers impact changes in river morphology. Alluvial river channels are also classified with respect to the total sediment load delivered to the channel. An excess of total load causes deposition, a deficiency causes erosion, and between the extremes lays the stable channel. Moreover, suspended sediment is a dominant factor in the Ganges and Brahmaputra Rivers. For Brahmaputra, the ratio of the bedload discharge to the suspended sediment discharge was 10-25(Okada, 2016). SSC is also an indicator of river planform. It is important to accurately monitor and archive synoptic SSC data of rivers to understand and track changes in river morphology and water quality.

Suspended sediments are significant for sustaining complex river ecosystems and aquatic life. Many human activities in or near aquatic habitats re suspend bottom sediments and create turbid conditions that differ in scope, timing, duration, and intensity from the resuspension events induced by storms, freshets, or tidal flows. Dredging of navigation channels is one such source of bottom disturbance. Suspended sediments can elicit a variety of responses from aquatic biota, primarily because many attributes of the physical environment are affected. Physical impacts from increased concentrations of suspended sediment on aquatic life can be detrimental, for example, resulting in egg abrasion, reduced bivalve pumping rates, and direct mortality (Wilber and Clarke, 2001). However some species of fishes in alluvial rivers thrive in turbid and sediment rich conditions. Previous

studies reveal that several species actively prefer turbid over clear water conditions; using turbid conditions to facilitate feeding and avoidance behaviors (Cyrus and Blaber, 1987). Also sediments provide essential nutrients for unique local ecosystem to survive and flourish.

1.2 Constraints in Acquisition of SSC Data

The task of obtaining and reliable and constant spatio-temporal SSC data of rivers in Bangladesh is severely limited. These limitations include size and extent of rivers, financial and economic constraints; lack of experienced personnel. Although in situ measurement techniques of suspended sediment are continually changing, it is generally accepted that they do not completely satisfy requirements. Instruments used traditionally to evaluate SSC have been limited to single location, and therefore variations in SSC have been obtained by profiling or by using a fixed vertical array of measuring devices. Mechanical measurement techniques are both time consuming and have poor temporal resolution. There are additional problems with regard to logistics; problems in deployment and calibration of devices. Acoustic Doppler profilers using acoustic backscatter to measure suspended sediment concentrations in orders of magnitude are being used widely recently (Gray and Gartner, 2009). The technology is relatively robust and generally immune to effects of biological fouling. However, these devices have constraints in terms of spatial coverage. Conventional techniques are often constrained in their capability to provide comprehensive spatial and temporal data of SSC (Crawford and Hay, 1993; Sheng and Hay, 1988; Thorne and Hardcastle, 1997; Thorne et al., 1993).

1.3 Significance of SSC in the Ganges-Brahmaputra Rivers

The Ganges-Brahmaputra Rivers System carries the world's highest yearly sediment loads of approximately one billion tons (Milliman and Meade, 1983; Milliman and Syvitski, 1992b). Due to the large size and extent of these rivers, study of sediments and their spatial-temporal characteristics in the delta has been restricted (Rice, 2007). Approximately 33% of the annual sediment load is deposited in the river flood-plain (Goodbred Jr and Kuehl, 1998; Goodbred

and Kuehl, 1999), 21% is deposited in the beds of the subaqueous delta (Michels et al., 2003), 20% contributes to subaqueous delta progradation in the foreset beds, and 25% is conveyed to the Swatch of No Ground Canyon (Goodbred and Kuehl, 1999). 1-2% of the annual sediment load contributes to the prograding subaerial delta (Allison, 1998). Suspended Sediment Concentration is therefore a very useful parameter in the study of alluvial rivers such as Ganges, Brahmaputra and Meghna. Reliable historical SSC data is required to observe and predict aggradation and degradation of river beds, erosion and accretion of river banks, and to carry out various hydro-morphological analysis.

1.4 Remote Sensing using Landsat

From 1972, Landsat satellites have consistently acquired space-based images of the Earth's land surface, coastal shallows, and coral reefs. Open-access Landsat data are being utilized by government, commercial, industrial, civilian, military, and educational communities throughout the world. These data support a plethora of applications in areas such as global change research, studies on water bodies, agriculture, forestry, geology, resource management, geography, mapping, water quality, and coastal studies. Landsat satellites acquire images of the Earth's surface along the satellite's ground track in a 185-kilometer-wide swath as the satellite moves in a descending orbit over the sunlit side of the Earth. Landsat 7 orbits the Earth at an altitude of 705 kilometers. It completes orbit every 99 minutes, 14 full orbits per day, and covers every geographic point on Earth once every 16 days. Although each satellite has a 16-day temporal resolution, their orbits allow 8-day repeat coverage of any Landsat scene area on the globe. Landsat 7 carries the Enhanced Thematic Mapper Plus (ETM+), with 30-meter visible, near-IR, and SWIR bands, a 60-meter thermal band, and a 15-meter panchromatic band (USGS, 2013). Satellite remote sensing offers a feasible alternative option of acquiring SSC data over large spatial extent and high temporal repeatability.

1.5 Scope of the Study

The Padma River starts downstream from the point where the Ganges and Brahmaputra Rivers confluence. In this thesis, satellite remote sensing of SSC in the Padma River was focused upon. Multiple Landsat ETM+ images were processed; cloud-free Landsat-7 ETM+ images of both monsoon and post monsoon seasons, extending between 2000 and 2010 were used in this study. Rarity of Landsat images during monsoon season was a notable aspect. Multiple regression and correlation analyses were applied in this study. Open source GIS software was used to generate spatial distribution maps. Scatter plots and their respective coefficient of determination were used at multiple stages of this study.

1.6 Objectives of the Study

- i. To establish a correlation between suspended sediment concentrations and spectral reflectance of the Padma River and to use that correlation to estimate its historical suspended sediment concentrations.
- ii. To investigate the relationships between SSC levels and corresponding spatio-temporal variations in the channel hydro-morphology of the Padma River.

Chapter 2

Literature Review

2.1 Application of Remote Sensing in Retrieval and Monitoring of SSC Values

Since Landsat images became available in 1972, they have been used for monitoring of inland and coastal water bodies, including retrieval of quantitative data concerning the water area. One of the earliest studies showed that quantitative estimates of suspended sediment concentration of surface water could be made using reflected solar radiation (Ritchie et al., 1976). Another one of the earliest studies developed a model for obtaining volume spectral reflectance from the surface radiance of a water body, and spectrometer data, showing that multispectral algorithms exist which can relate volume spectral reflectance to either nonfilterable residue or nephelometric turbidity with accuracy, and turbidity had emerged as the best suited for measurement by remote sensing techniques for reasons of accuracy and signature transferability (Holyer, 1978).

Turbidity can be quantified directly using a light turbidimeter, or visually using Secchi disc depth. Because sediment concentration is often the primary control on turbidity, the two quantities are frequently treated similarly with respect to remote sensing (Ritchie et al., 2003). In 1988, a study suggested that SSC-Spectral Reflectance relationship is difficult to both quantify and utilize. It is difficult to quantify because of the many environmental factors that disturb the relationship. These include the atmosphere, sensing geometry, water/atmosphere boundary, water components and concentration of suspended sediments. It is difficult to utilize because of the problems associated with sampling the SSC that is necessary to both train and test any estimation procedure (Curran and Novo, 1988). Figure 2.1 shows the results of a 1972 laboratory study (Scherz, 1972) on the effect of SSC on the reflectance of red light, and was one of the first to demonstrate the non-linear relationship between spectral reflectance and SSC. Spectral reflectance is not linearly related to SSC; it is

controlled by many factors including the sediment properties such as size, mineralogy and color (Rimmer et al., 1987).

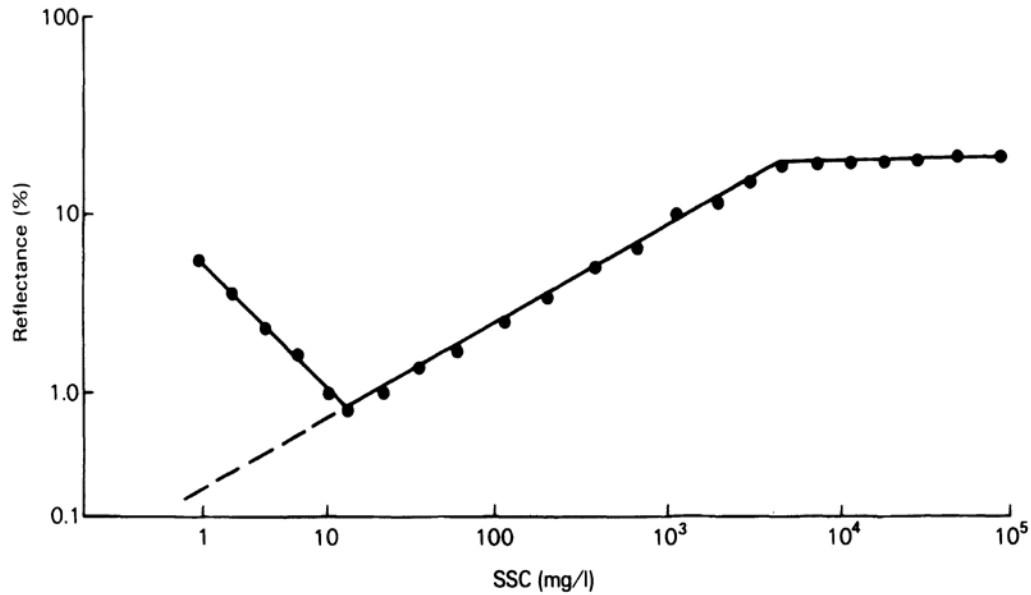


Fig. 2.1: Effect of SSC on the reflectance of red light tested in laboratory (Scherz, 1972)

2.2 Constraints in the Estimation of SSC from Spectral Reflectance

The estimation of SSC from remotely sensed spectral reflectance has followed all or, more usually some of the generic five stages mentioned below (Curran, 1987; Tassan, 1987).

- i. Simultaneous measurement of SSC and spectral reflectance.
- ii. Correct, as far as possible, for environmental influences on (i).
- iii. Derive an empirical relationship between corrected SSC and spectral reflectance on a training set of data.
- iv. Use corrected spectral reflectance and the relationship in (iii) to estimate SSC.
- v. Determine the accuracy of SSC estimation using a testing set of corrected SSC data.

However, majority of the studies terminated at stage (iii) on the assumption that a statistically significant correlation between SSC and spectral reflectance is the foundation for accurate estimation.

A vast majority of previous works have simply inverted a SSC-spectral reflectance, regression relationship (Curran and Hay, 1986) which violates three assumptions upon which such regression is based:

- SSC on spectral reflectance is the same as spectral reflectance on SSC
- There is no error in the measurement of SSC
- The error in spectral reflectance is unrelated to SSC

Given the small sample size in each case their conclusions were necessarily tentative. At that moment the single largest limitation to the successful implementation of the previously mentioned five stages is the problem of sampling aerially, vertically and temporally varying SSC synchronously with spectral reflectance. The majority of early studies have taken an inadequate number of random samples to try and characterize areal variability (Curran and Novo, 1988). Another study extracted of in situ information from multispectral satellite data with the use of empirical algorithms (Topliss et al., 1990). However these basic statistical relationships were later improved using artificial neural network approach. A neural network approach was shown to be useful in modeling the transfer function and water quality parameters of chlorophyll and suspended sediment concentrations and the received radiances of the Landsat Thematic Mapper. The network combined with Landsat thematic mapper images was shown to be applicable for studying water quality of coastal areas (Keiner and Yan, 1998). Spectral mixture analysis have also been successfully used to map SSC (Matsushita and Fukushima, 2009; Mertes et al., 1993).

2.3 Methodologies of Estimating SSC using Remotely Sensed Satellite Data

The principal methodological difference among such studies is the choice of spectral band(s) from which to extract reflectance measurements (Pavelsky and Smith, 2009). Single band satellite measurements from the Moderate Resolution Imaging Spectroradiometer (MODIS) on Aqua have been used to quantify the Mississippi River plume following the intense rainfall and massive flood along the Mississippi River and its tributaries during the spring of 2008. The shortwave infrared (SWIR) atmospheric correction algorithm was then used to derive the total suspended matter (TSM) concentration and the spectral optical features of the Mississippi River plume (Shi and Wang, 2009).

Single band of IKONOS satellite, as shown in Figure 2.2, was shown to have positive correlation with ground measured turbidity in the lower Charles River in Boston, United States of America, which demonstrated the usability of high-resolution satellite data for mapping turbidity in the lower Charles River (Hellweger et al., 2007).

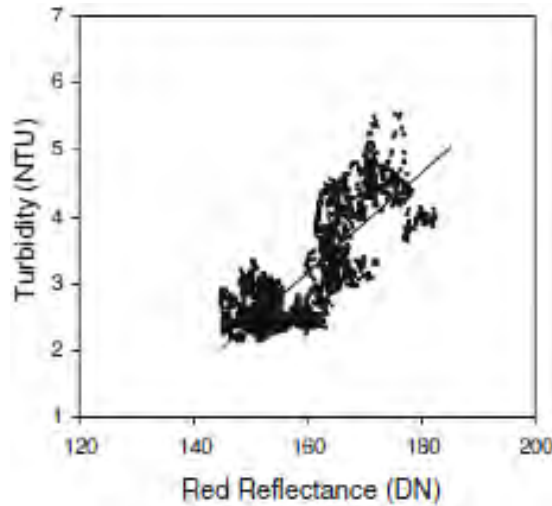


Fig. 2.2: Correlation between ground-measured turbidity and satellite-observed red reflectance (Hellweger et al., 2007)

AVHRR satellite imagery have been used to monitor in situ water quality data; multiple in situ water quality data and reflectance were used to calibrate a general optical equation (Woodruff et al., 1999). Some studies have also conflated red reflectance with reflectance in one or multiple other visible bands to create robust relationships, especially in the case of varying sediment color. Data from the Chinese Moderate Resolution Imaging Spectroradiometer (CMODIS), loaded on the China's SZ-3 spacecraft, have been used for concentration retrieval of the suspended sediment. Using an empirical line method, the CMODIS radiance was converted to the water-leaving reflectance, and is applied to inversion of the suspended sediment concentrations in the Yangtze River estuary. The concentrations ranging between 0 mg/L and 1000 mg/L are well validated by the field measurement data (Han et al., 2006).

The use of a near infrared band for Total Suspended Matter (TSM) retrieval in surface waters has been suggested (Ritchie et al., 1976). Near Infrared bands have the least impacts from chlorophyll and colored dissolved organic carbon. Furthermore, shorter wavelengths integrate over a larger water column while penetration depth at 833 nm is small (much less than 1 m in turbid waters). The latter corresponds to the depth of the in situ water sampling. Although single-bands reflectance in the near-IR (746, 774, 803, 833, or 862 nm) performed well for the shipborne reflectance (Sterckx et al., 2007). The use of total reflectance combining bands 1, 2 and 3 of ASTER and SPOT images seemed to generate stronger statistical relationship compared to only red band (Figure 2.3). To assess detailed spatial patterns in SSC in the Peace Athabasca Delta (PAD), Canada, robust positive relationships between in situ suspended sediment concentration (SSC) and remotely sensed visible/near-infrared reflectance for four days in 2006 and 2007 were applied, revealing strong variations in water sources and flow patterns, including flow reversals in major distributaries (Pavelsky and Smith, 2009).

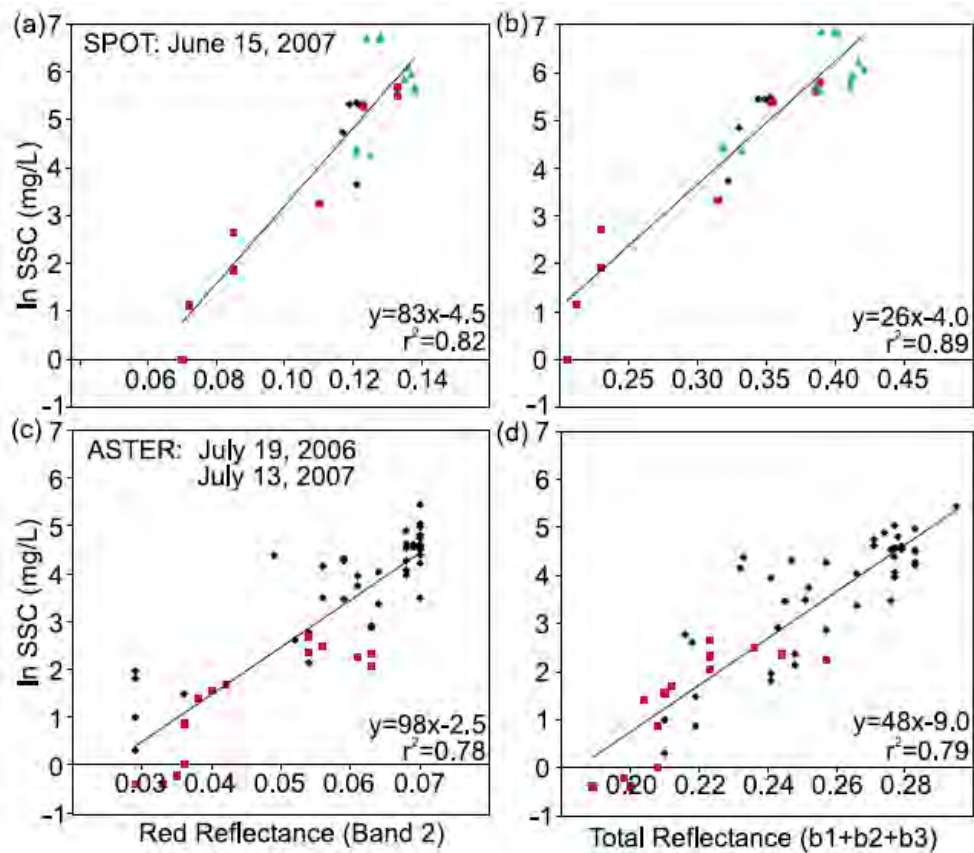


Fig. 2.3: Scatterplots showing the natural logarithm (ln) of in situ SSC measurements and red

reflectance (band 2) and total reflectance (band 1 + band 2 + band 3) from one high resolution SPOT image acquired on June 15, 2007 and two ASTER images acquired on July 19, 2006 and July 13, 2007. In each case, the use of total reflectance rather than red reflectance results in a stronger statistical correlation indicated by the higher r^2 . Points are colored according to region. In the case of total reflectance, results suggest that mean divergence from the overall regression line does not differ by region (Pavelsky and Smith, 2009)

Multiple studies have demonstrated that water reflectance in the NIR and visible spectral regions (bands 1-4) of Landsat images correlate quite strongly with SSC (Ritchie and Schiebe, 2000). Therefore, reflectance is usable as an indicator of SSC for inland and coastal waters. One study demonstrated that the characteristics of the MODIS Terra instrument provide data well suited for the study of suspended matter in dynamic coastal waters (Figure 2.4). The moderately high resolution of MODIS 250 m data was useful for mapping small-scale features of TSM concentration in different inland and coastal waters (Miller and McKee, 2004).

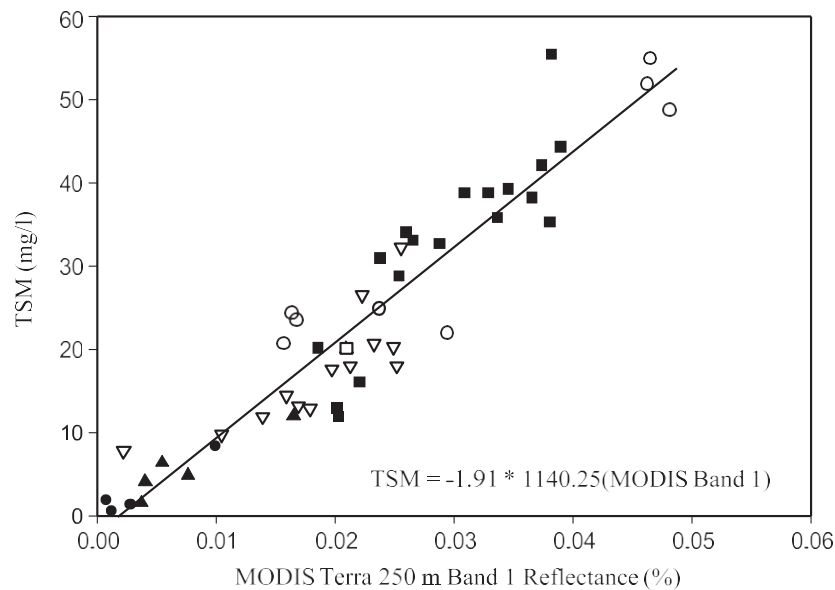


Fig. 2.4: Suspended Matter (TSM) concentration as a function of atmospherically corrected MODIS Terra 250 m band 1 reflectance. TSM data were obtained from six field campaigns: Mississippi Sound, 5/16/2001 (o); Mississippi River Delta (MRD), 3/17/02 (•); Lake

Pontchartrain (LP), 5/19/02 (■); LP, 5/23/02 (D); MRD, 7/15/03 (▲); and MRD, 10/20/03 (□). The line is the least-squares fit to the data (Miller and McKee, 2004).

Previous studies have also shown water bodies with higher turbidity demonstrate much stronger scattering compared to waters with lower turbidity (Kirk, 1994). Digital Numbers (DN)s have been directly used in past studies to retrieve SSC values from water using satellite remote sensing. Digital spectral data from 14 Landsat MSS scenes of Moon Lake in Coahoma County, Mississippi were analyzed and compared with ground measurements of total solids and suspended sediments in the lake surface water for the period between January 1983 and May 1985. Coefficients of determination of greater than 0.81 were calculated between MSS Band 2 (0.6-0.7 μm) or Band 3 (0.7-0.8 μm) and suspended sediments or total solids. Coefficients of determination for multiple regression (Figures 2.5-2.9) using three or four MSS bands were greater than 0.90 (Ritchie et al., 1987).

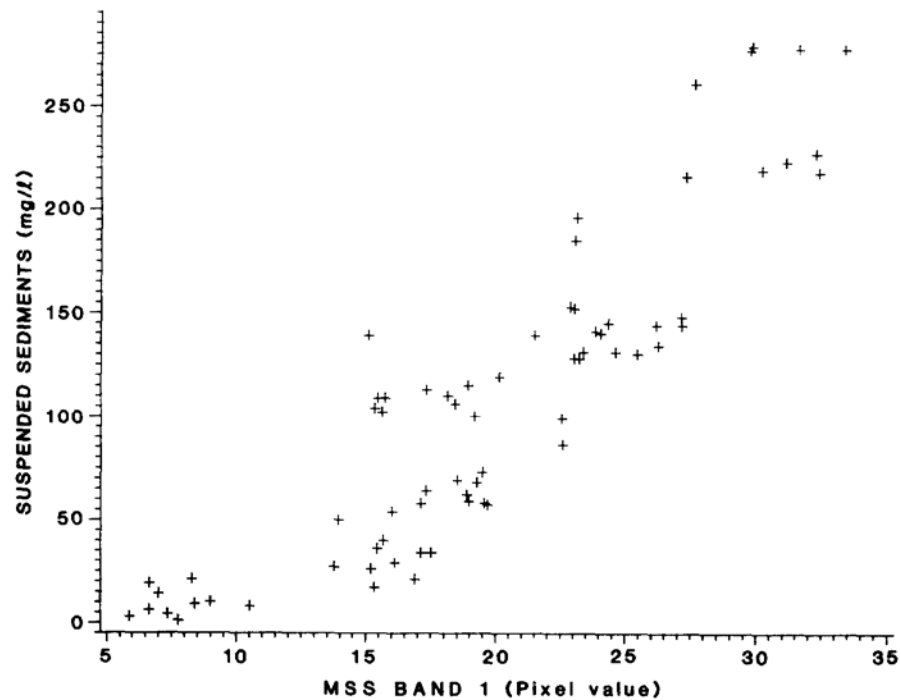


Fig. 2.5: Plot of the concentrations of suspended sediments with base pixel values for Landsat Multispectral Scanner (MSS) Band 1 data (Ritchie et al., 1987)

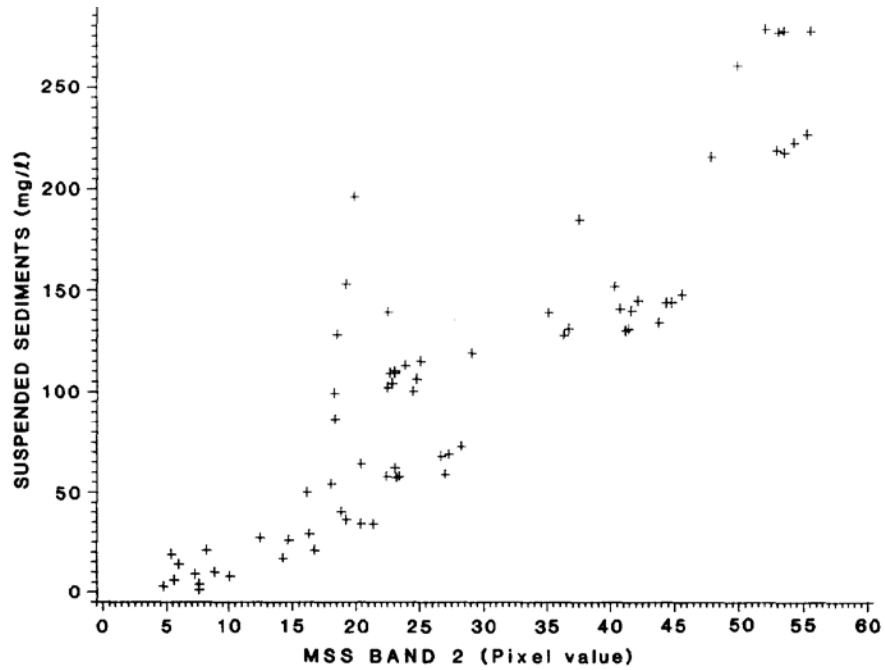


Fig. 2.6: Plot of the concentrations of suspended sediments with base pixel values for Landsat Multispectral Scanner (MSS) Band 2 data (Ritchie et al., 1987)

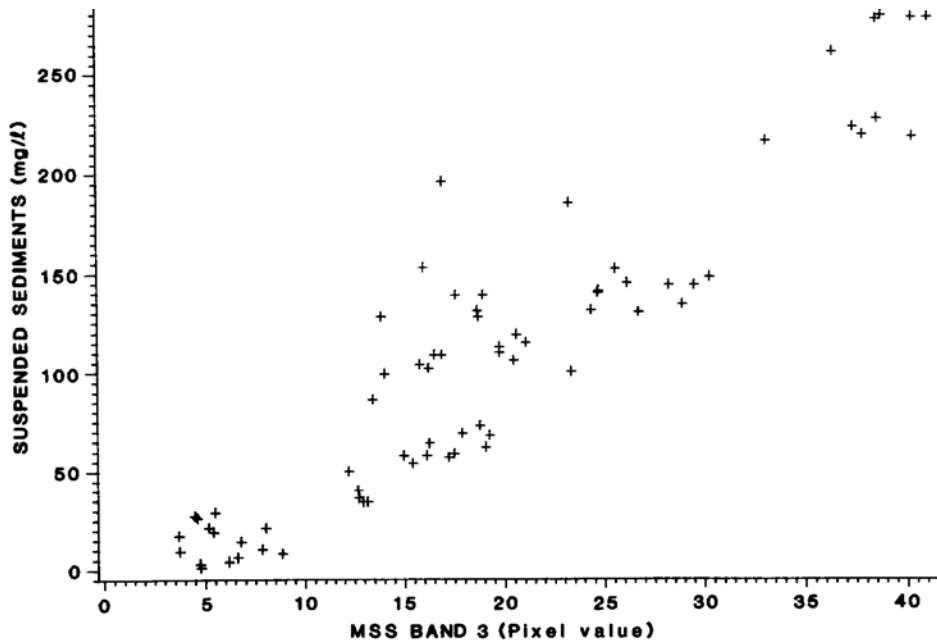


Fig. 2.7: Plot of the concentrations of suspended sediments with base pixel values for Landsat Multispectral Scanner (MSS) Band 3 data (Ritchie et al., 1987)

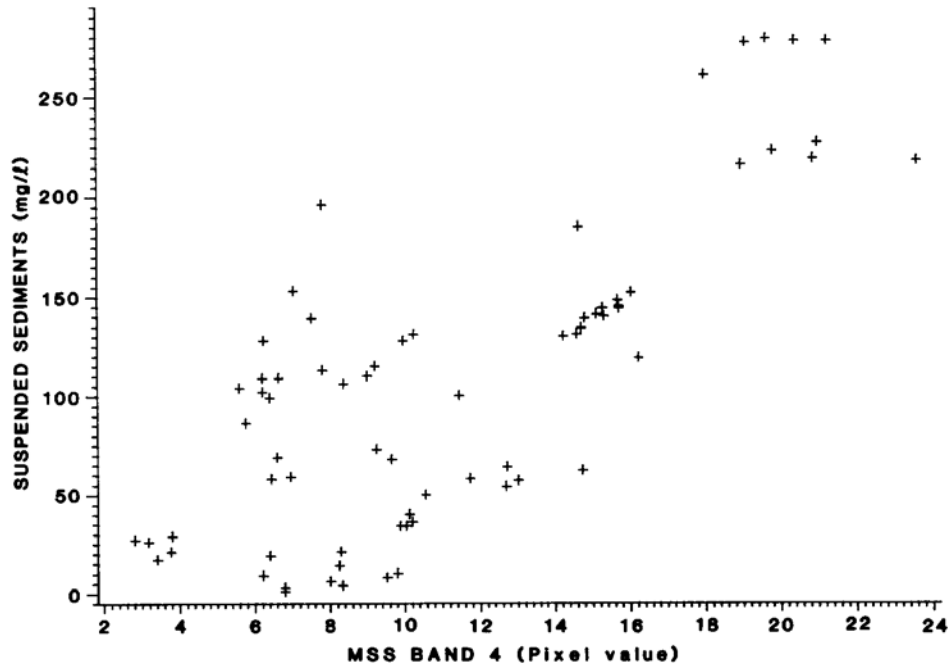


Fig. 2.8: Plot of the concentrations of suspended sediments with base pixel values for Landsat Multispectral Scanner (MSS) Band 4 data (Ritchie et al., 1987)

Physically quantified values of spectral radiance, which is converted from DN through in-flight calibration sensor parameters, have also been used to indicate SSC values for coastal waters. Digital data from Landsat's Multiple Spectral Scanners (MSS) were used to calculate the amount of radiation received from sea level at the position of the satellite. After assessing the atmospheric effects, on the radiance data, the amount of radiance was then related to sediment concentration (Aranuvachapun and LeBlond, 1981). An earlier study had also applied a single band of MSS data to investigate correlation between radiance and suspended sediments or suspended solids (Figure 2.8).

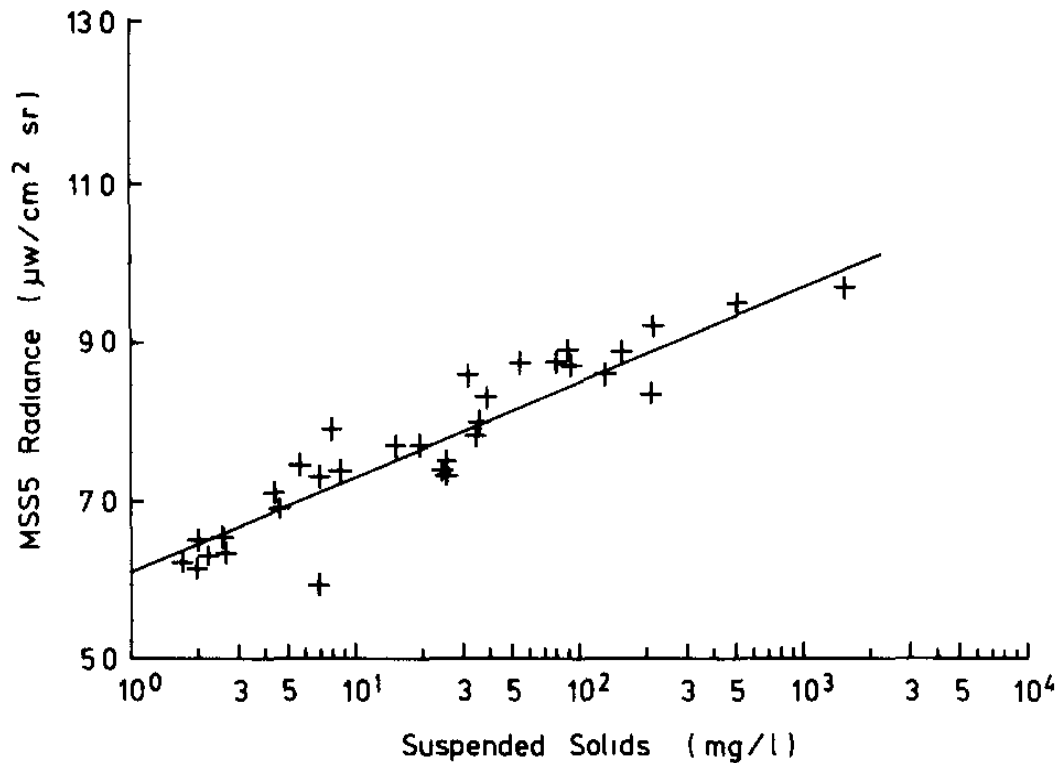


Fig. 2.9: Graph of MSS radiance in band 5 plotted against suspended solids (Munday and Alföldi, 1979)

However reflectance values, especially exo-atmospheric or top of atmosphere reflectance have been the most widely used for indicating SSC; for example, Band 3 (Red) of SPOT- XS2 demonstrated strong correlation with SSC within a range of 0-10 ppm. Similarly, MODIS Terra Band 1 showed significant correlation with SSC range of 0-60 ppm. Reflectance in the Band 2 and Band 4 of Landsat ETM+ have been used in the past to retrieve SSC values (Ouillon et al., 2004). Reduction of the influence of particle grain size and refractive index variation was shown to be possible through use of reflectance ratio. Also reflectance ratios of specific spectral regions demonstrated quite good correlation with SSC (Doxaran et al., 2002). Information from the Landsat 5 (TM sensor), Landsat 7 (ETM sensor) and SAC-C (MMRS sensor) satellites have been used in combination with on-site measurements to study the spatial and temporal characteristics of permanent lakes in the Ibera macrosystem in Argentina (Cózar et al., 2005).

High Resolution Ikonos Multispectral Imagery have been used to retrieve Total Suspended Solids (TSS) in a study conducted on Istanbul, Turkey (Ekercin, 2007). Multi regression of dependent variable TSS study showed that all spectral bands contribute to the variance in TSS. Therefore, all spectral bands were used to develop a final model to predict TSS. Blue, and NIR bands have negative, green and red bands have positive relationship with TSS. All bands significantly contributed 97.24% of the variance in TSS. The model was then used to generate spatial variation map of the study area (Figure 2.9).

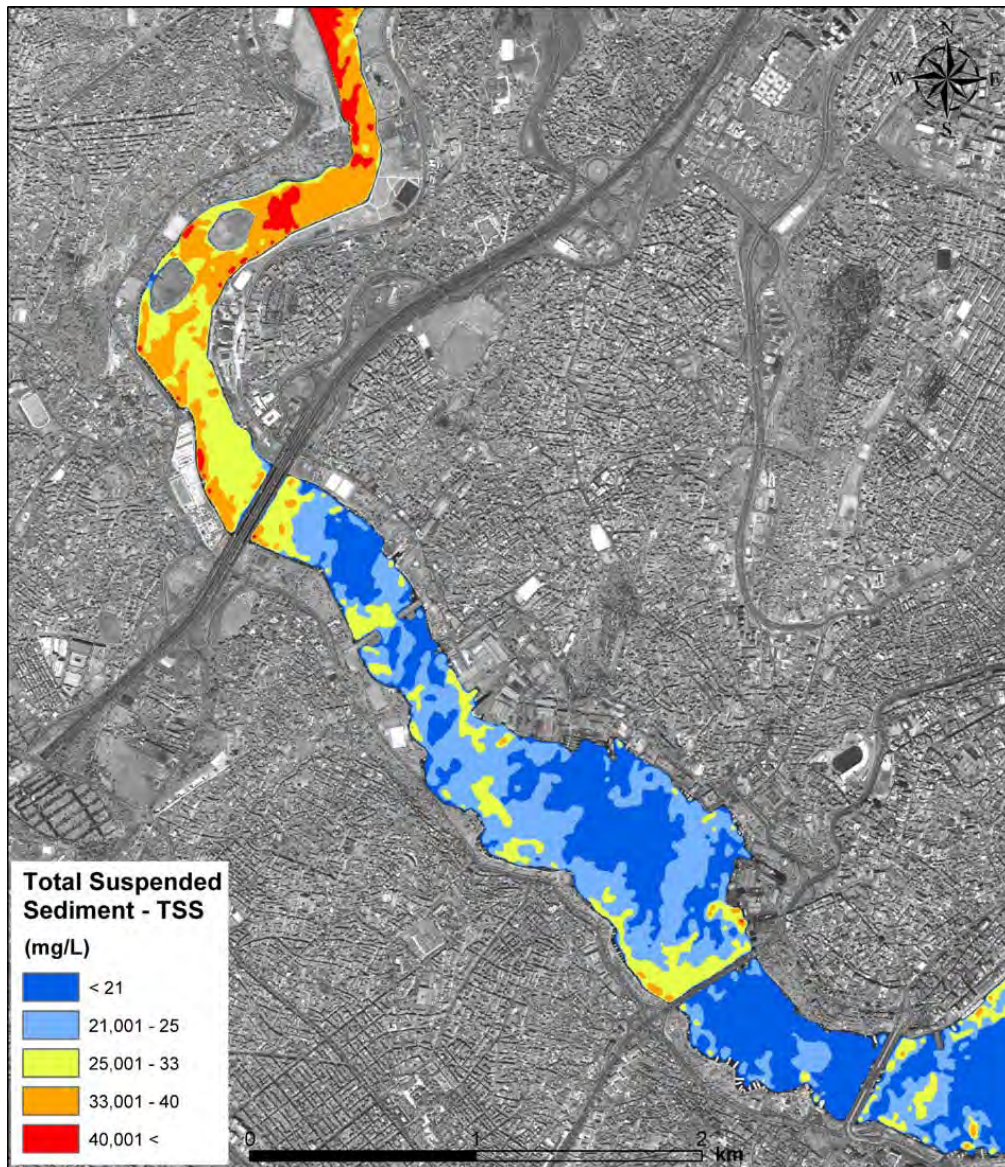


Fig. 2.10: Distribution of TSS over the study area in Istanbul on 04 June 2005. The base image is 04/06/2005 dated IKONOS Pan data (Ekercin, 2007)

Algorithms to define the relationship between in situ SSC and corresponding spectral radiance or reflectance have been developed to indicate SSC directly using satellite images (Pavelsky and Smith, 2009; Reddy and Srinivasulu, 1994; Xia, 1993). Most of these studies investigated relations for water bodies such as lakes, reservoirs and coastal regions; mainly waters with very low to moderate turbidity. Also, many of their concentrations were on water quality (Zhang et al., 2003) aspects rather than morphological aspects associated with rivers, especially alluvial rivers.

2.4 Satellite Remote Sensing of SSC in Large Alluvial Rivers

In terms of rivers, very few studies have been undertaken regarding satellite remote sensing of parameters such as SSC. Even fewer studies have concentrated on the relationship between remotely sensed SSC and characteristics of alluvial rivers, such as cross section, discharge, flow velocity and water levels. Especially highly turbid large rivers have been largely ignored when it comes to the remote sensing of suspended sediments. A study concerning Yangtze River in China used multi-temporal Landsat ETM+ to estimate its SSC (Wang et al., 2009). Using an effective easy-to-use atmospheric correction method that does not require in situ atmospheric conditions, retrieved water reflectance of Band 4 was found to be a good SSC indicator within the large SSC range 22–2610 mg /l (Figure 2.11). The regression relation between SSC and water reflectance of Band 4 appeared to be able to provide a relatively accurate SSC estimate directly from Landsat ETM+ images for the Yangtze River from the upper, the middle to the lower reaches. Using the regression relation, SSC spatial maps were generated for upper, middle and lower Yangtze River (Figure 2.12-2.14)

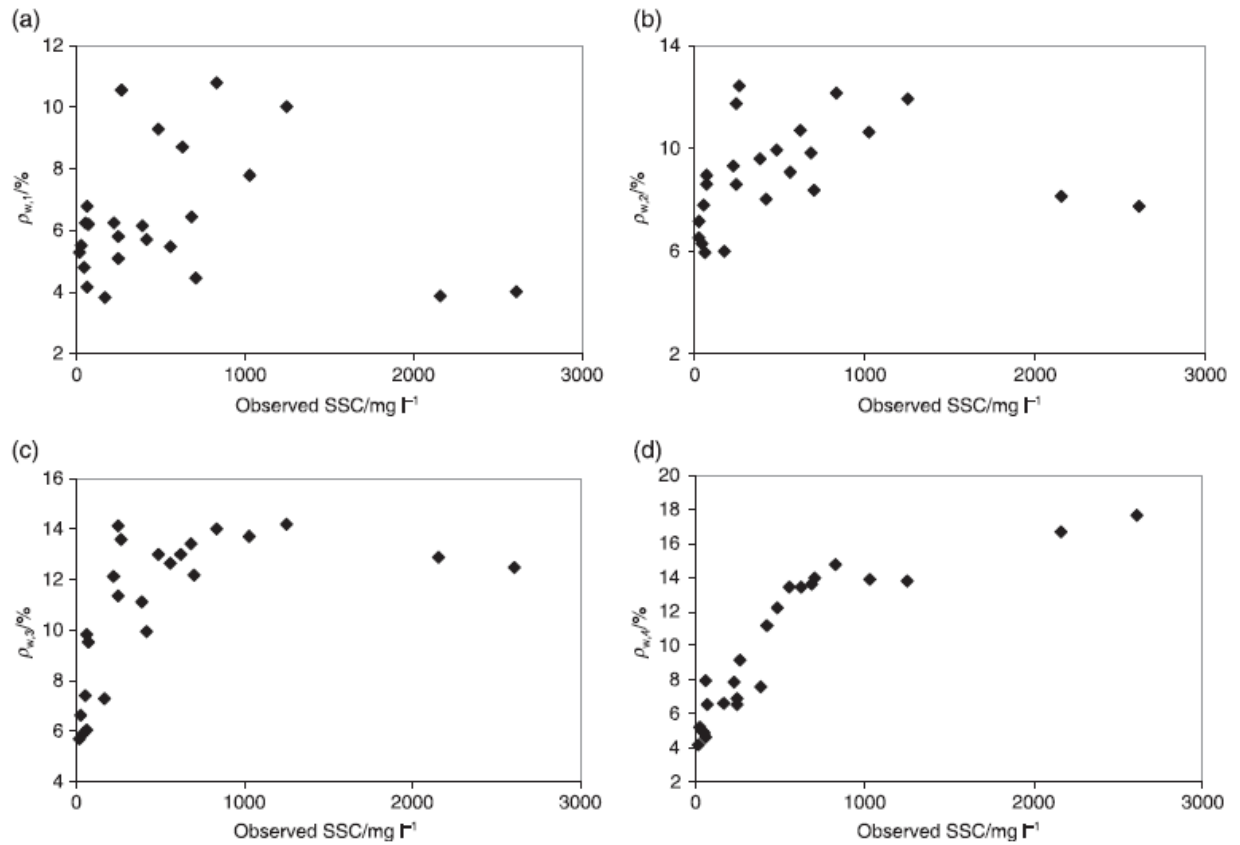


Fig. 2.11: Relation between SSC and water reflectance at Bands 1–4 in the Upper and Middle Yangtze River: (a) Band 1; (b) Band 2; (c) Band 3; (d) Band 4 (Wang et al., 2009)

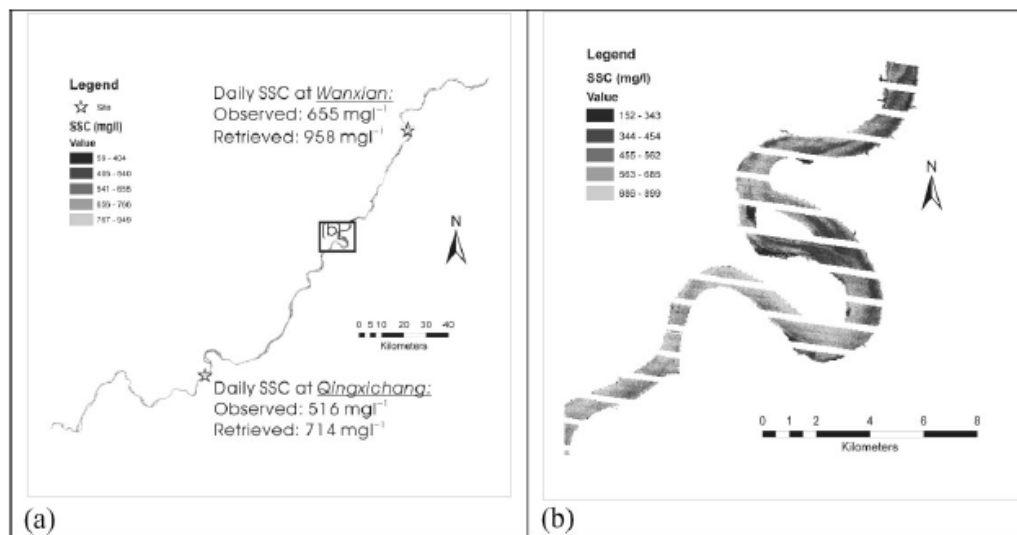


Fig. 2.12: SSC distribution map (a) and enlarged part of it (b) in the Upper Yangtze showing

the spatial variations of SSC. SSC values were retrieved directly from a Landsat ETM+ image (Wang et al., 2009)

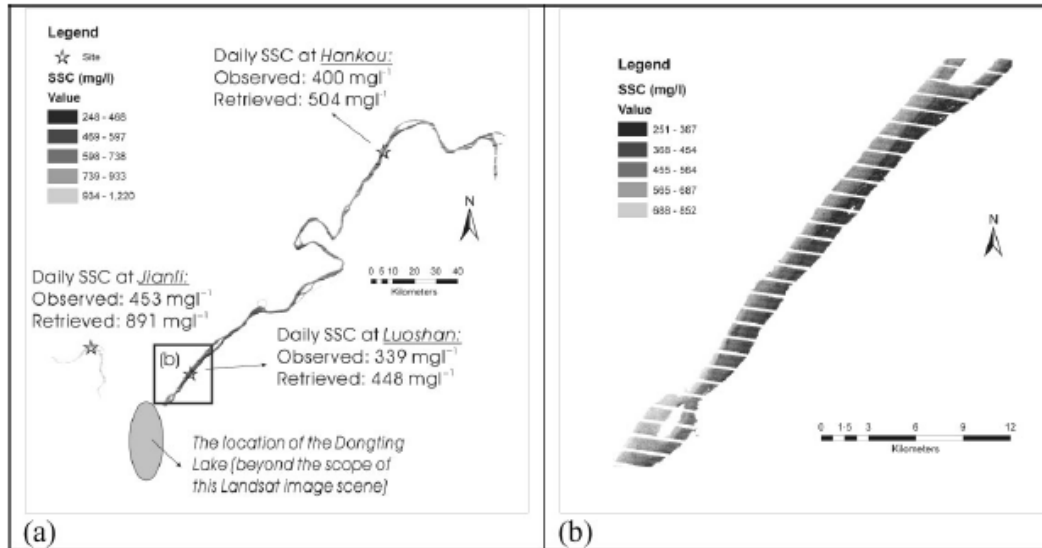


Fig. 2.13: SSC distribution map (a) and enlarged part of it (b) in the Middle Yangtze showing the spatial variations of SSC values retrieved directly from a Landsat ETM+ image (Wang et al., 2009)

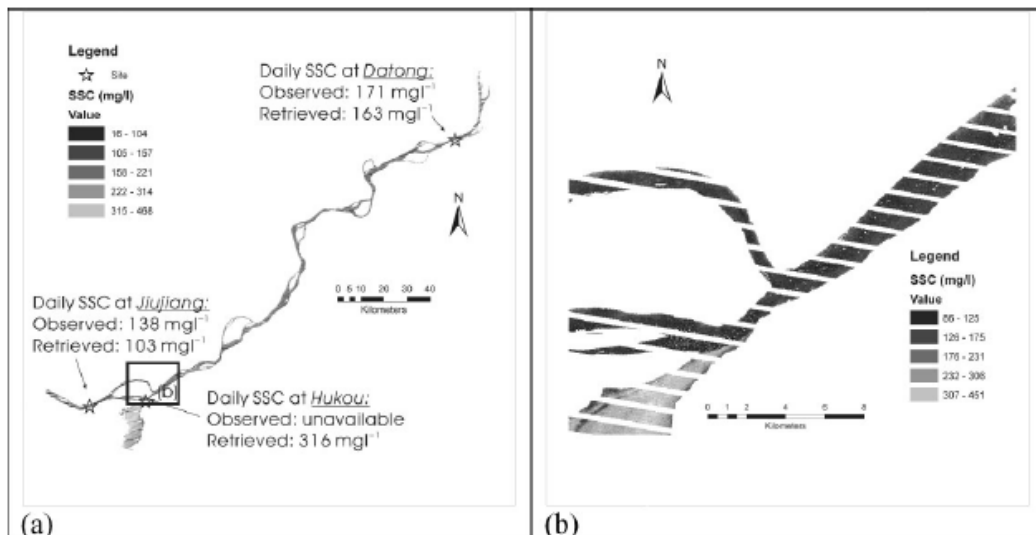


Fig. 2.14: SSC distribution map (a) and enlarged part of it (b) in the Lower Yangtze showing the spatial variations of SSC. SSC values were retrieved directly from a Landsat ETM+ image (Wang et al., 2009)

Another study concerning large turbid river presented a method of estimating SSC of the Yangtze at Jiujiang using time-series satellite data of high temporal resolution Terra MODIS (Wang and Lu, 2010). It was found that differences in water reflectance between Band 2 and Band 5 could provide relatively accurate SSC estimation even when in situ atmospheric conditions were unknown (Figure 2.15). After validation (Figure 2.16-2.17), mean absolute relative error (ARE) and relative root mean square error (RRMSE) were found to be relatively low (i.e., 25.5% and 36.5%, respectively). This empirical relationship was successfully applied to the estimation of SSC at Datong in the Lower Yangtze River, although the SSC values were generally underestimated (Wang and Lu, 2010). This study suggested that Terra MODIS could be used to estimate SSC in large turbid rivers, although some influencing factors required further study to improve the accuracy of SSC estimation.

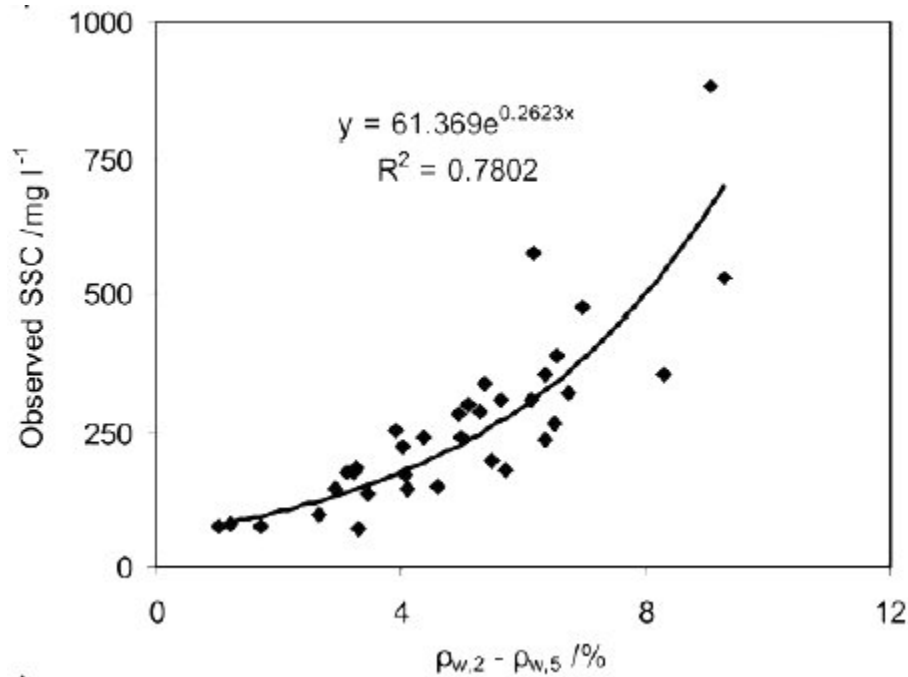


Fig. 2.15: Regression relationship between SSC and water reflectance between band 2 and band 5 (Wang and Lu, 2010)

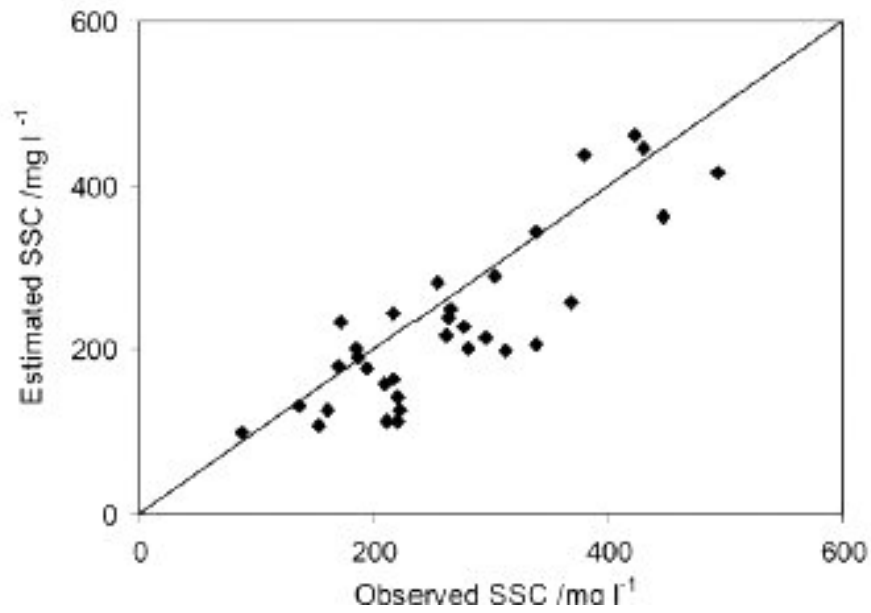


Fig 2.16: Scatter plot of observed SSC against estimated SSC of the Lower Yangtze River (n=33), where the line indicates a 1:1 relationship (Wang and Lu, 2010)

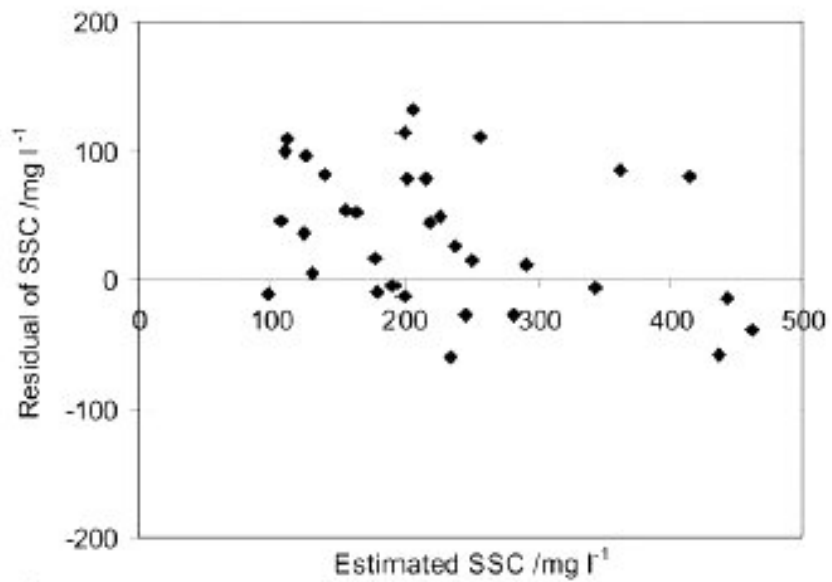


Fig 2.17: Residual of SSC versus estimated SSC (Wang and Lu, 2010)

Another notable study studied the monitoring of suspended sediment load in the Mekong River; the applicability for monitoring suspended sediment load (SSL) in the Mekong River over temporal and spatial dimensions was investigated (Fleiflea, 2013). Landsat scenes captured between 1988 and 2000, including 110 Thematic Mapper (TM) images and 21 Enhanced Thematic Mapper Plus (ETM+) images, were analyzed in correspondence with ground observations. The three visible and near infrared bands were included in the analysis. The polynomial relationship of the NIR Exoatmospheric reflectance, band 4 wave length: 760- 900 nm, to SSL based on the ground observations at 9 sites along the river demonstrated the best agreements (overall R^2 , 0.76) (Figure 2.18-2.19). Subsequently, the equation enabled reasonable estimation of the suspended sediment load longitudinal profiles and its temporal changes. Thus, the results confirmed a high applicability of satellite image for monitoring SSL in relatively large rivers such as the Mekong River (Fleiflea, 2013).

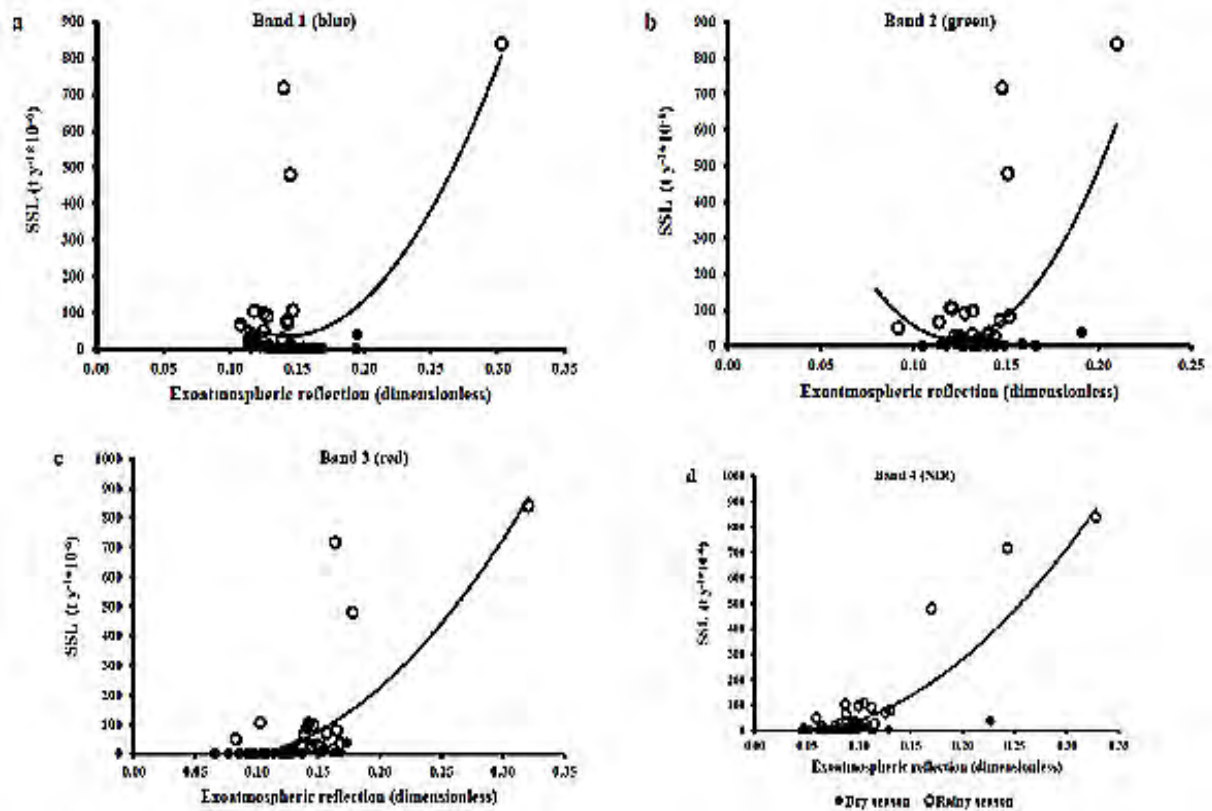


Fig 2.18: Scatter plots and best-fit curves for the relationship between SSL and Exoatmospheric reflectance (a) band 1, $R^2=0.436$; (b) band 2, $R^2=0.358$; (c) band 3, $R^2=0.566$; (d) band 4, $R^2=0.76$ (Fleiflea, 2013)

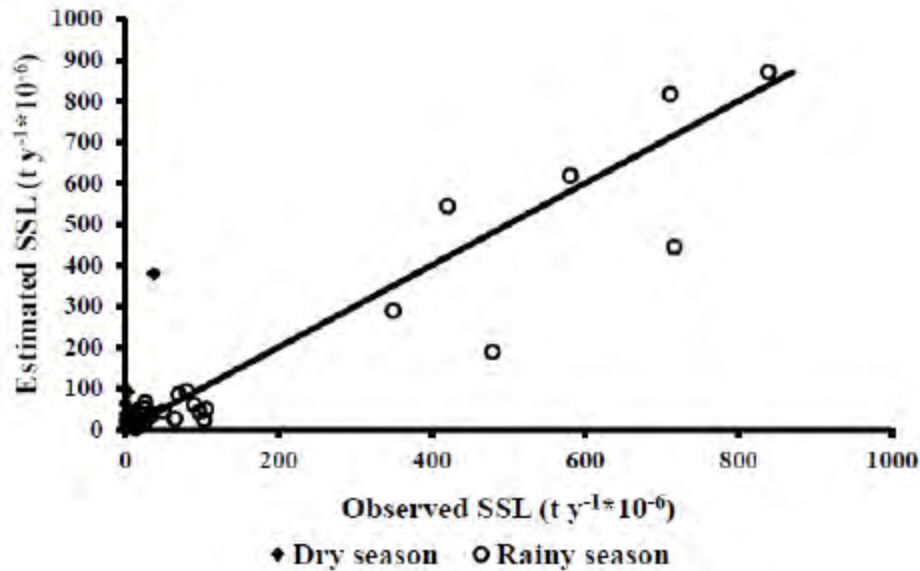


Fig 2.19: Scatter plot of predicted values by the polynomial model based on NIR band Exoatmospheric reflectance and measured values of SSL with 1:1 fit line (Fleiflea, 2013)

One study applied spectral mixture analysis to estimate the concentration of suspended sediment in surface waters of the Amazon River wetlands from Landsat MSS and TM images (Mertes et al., 1993). One study regarding the satellite remote sensing of suspended sediments in Bangladesh is on the Ganges and Brahmaputra Rivers using older Landsat TM and AVHRR data (Islam et al., 2001). Although this study made use of five data points to develop relationship between suspended sediment and DN values directly, only three images were used. A relationship between reflectance of TM band 3 and suspended sediment concentration (SSC) was established during this study (Figure 2.20). Another similar study (Islam et al., 2002) concentrated on the Distribution of suspended sediment in the coastal sea off the Ganges–Brahmaputra River mouth. However, no comprehensive study regarding the remote sensing of SSC in the Padma River has yet been published for the large alluvial Padma River in Bangladesh.

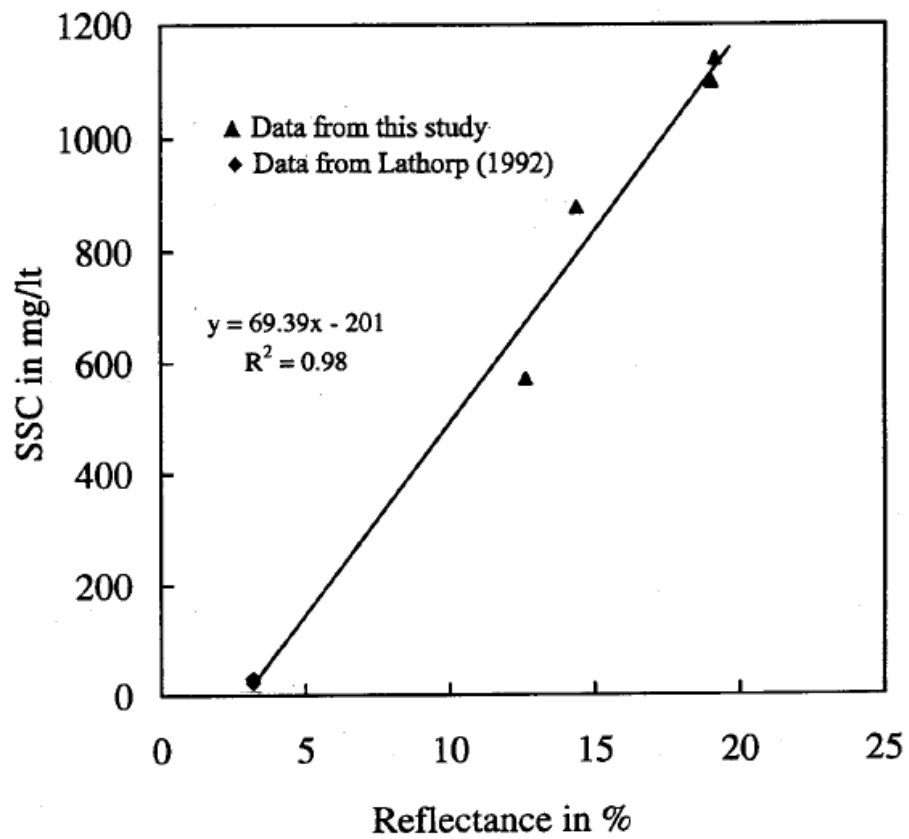


Fig 2.20: Relationship between reflectance of TM band 3 and suspended sediment concentration (SSC) for Ganges-Brahmaputra Rivers (Islam et al., 2001)

Chapter 3 - The Ganges-Brahmaputra Rivers System

3.1 Significance of Geographical Location

More than 2% of the world's six billion population reside in the Bengal Basin, an area of about 200,000 km², covering most of Bangladesh and parts of eastern India, and is the world's largest fluvio-deltaic system (Alam et al., 2003; Coleman, 1976). The annual flow of the Brahmaputra River from China to India is 165.4 billion cubic metres (BCM), from Bhutan to India 78 BCM, and from India to Bangladesh 537.2 BCM (Rasul, 2015). The annual flow of the Ganges River from China to Nepal is 12 BCM. All the rivers in Nepal drain into the Ganges River; the annual flow from Nepal to India is 210.2 BCM. The annual flow of the Ganges from India to Bangladesh is 525 BCM (Rasul, 2015). The major source of water is the summer monsoon and snow and ice melt from the Himalayas. Water regimes are strongly influenced by the monsoon. About 84% of the rainfall occurs from June to September, and 80% of the annual river flow takes place in the four months from July to October (Sood and Mathukumalli, 2011). The drastically reduced rainfall from November to March has created a flood-drought syndrome in the basin. While huge amounts of water during the monsoon period trigger floods and other hazards, the water in the dry season is insufficient to meet the requirements for irrigation and navigation or to maintain the minimum environmental flow in the rivers. Considerable areas in the Ganges-Brahmaputra region often suffer from both floods and droughts, which cause huge economic and social losses (Sood and Mathukumalli, 2011).

The Bengal basin also represents the world's largest sediment dispersal system and has formed the world's biggest submarine fan, known as the Bengal fan (Kuehl et al., 1989). River Ganges enters into the Bengal basin from the northwest after draining the Himalayas and about 2500 km through India. The Ganges divides into two distributaries; the River Padma flows southeast toward the confluence with the River Brahmaputra in Bangladesh (Mukherjee et al., 2009). The Brahmaputra channel belt shows a rapid lateral migration of as much as 800 m/year (Allison, 1998). Physiographically, the Bengal basin can be divided into two major units, the Pleistocene uplands and Holocene sediments (Heroy et al., 2003).

3.2 Geologic History of the Ganges-Brahmaputra Basin

The eastern part of the Bengal basin is mostly floored with Quaternary sediments deposited by the Ganges, Brahmaputra and Meghna rivers and their numerous tributaries and distributaries. The Ganges River rises near the Tibet-India border and flows southeast across India into Bangladesh. Its drainage basin lies predominantly in highly weathered sediments and volcanics, with the result that a heavy clay load is imposed on the channel. The Brahmaputra River has its source within Tibet along the northern slope of the Himalayas and flows across Assam into Bangladesh. This drainage basin contains very young and unweathered sedimentary rocks, and little clay is available for transport. The bedload thus consists predominantly of silt and fine sand. Of the two rivers, however, the Brahmaputra has the slightly higher total sediment concentration. The sediments within the rivers of Bangladesh, therefore, consist primarily of fine sands and silts, with little clay matrix. Being recently deposited, the sediments contain high water content and are loosely compacted. The nature of these sediments and the great amount of material imposed on the channels by the watershed causes the rivers constantly to adjust their bed configurations to differing flow regimes. Thus the sediments of the Brahmaputra and Ganges rivers are not only deposited in millions of tons but are also highly susceptible to erosion when flow conditions change. Within Quaternary times both rivers have occupied and abandoned numerous distinct courses (Coleman, 1969). Geologic map of the greater Bengal basin has been shown in Figure 3.1.

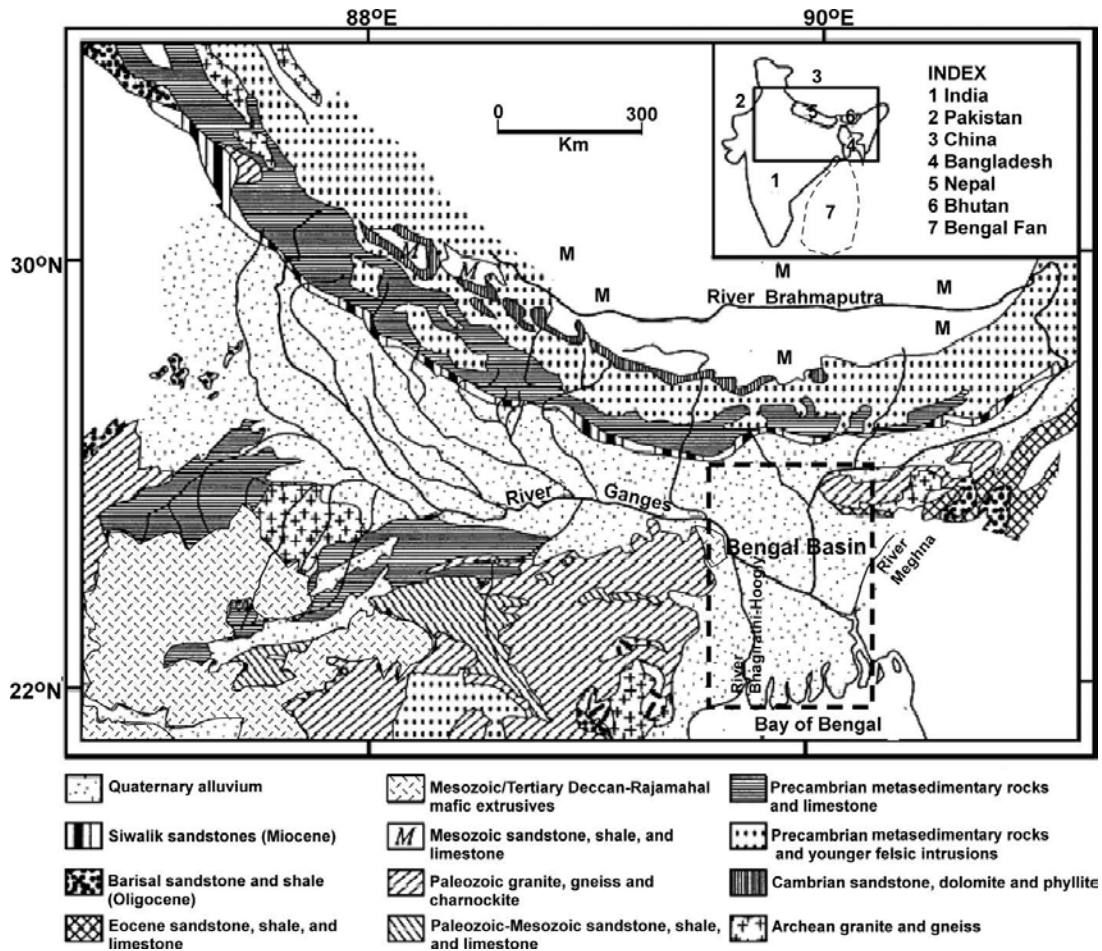


Fig. 3.1: Geologic map of the Bengal basin (Heroy et al., 2003)

3.3 Nature of Sediment Transport along the Ganges-Brahmaputra Rivers

The Ganges-Brahmaputra River transports approximately 1×10^9 tonnes of sediment per year, ranking it highest in the world among the river systems (Milliman and Syvitski, 1992a). An estimated 80% of this sediment load is delivered while southwest monsoon prevails from June to September (Coleman, 1969), rendering the system especially vulnerable to regional-scale climatic forcing. Approximately $8.5 \times 10^{12} \text{ m}^3$ of Ganges-Brahmaputra sediment has been stored in the Bengal basin since ca. 11 000 year before present (Goodbred and Kuehl, 2000). At the margin of the continent, the Ganges-Brahmaputra sediment load drains through the Bengal basin. The Bengal basin consists of approximately $1 \times 10^5 \text{ km}^2$ of flood-plains and delta-plains. The Padma, like Ganges and Brahmaputra is a very dynamic river; amounts

of deposition, accretion and lateral channel migration are very high. Fluvial sediment delivery to the GBM delta is projected to increase under the influence of anthropogenic climate change, albeit with the magnitude of the increase varying according to the specific catchment being considered. By the middle part of the 21st century, sediment loads are projected to increase by between 16% and 18% for the Ganges, and between 25% and 30% for the Brahmaputra River (Darby et al., 2015). A representation of the sediment budget of the GBM delta based on this study has been shown in Figure 3.2. The Padma River rearranges its channel every year and overbank inundation dispenses river's sediment load over the delta. Alluvial sediments are necessary for regulating soil fertility in the GBM delta, but this pattern is also detrimental to the lives and livelihoods of people. Over the last thirty years, erosion has devoured hundreds of thousands hectares of arable land along the Ganges, Brahmaputra and Padma banks. SSC is a major parameter in understanding and predicting river evolution, and therefore of significance in Bangladesh.

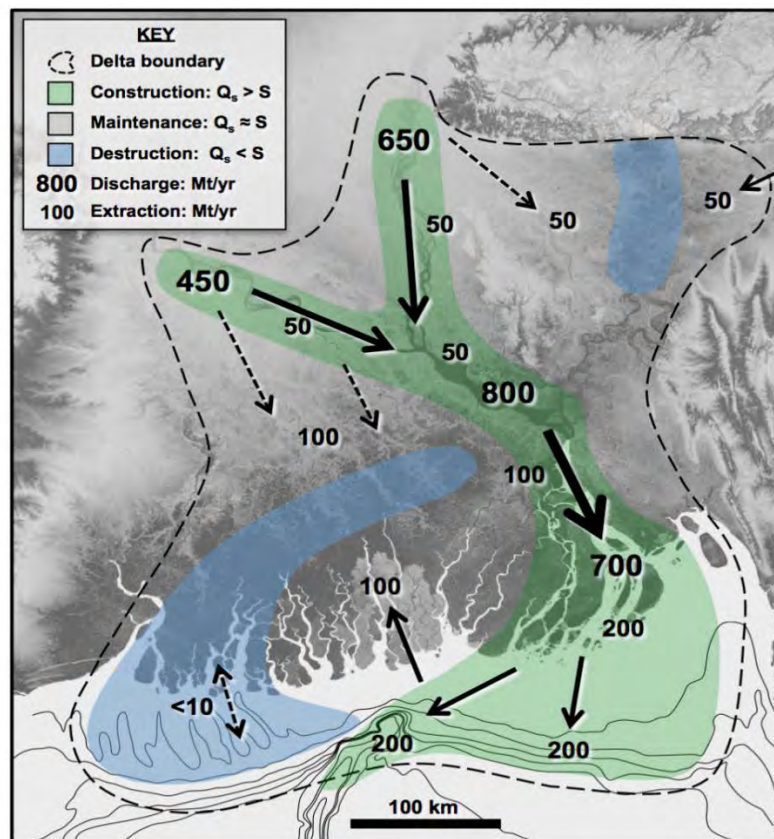


Fig. 3.2: Predicted sediment budget of the GBM delta (Courtesy - ESPA Deltas Project)

3.4 Morphology of the Ganges-Brahmaputra System

Most of the major rivers can generally be grouped into three types: braided, straight, and meandering. The presence of only one alluvial island (braid or, locally in Bangladesh, char) is sufficient to make the channel braided, but most braided rivers show several islands between channel banks (Figure 3.3). The chars are a product of the river itself and are composed of both bedload and suspended sediment. In plan view, the chars are asymmetrically diamond-shaped or triangular, with one point of the triangle pointed upstream. Although these two major shapes are most common, other types can be found. Generally the islands are unstable and change their location frequently. However, under certain conditions, such as stabilization by vegetation, they become semi-permanent. Since most chars modify their size, shape and location from time to time, they cause drastic changes in cross-sectional area at any one point. Brahmaputra can be classified as braided. The detailed processes responsible for the formation of a braided river are still poorly understood. Many published works deal specifically with the process of braiding, but little agreement can be found, and the hydraulic parameters of a braided stream are extremely complex (Coleman, 1969). Ganges is a sediment laden, wide, meandering river. Its annual mean predicted sediment load is 498.8×10^6 tons (Islam and Jaman, 2006). A geomorphic map of the Bengal basin has been shown in Figure 3.4.

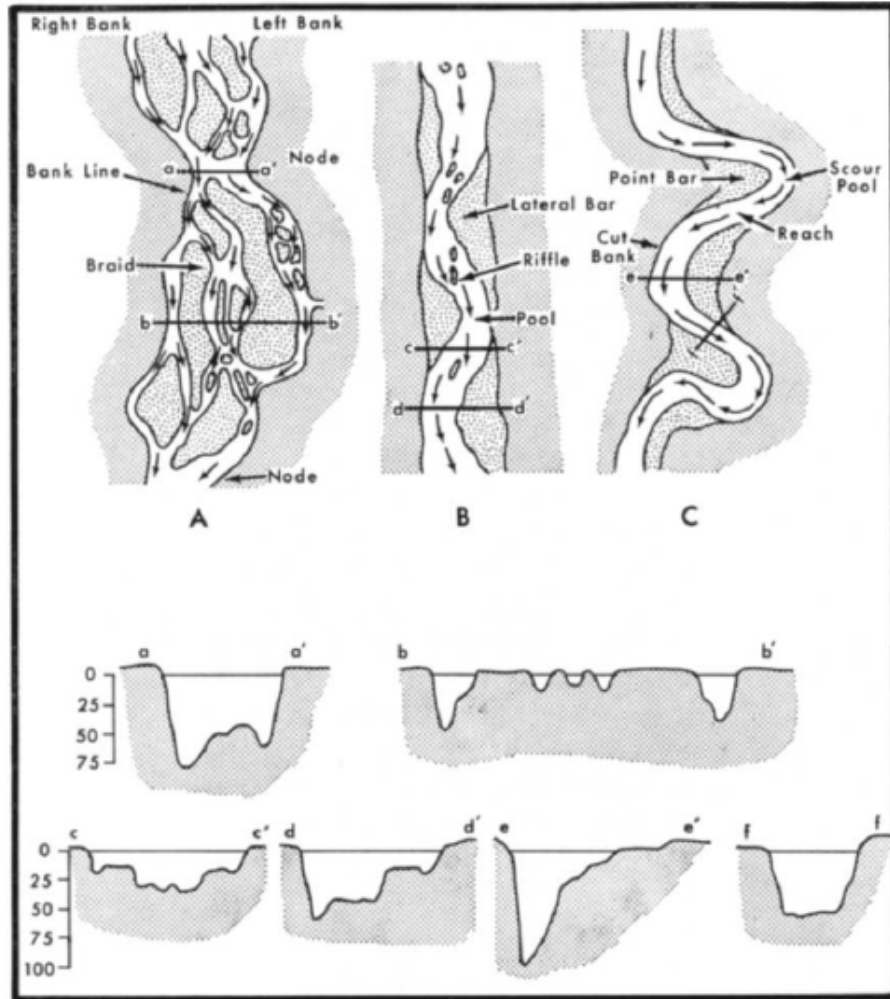


Fig 3.3: River channel patterns and typical cross-sections: A. braided; B. straight; C. meandering (Coleman, 1969)

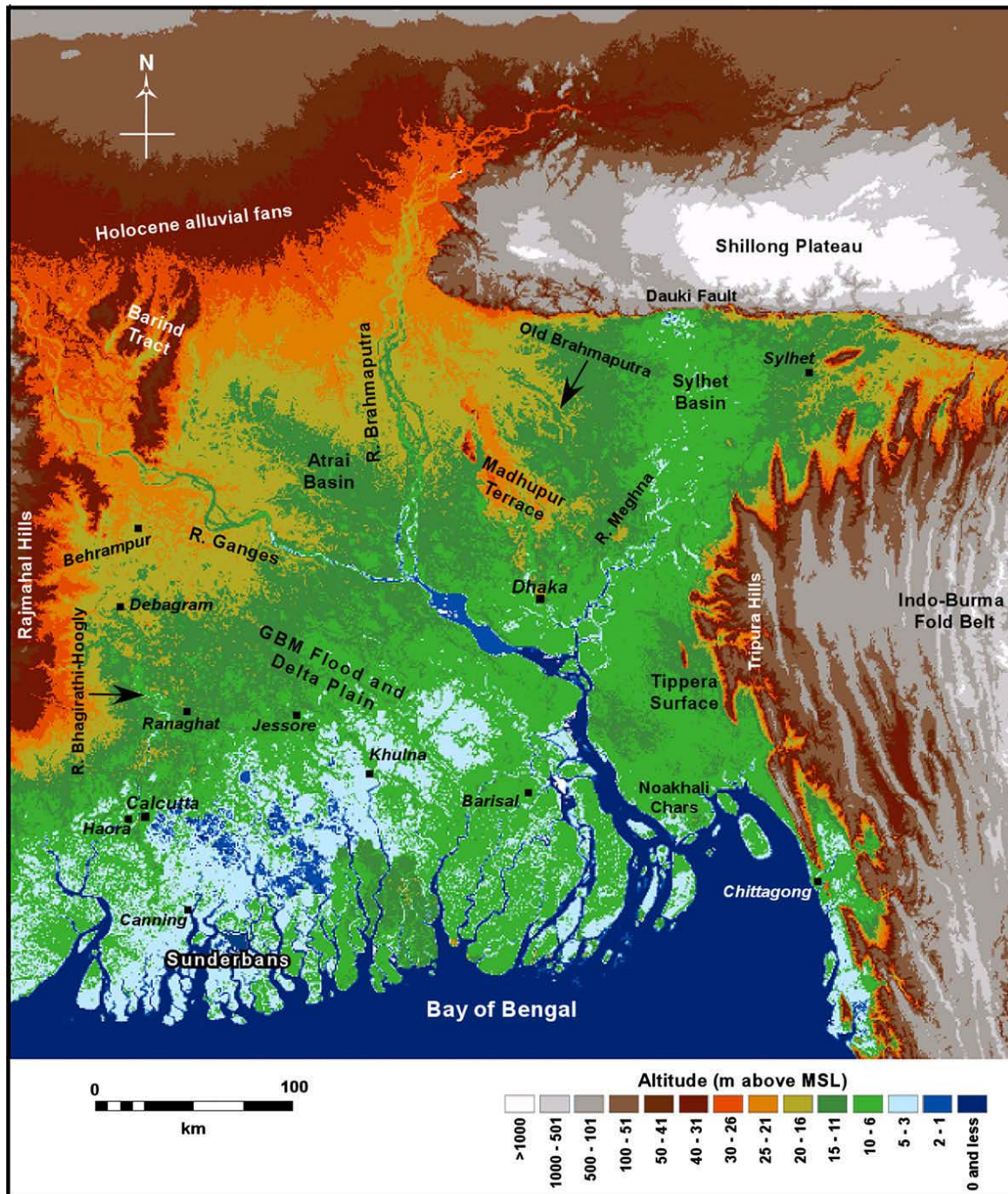


Fig. 3.4: Geomorphic map of the Bengal basin and surroundings superimposed on the SRTM-90 m digital elevation model (DEM) (Mukherjee et al., 2009)

3.5 Location of Gauging Station at the Padma River

Padma River in Bangladesh starts after the Ganges and the Brahmaputra Rivers conflate, flowing towards southeast until it conflues with the Meghna River near the Bay of Bengal. Secondary data procured from Bangladesh Water Development Board (BWDB) corresponding to their gauging station at Mawa SW 93.5L (23°28' N & 90°15' E) were used in this study. This station is the only reliable historical measured data point source currently available in Bangladesh for the Padma River; therefore specifically chosen for this study (Figure 3.5).

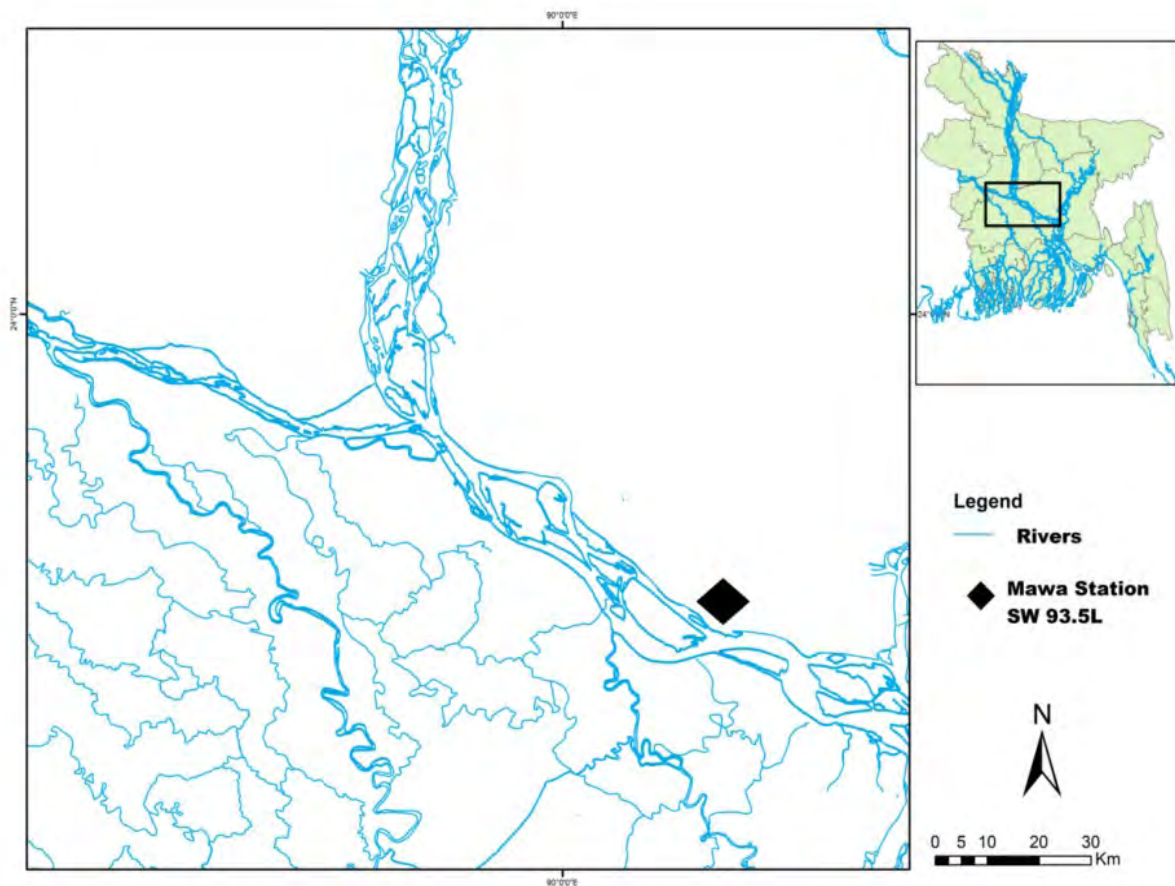


Fig. 3.5: Location of in situ data collection point

Chapter 4

Data Collection

4.1 In situ SSC Data Acquisition by BWDB

The procedure for collection of in situ suspended sediment data was observed as a part of this study. Bangladesh Water Development Board (BWDB)'s non-tidal discharge station consists of a pilot station and a survey catamaran. The catamaran is a vessel equipped with various measurement devices including Global Positioning System (GPS) and measurement devices for suspended sediment. A series of pictures (Figure 4.1-4.9) depicting the sequence of steps in the measurement of suspended sediment has been given below.



Fig. 4.1: Bangladesh Water Development Board's water survey catamaran stationed at Mawa 93.5L gauge station



Fig. 4.2: An automatic pulley system used to lift and submerge gauging equipment



Fig. 4.3: Sediment gauging equipment being prepared for sample collection



Fig. 4.4: Sediment sampling equipment being lowered for water sample collection



Fig. 4.5: Sediment sampling equipment being lifted up after water sample collection



Fig. 4.6: Water sample being transferred to another container from sediment sampling equipment



Fig. 4.7: Sample being transferred from the container to the measurement tube using a funnel



Fig. 4.8: Measurement tubes being separated after collection of sample



Fig. 4.9: Samples in measurement tubes being stored to be transferred to laboratory for testing

The measurement protocol starts with spatially accurate placement and anchoring of survey catamaran using GPS device. A measuring probe specifically designed for the purpose of

collecting turbid water from rivers is lowered into the water through a gap at the middle of the vessel with the aid of an automated pulley (Figure 4.4). The mouth of the probe is opened and the device is sunk about 1-2 meters into the flowing river water. After about 2 minutes the probe is lifted upwards and the water trapped inside of it is collected in a container (Figure 4.5). A test tube is setup below a funnel in an upright platform and the sample water is drained into it for exactly 1 minute (Figure 4.7). Thereafter the test tubes are sealed and stored in crates (Figure 4.9) and transferred to BWDB's lab where the concentration of sediments and sediment sizes are recorded at a later time.

The Padma's sediment values vary greatly between different seasons; a stark contrast could be seen between monsoon and post-monsoon seasons. Generally during dry season, the suspended sediment values are depleted greatly; nearing zero values. In the monsoon season however, the SSC values exceed 1000 ppm making the Padma's water highly turbid. These data are available at BWDB's data archives on special request and upon following specific formalities. Complete sets of data procured from BWDB have been included in the appendices. A sample set of sediment data provided by BWDB on the Mawa 93.5L station for the year 2001 has been demonstrated below (Table 4.1). The maximum sand concentration was chosen for this study on the basis of Padma being a large alluvial river and it mostly conveys one type of suspended sediment i.e. sand. Measured data between the years 2000-2012 was used in this particular study.

Table 4.1: An example of the Padma's sediment data set provided by the BWDB

| River Name | Station Name | Station ID | Date | Sand kg/s | Fine kg/s | Max Sand Concentration (PPM) |
|--------------|--------------|------------|-----------|-----------|-----------|------------------------------|
| Ganges-Padma | Mawa | SW93.5L | 6/2/2004 | 0.2674982 | 0 | 144.9 |
| Ganges-Padma | Mawa | SW93.5L | 6/9/2004 | 0.190087 | 0 | 209.3 |
| Ganges-Padma | Mawa | SW93.5L | 6/16/2004 | 0.259717 | 0 | 128.8 |

4.2 Acquisition of Landsat Data

Landsat 7 Enhanced Thematic Mapper (ETM+) images were selected as the remotely sensed data for this study. The Landsat's temporal resolution is 16 days and its spatial resolution is 30 m, meaning that images for a specific path and row are available every 16 days. Landsat being sun-synchronous, it generates day images only. These images are available for download upon request from United States Geological Survey (USGS) specified websites such as earthexplorer.usgs.gov and glovis.usgs.gov. For acquiring Landsat 7 data from its historical data archives, earthexplorer.usgs.gov was chosen. USGS offers open access to Level 1G product to users; L1G is a radiometrically and geometrically corrected Level 0R image. The correction algorithms used the spacecraft model and sensor, using images generated by in-flight computers during data acquisition events. Primary inputs are the Payload Correction Data, which includes the attitude and ephemeris profiles, the definitive ephemeris (if available) and the Mirror Scan Correction Data (MSCD). Although terrain corrected L1Gt products were available upon special request, they were not applicable for the current study which only deals with reflectance from surface water. Landsat 7 captures visible bands in the spectrum of blue, green, red, near-infrared and mid-infrared (bands 1-5 & 7). It is also equipped with thermal infrared channel (band 6) with a spatial resolution of 60 m. Landsat 7 data were glitch-free up to 2003, then there was a mechanical disturbance in the Scan Line Corrector (SLC); therefore images resulted in partially missing data. However, the SLC error did not have any significant implication regarding this study, and therefore correction was not necessary.

Upon creating an USGS EROS account at www.earthexplorer.usgs.gov an Email connection was established between user and website. For access to desired data, the polygon of corresponding image was selected by inputting Path and Row numbers of 137 and 44 respectively. This polygon covers the entire length of the Padma River and portions of the Brahmaputra and Ganges inside Bangladesh. After selecting the desired date and type of product an order was placed for processed L1G product. It is to be noted that the months of June to September were considered to be in Monsoon season. October and November were taken as post monsoon months. Thereafter download links were sent to user emails from USGS EROS when the products were ready. The downloaded products were compressed in a

zip file; upon expanding, images corresponding to the 8 bands of Landsat 7 were revealed along with some other data files which included the metadata file consisting of relevant information required in this study. Figure 4.10 shows an example of a true color composite Landsat ETM+ image. List of all Landsat 7 ETM+ images used in this study have been mentioned in appendix-F.

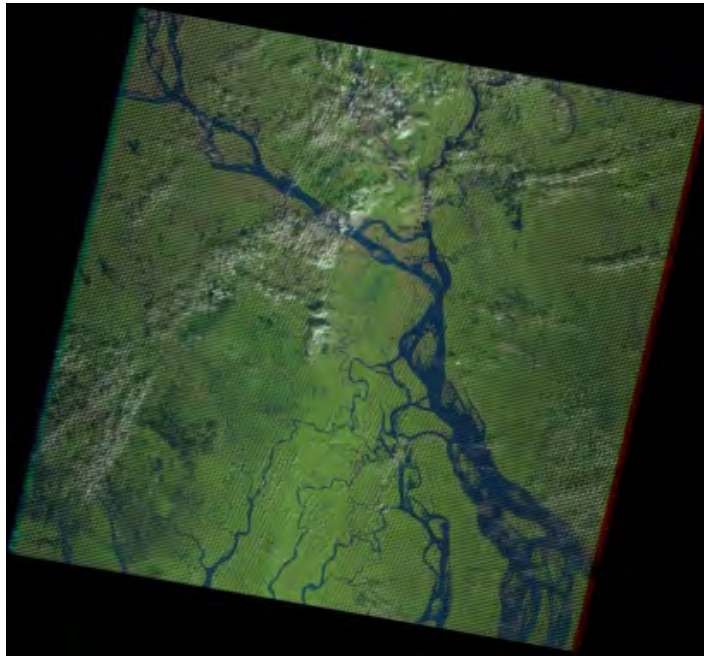


Fig. 4.10: Example of True Color Landsat 7 ETM+ Product (Polygon Path 137 & Row 44)

4.3 Hydro-morphological Data Collection

Water level, discharge, flow velocity and cross section data corresponding to sediment data were also procured from the Bangladesh Water Development Board through appropriate acquisition procedure. These data sets were used for morphological analyses later in this study. Appendix-B contains these detailed data tables as provided by BWDB.

Chapter 5 - Satellite Image Processing

5.1. Processing Landsat Data

Landsat ETM+ L1G products between the years 2000-2010 were processed for analysis in this study. List of all Landsat data sets used in this study has been provided in the appendix (Appendix-F) section. These images were selected based on two broad temporal categories, i.e. monsoon and post-monsoon season images. The months of June to September were considered to inside monsoon, whereas the months of October and November were deemed to be in post-monsoon season. Landsat images were processed using ILWIS.

Integrated Land and Water Information System (ILWIS) is a remote sensing and GIS software which integrates image, vector and thematic data in one unique and powerful package on the desktop. ILWIS delivers a wide range of features including import/export, digitizing, editing, analysis and display of data, as well as production of quality maps (www.52north.org).

The procedure for extraction of Digital Number (DN) begins with the importing of Raster images as Tagged Image File Format (.TIF). Input files are found in the folder containing decompressed Landsat data corresponding to specific bands. Because bands 1-4 have been proven by previous multiple researches to have the best relationship with suspended sediment reflectance, as mentioned in previous chapters; only data corresponding to aforementioned bands of specific wavelengths were imported. Upon importing, Raster Operation was initiated and with the aid of MapList Calculation function, raster images corresponding to the four bands were aggregated to be viewed as Color Composite images. To obtain True Color Composite images, the bands Blue, Green and Red were mapped to their corresponding layers. Thereafter, the pixel information window was accessed and the study area was focused upon by zooming in on the coordinates Latitude 23° 28' N and Longitude 90° 15' E. For each image, five cloud-free points across the length of the Padma River at Mawa 93.5L station were chosen and their corresponding band pixel values were recorded. A screenshot of the ILWIS interface has been provided later (Figure 5.1). The process was repeated for each of the downloaded product until band-wise pixel values, corresponding to the study

area, were acquired for all the downloaded L1G products. To ensure that no submerged sand bar could interfere with the desired reflectance, band combination RGB=754 was used which sharply separated land and water. Also band 4 is sensitive to shallow water depths (Poonawala et al., 2006). Hazy portions of the images were avoided as much as possible. Atmospheric correction was skipped because the individual images had very small angular range and it is almost impossible to carry out effective atmospheric correction if in situ atmospheric conditions are unknown (Wang and Lu, 2010). Thus, atmospheric correction was considered to have minimal effect on upcoming correlation analyses.

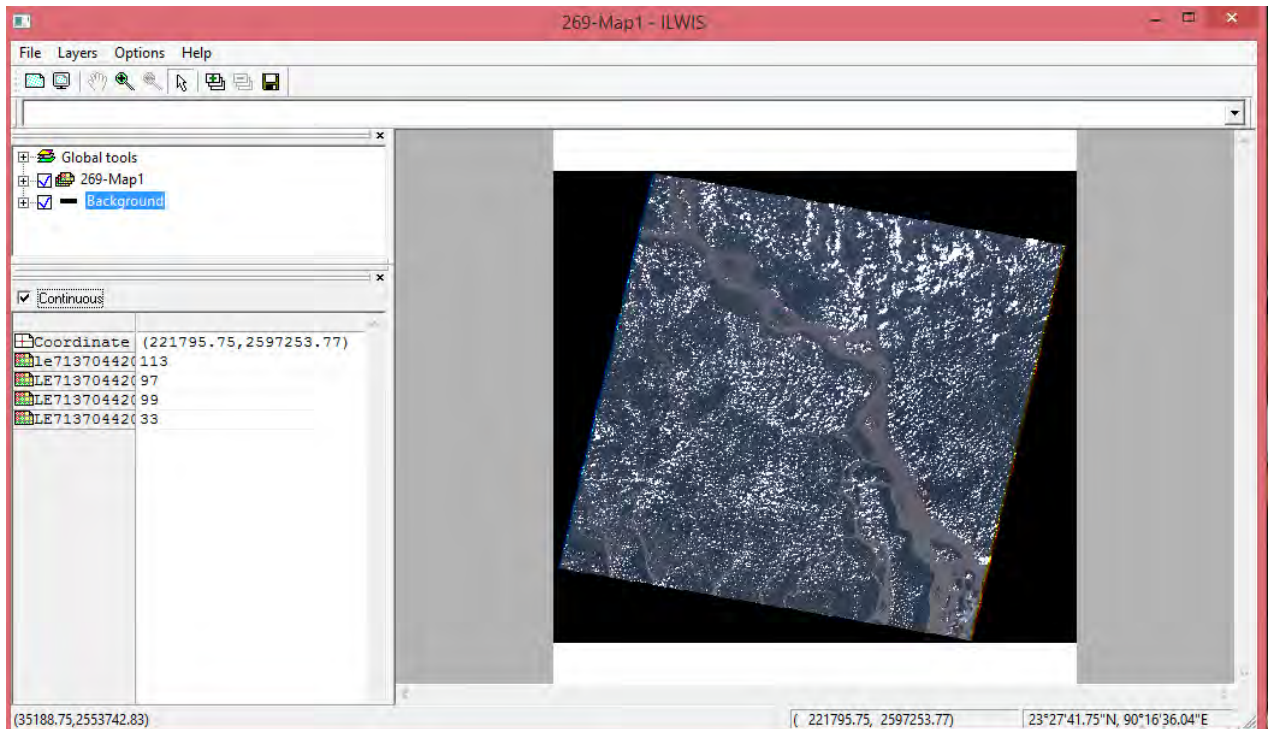


Fig. 5.1: Screenshot of ILWIS while extraction of DN with pixel information

It is worthy stating that Landsat ETM+ DN values range between 0 to 255 because these images are 8-bit data systems. Although these DNs are useful values, they are not physically meaningful. Therefore DN values for the four bands and each individual image were converted to physical values of radiance using the satellite's in-built sensor calibration parameters. Due to the enormous volume of data tables used for recording DN, the data record tables have been attached in the appendix section (Appendix-C). The highlighted row is the average of the DN from five individual data points for each of the four bands (B1-B4).

5.2. Conversion of DN into Radiance

Transformation of raw Landsat ETM+ Digital Numbers into physical values of radiance involves the following formula [1] (Fleiflea, 2013).

$$L\lambda = ((L_{\max} - L_{\min})/255)DN + L_{\min} \quad [1]$$

Where, $L\lambda$ is the spectral radiance ($m W cm^{-2} sr^{-1} \mu m^{-1}$), L_{\max} is the radiance measured at detector saturation ($m W cm^{-2} sr^{-1} \mu m^{-1}$) and L_{\min} is the lowest radiance ($m W cm^{-2} sr^{-1} \mu m^{-1}$). The radiance at detector saturation and lowest radiance values for bands of each image is available inside their corresponding metadata files attached with L1G products.

5.3. Conversion of Radiance into Top of Atmosphere Reflectance

Top of Atmosphere or Exoatmospheric Reflectance corrects for the earth-sun distance and solar angle errors. Reflectance is the proportion of the radiation striking a surface to the radiation reflected off of it. Thus to increase the accuracy of results, it was preferable to convert those radiance values into Exoatmospheric reflectance values. The following formula [2] (Fleiflea, 2013) was used for conversion.

$$p\lambda = (\pi d^2 L\lambda / E_o\lambda \cos\theta_s) \quad [2]$$

Where, $p\lambda$ is the ToA or Exoatmospheric Reflectance as a function of the band width λ , d^2 is the factor which corrects the variation in solar irradiances due to varying earth-sun distance at different times of the year. The value of d for each image was acquired from a table provided by USGS which consists of d values corresponding to the day of year. $E_o\lambda$ or F_i is the mean solar Exoatmospheric Irradiance ($W\mu m^{-2}$); θ_s represents the Solar Zenith Angle in radians which was obtained by subtracting the Solar Elevation Angle from 90 degrees.

To alleviate the volume of tasks regarding these two conversions of 32 Landsat ETM+ images, each with four bands, excel function sheets were created where input average DN data was converted directly into reflectance values. The Earth-sun distance correction factor (d) table provided by USGS/NASA has been attached in the appendix section (Appendix-D).

The resultant Top of Atmosphere or Exoatmospheric Reflectance values for the bands (B1-B4) corresponding to Day of Year between 2000 and 2010 have been listed in the table below (Table 5.1). These band specific reflectance values were used in correlation and regression analyses of this study. The application and significance of these data sets have been discussed in next chapters.

Table 5.1: Resultant ToA reflectance (dimensionless) values

| Year | Mawa 93.5L ToA Reflectance | | | | |
|------|----------------------------|-------|-------|-------|-------|
| | Day of Year | B1 | B2 | B3 | B4 |
| 2000 | 235 | 0.173 | 0.166 | 0.171 | 0.146 |
| | 283 | 0.159 | 0.148 | 0.137 | 0.114 |
| | 299 | 0.172 | 0.158 | 0.144 | 0.120 |
| | 331 | 0.184 | 0.164 | 0.144 | 0.164 |
| 2001 | 189 | 0.188 | 0.187 | 0.183 | 0.164 |
| | 221 | 0.175 | 0.171 | 0.167 | 0.146 |
| | 269 | 0.163 | 0.152 | 0.142 | 0.120 |
| 2002 | 256 | 0.163 | 0.159 | 0.152 | 0.122 |
| | 304 | 0.156 | 0.145 | 0.129 | 0.102 |
| 2003 | 227 | 0.175 | 0.165 | 0.167 | 0.131 |
| | 307 | 0.174 | 0.160 | 0.151 | 0.126 |
| | 323 | 0.171 | 0.157 | 0.143 | 0.162 |
| 2004 | 182 | 0.206 | 0.198 | 0.192 | 0.175 |
| | 230 | 0.200 | 0.196 | 0.191 | 0.176 |
| | 246 | 0.216 | 0.201 | 0.193 | 0.187 |
| | 294 | 0.105 | 0.103 | 0.098 | 0.112 |
| 2005 | 280 | 0.176 | 0.162 | 0.149 | 0.131 |
| 2006 | 139 | 0.157 | 0.147 | 0.132 | 0.101 |
| | 299 | 0.165 | 0.162 | 0.150 | 0.115 |
| 2007 | 270 | 0.162 | 0.160 | 0.159 | 0.130 |
| | 302 | 0.113 | 0.111 | 0.105 | 0.119 |
| | 334 | 0.173 | 0.161 | 0.138 | 0.143 |
| 2008 | 177 | 0.191 | 0.190 | 0.185 | 0.154 |
| | 209 | 0.173 | 0.174 | 0.174 | 0.153 |
| | 273 | 0.161 | 0.173 | 0.171 | 0.153 |
| | 289 | 0.169 | 0.162 | 0.155 | 0.128 |
| | 305 | 0.107 | 0.102 | 0.094 | 0.101 |
| 2009 | 163 | 0.206 | 0.196 | 0.183 | 0.148 |
| | 291 | 0.129 | 0.122 | 0.117 | 0.121 |
| 2010 | 182 | 0.187 | 0.181 | 0.175 | 0.156 |
| | 294 | 0.163 | 0.158 | 0.151 | 0.124 |

Chapter 6

Development of SSC- Spectral Reflectance Relationships

6.1. Investigating SSC-ToA Reflectance for Individual Bands

To investigate which band or what combination of bands of Landsat ETM+ provide the strongest correlations. For the purpose of analysis the ToA Reflectance values were converted to ToA% values. Thereafter XY scatter plot were drawn for each of the four bands. For each scatter plot, a best-fit polynomial curve was plotted and its Coefficient of Determination (R^2) was found out (Figure 6.1-6.4). The results have been demonstrated and discussed below.

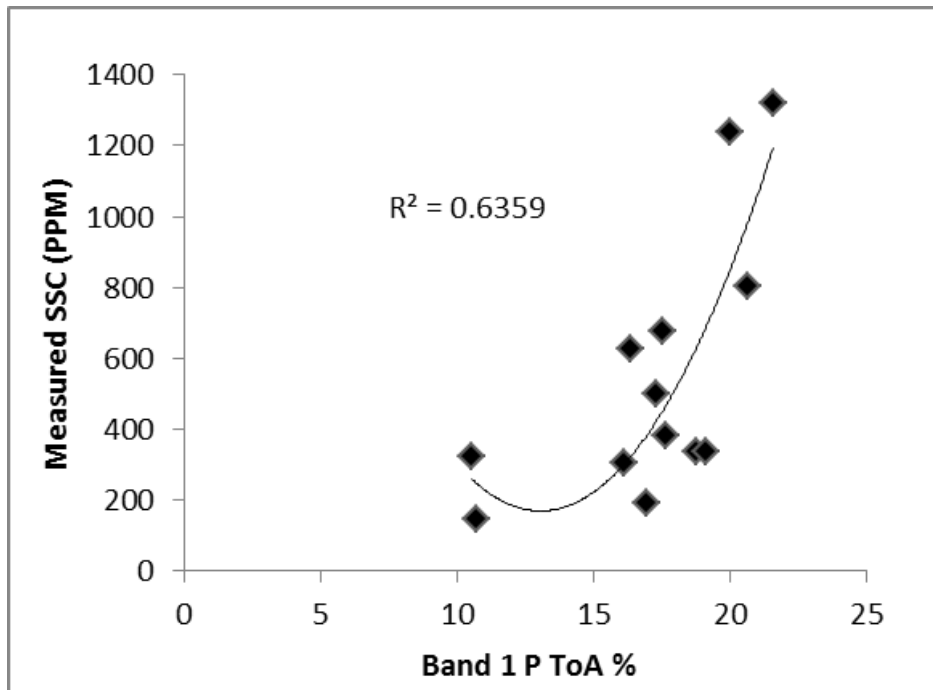


Fig. 6.1: Scatter plot of measured SSC versus ToA reflectance percentage of band 1

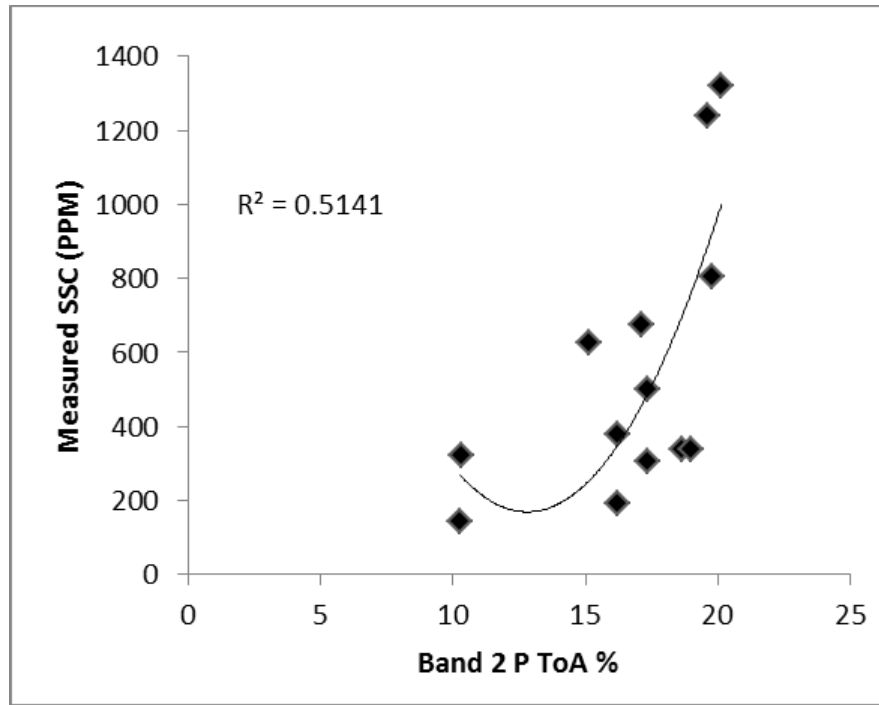


Fig. 6.2: Scatter plot of measured SSC versus ToA reflectance percentage of band 2

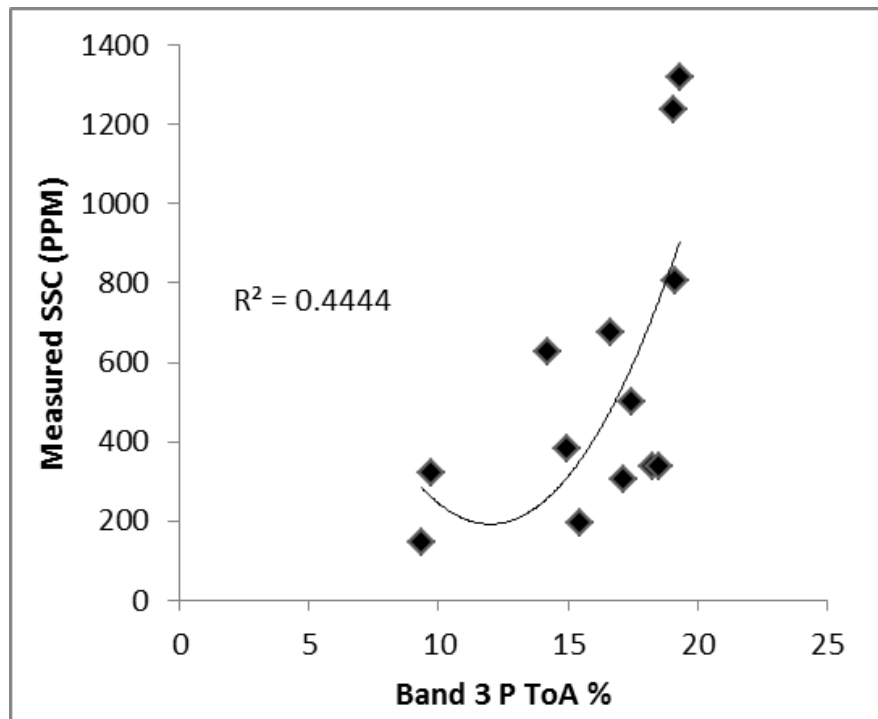


Fig. 6.3: Scatter plot of measured SSC versus ToA reflectance percentage of band 3

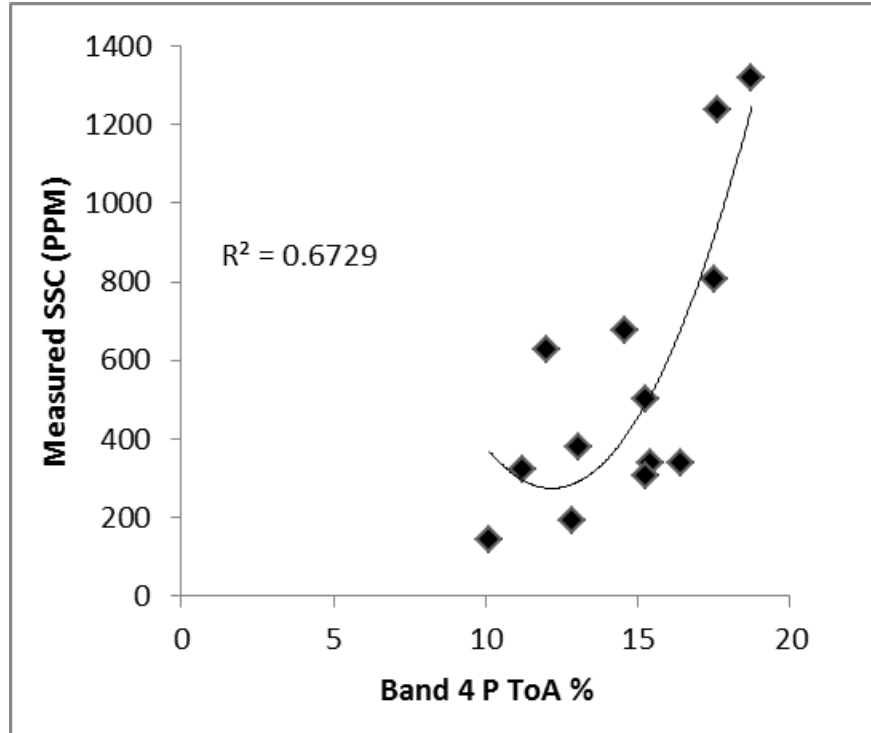


Fig. 6.4: Scatter plot of measured SSC versus ToA reflectance percentage of band 4

The purpose of these correlation analyses is to investigate any statistically significant relationship between two variables. In this case it was to investigate which band's reflectance values. R^2 values indicate the strength of correlation; ranging between 0-1, the closer to 1 the stronger is the agreement between two variables. R^2 for bands 1, 2, 3 and 4 were 0.6359, 0.5141, 0.4444 and 0.6729 respectively. Although reflectance at band 1 shows significantly strong relationship with measured SSC, band 4 ($R^2= 0.6729$) demonstrated the strongest statistical relationship among the four, which is consistent with previous studies (Sterckx et al., 2007; Wass et al., 1997). Therefore band 4 (Near Infrared) was chosen as the indicator for SSC. Near Infrared spectrum is sensitive to SSC and relative to shorter wavelength bands, also less influenced by bottom reflectance in environments with shallow water (Tolk et al., 2000). Owing to the non-linear nature of the data, curvilinear polynomial equation [3] was chosen. The polynomial relationship obtained from the best-fit curve can be stated as,

$$SSC = 22.565 (B4)^2 - 549.27(B4) + 3616.7 \quad [3]$$

Where 'SSC' is the Suspended Sediment Concentration (ppm) and 'B4' is the Band 4 ToA reflectance percentage. Polynomial relationship, which provided the best coefficient of

determination values, was chosen over linear (Figure 6.5), exponential (Figure 6.6) and log formulations (Figure 6.7), after applying them similarly to examine the relationship between SSC and reflectance percentage values. In order to validate the regression relation between SSC and band 4 reflectance percentage values, scatter plot of predicted values of SSC from equation [3] versus measured values of SSC was drawn and the Root Mean Square Error (RMSE) was extracted (Figure 6.8). Thereafter the residuals were also plotted against measured SSC (Figure 6.9). Relative error percentage was also demonstrated in an individual plot (Figure 6.10). A set of 13 Landsat ETM+ images were used to extract the estimated SSC and corresponding measured values were used for this purpose have been provided in table 6.1.

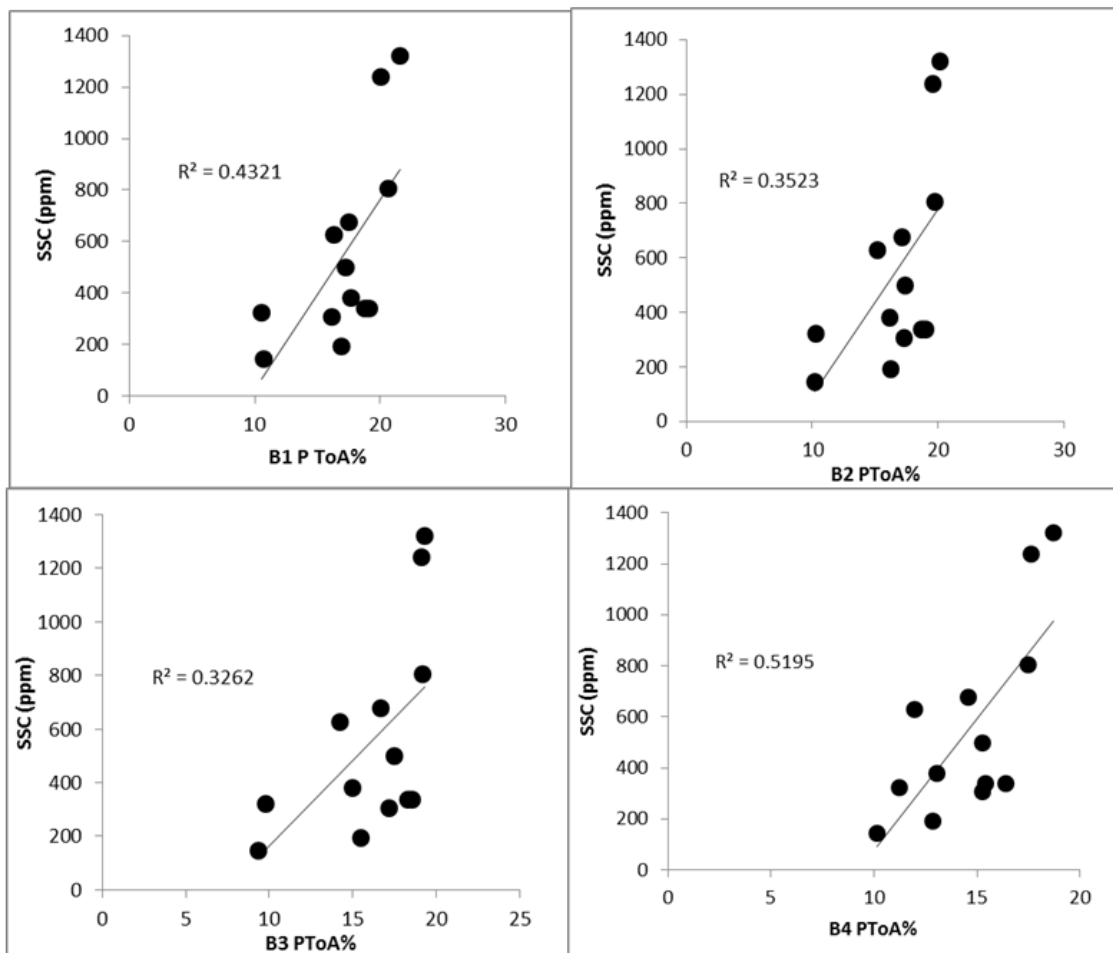


Fig. 6.5: Scatter plot of measured SSC versus ToA reflectance percentage of bands 1-4 with linear trend lines

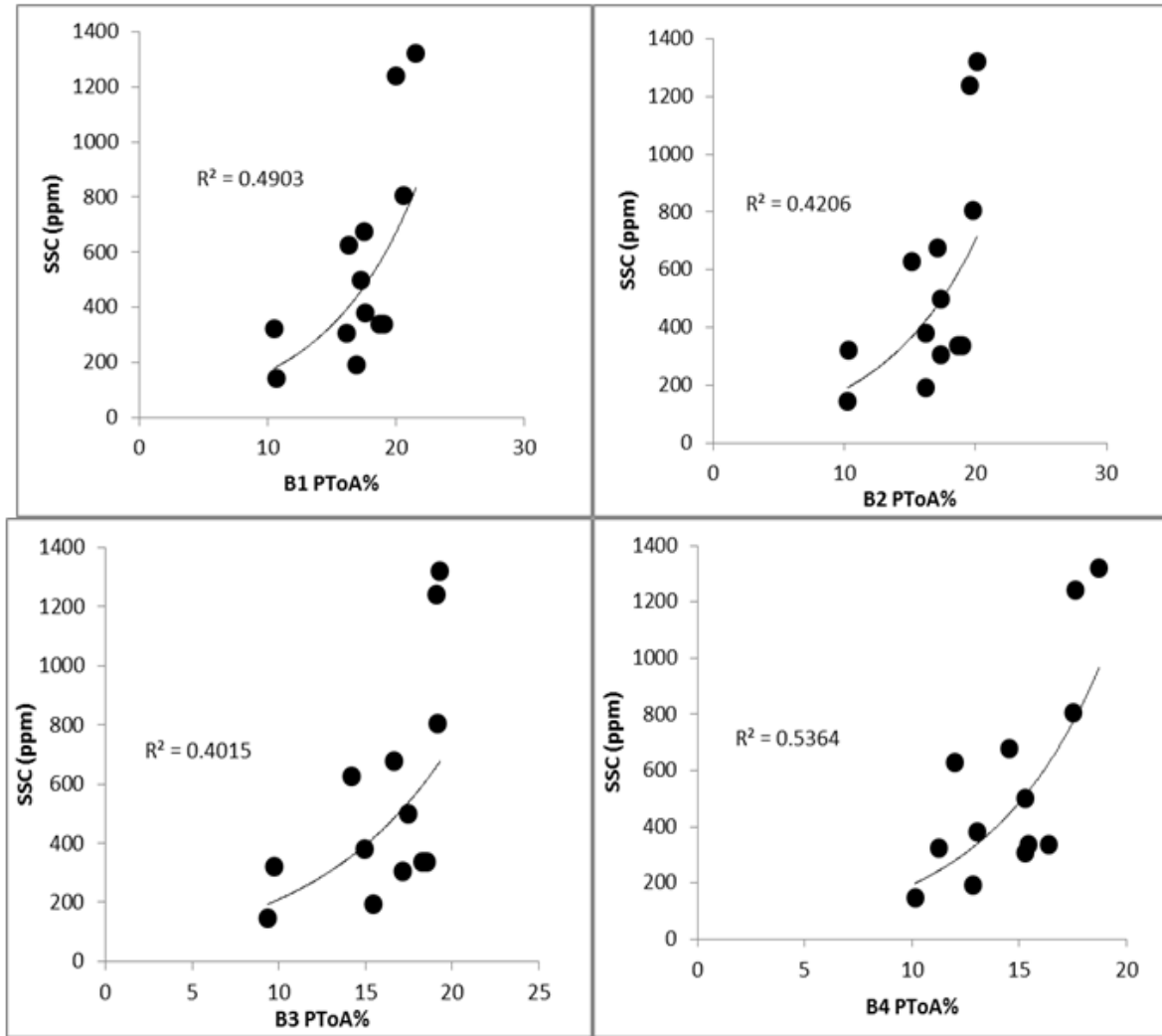


Fig. 6.6: Scatter plot of measured SSC versus ToA reflectance percentage of bands 1-4 with exponential trend lines

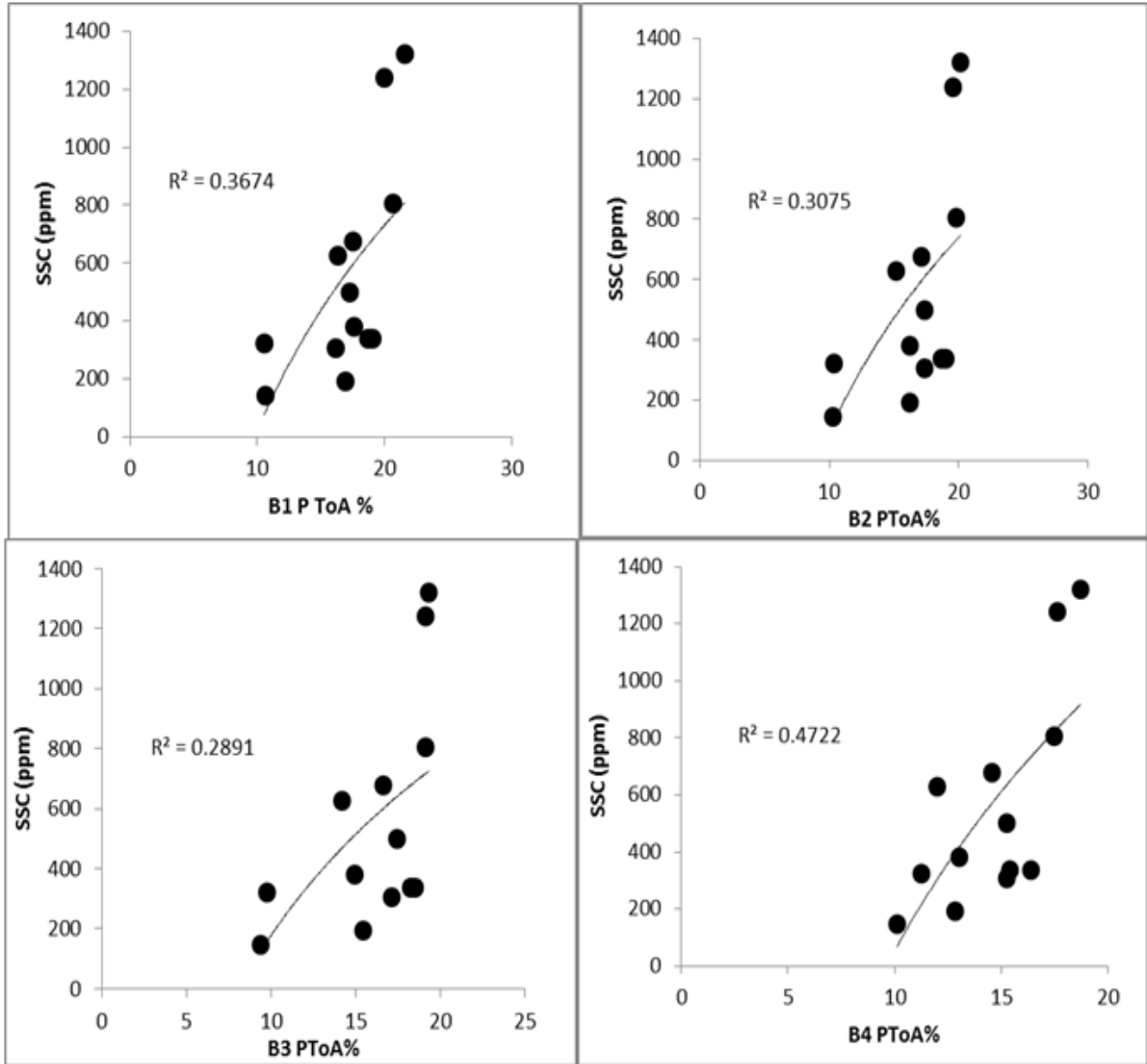


Fig. 6.7: Scatter plot of measured SSC versus ToA reflectance percentage of bands 1-4 with logarithmic trend lines

Table 6.1: Data sets used for validation of polynomial model [3]

| Date | Measured SSC (ppm) | Estimated SSC (ppm) | Residuals (ppm) | Squared Residuals | RMSE | Relative Error % |
|-----------|--------------------|---------------------|-----------------|-------------------|------|------------------|
| 1-Jul-10 | 460 | 543 | -83 | 6889 | 88.3 | -18.0 |
| 21-Oct-10 | 250 | 275 | -25 | 625 | | -10.0 |
| 12-Jun-09 | 435 | 434 | 1 | 1 | | 0.0 |
| 18-Oct-09 | 194 | 273 | -79 | 6241 | | -40.7 |
| 4-Aug-05 | 1047 | 1214 | -167 | 27889 | | -15.9 |
| 17-Jun-05 | 194 | 278 | -84 | 7056 | | -25.3 |
| 2-Jun-11 | 225 | 282 | -57 | 3249 | | -39.6 |
| 22-Sep-11 | 837 | 717 | 120 | 14400 | | 14.3 |
| 8-Oct-11 | 644 | 525 | 119 | 14161 | | 18.5 |
| 24-Oct-11 | 274 | 287 | -13 | 169 | | -4.7 |
| 20-Jun-12 | 354 | 276 | 78 | 6084 | | 22.0 |
| 22-Jul-12 | 564 | 595 | -31 | 961 | | -5.5 |
| 7-Aug-12 | 548 | 665 | -117 | 13689 | | -21.0 |

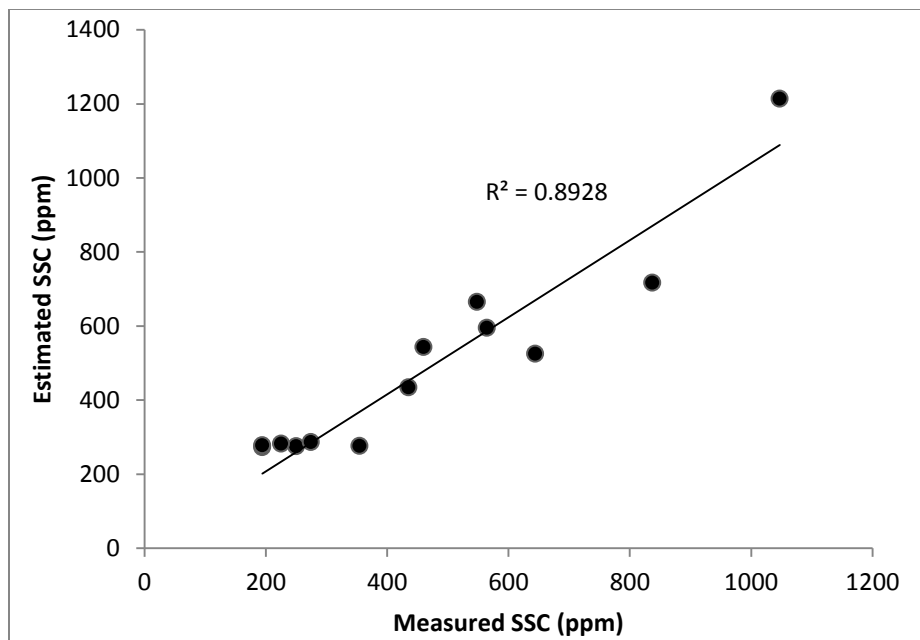


Fig. 6.8: Scatter plot of estimated SSC values by the polynomial model based on band 4 (Near Infrared) ToA reflectance and measured SSC data with 1:1 fit line. ($R^2=0.89$, $n=13$)

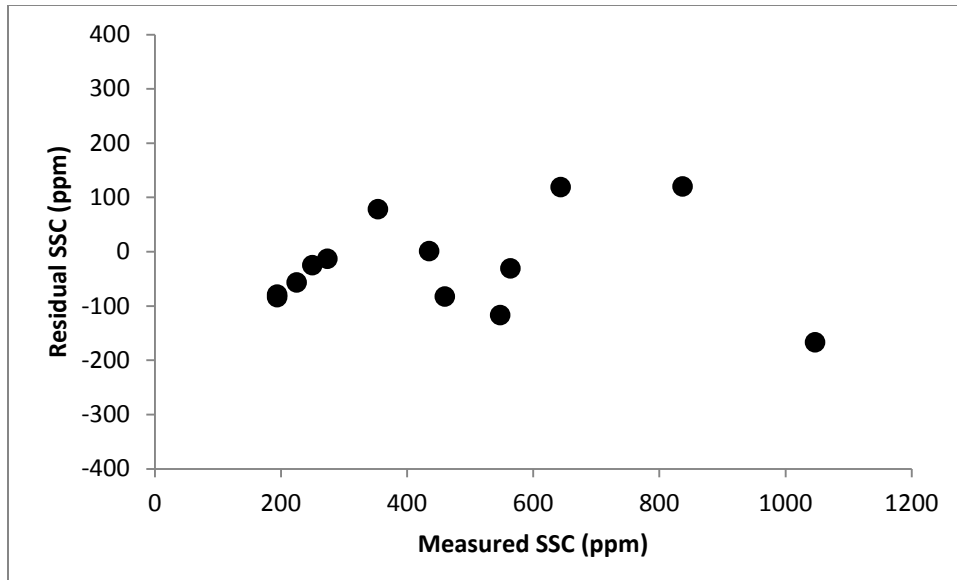


Fig. 6.9: Residue of SSC versus measured SSC

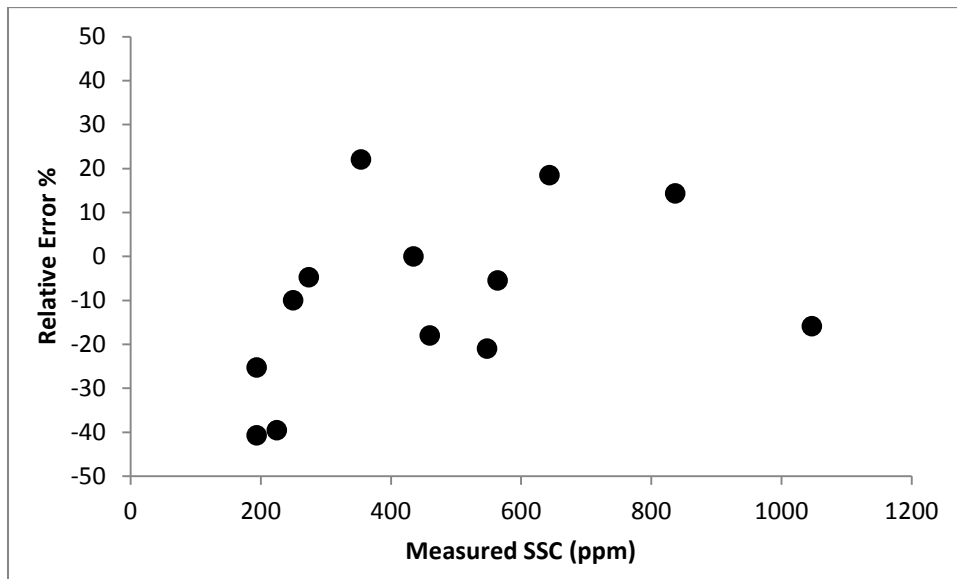


Fig. 6.10: Scatter plot of relative error percentage of estimated SSC from measured SSC (Average relative error is $\pm 18.11\%$)

Scatter plot of predicted SSC values from the polynomial equation [3] against in situ values of SSC with 1:1 fit line generated strong positive coefficient of determination of 0.89 and Root Mean Square Error (RMSE) of 88.3 ppm. The residual values of SSC were calculated by subtracting estimated values of SSC from the measured data. RMSE was extracted by

calculating the square root of average squared residual. Therefore, predicted values and measured values of SSC are in strong statistical agreement (Taylor, 1990), and that correlation does imply causation for the polynomial relationship. It is apparent that this model's prediction accuracy is better for higher values of SSC i.e. above 200 ppm to approximately 800 ppm. From the measured values of SSC, it is observed, the Padma River's SSC values usually range above 200 ppm for most of the time during monsoon and even during post-monsoon season; thus affirming this model's applicability. The average relative error is $\pm 18.11\%$.

6.2. Investigating Robust SSC- Spectral Reflectance Relationship

Some laboratory studies dealing with reflectance and SSC relationships suggested robust SSC-Reflectance relationships throughout the visible portion of the spectrum may augment the applicability of such models (Novo et al., 1989; Schiebe et al., 1992). Robust relationships are especially important in cases where sediment color varies greatly. Some studies have previously reflectance in the red band in combination with other reflectance of other visible bands to augment the models' robustness in the prospect of variation in suspended sediment color (Aranuvachapun and Walling, 1988; Dekker et al., 2001; Han et al., 2006; Lathrop et al., 1991; Wu et al., 2007). Padma being a large alluvial river, its overall sediment color remains relatively unvaried; the alluvial at the foothills of eastern Himalayas are formed by deposition from the north Bengal tributaries of the Ganges and Brahmaputra, these rivers have also dissected the Barind tract, and therefore coarse-grained sediments such as cobbles and sand dominate the Padma (Mukherjee et al., 2009). The four band reflectance percentage values were used as independent variables and measured SSC values were considered as dependent variables. The summary of multiple regression analysis has been listed below (Table 6.2-6.4). Graphical representation of this analysis is also provided (Figure 6.11).

Table 6.2: Output table of regression analyses

| | <i>Coefficients</i> | <i>Standard Error</i> | <i>t Stat</i> | <i>P-value</i> | <i>Lower 95%</i> | <i>Upper 95%</i> |
|-----------|---------------------|-----------------------|---------------|----------------|------------------|------------------|
| Intercept | -931.07 | 579.39 | -1.61 | 0.15 | -2267.15 | 405.01 |
| B1 PToa% | 280.62 | 182.26 | 1.54 | 0.16 | -139.68 | 700.91 |
| B2 PToA% | -473.49 | 568.76 | -0.83 | 0.43 | -1785.05 | 838.08 |
| B3 PToA% | 114.44 | 404.98 | 0.28 | 0.78 | -819.44 | 1048.31 |
| B4 PToA% | 186.85 | 70.10 | 2.67 | 0.03 | 25.20 | 348.50 |

Table 6.3: Summary of outputs of regression analyses

| <i>Regression Statistics</i> | |
|------------------------------|---------|
| Multiple R | 0.867 |
| R Square | 0.753 |
| Adjusted R Square | 0.629 |
| Standard Error | 227.632 |
| Observations | 13 |

Table 6.4: Residual output of regression analyses

| <i>Observation</i> | <i>Predicted SSC (PPM)</i> | <i>Residuals</i> |
|--------------------|----------------------------|------------------|
| 1 | 655.01 | -316.91 |
| 2 | 499.04 | 177.16 |
| 3 | 344.06 | 283.84 |
| 4 | 960.71 | -155.71 |
| 5 | 886.83 | 352.87 |
| 6 | 1302.00 | 18.20 |
| 7 | 357.19 | -35.19 |
| 8 | 503.95 | -123.45 |
| 9 | 440.14 | -102.04 |
| 10 | 543.42 | -43.42 |
| 11 | 208.64 | 97.26 |
| 12 | 309.35 | -116.15 |
| 13 | 181.38 | -36.48 |

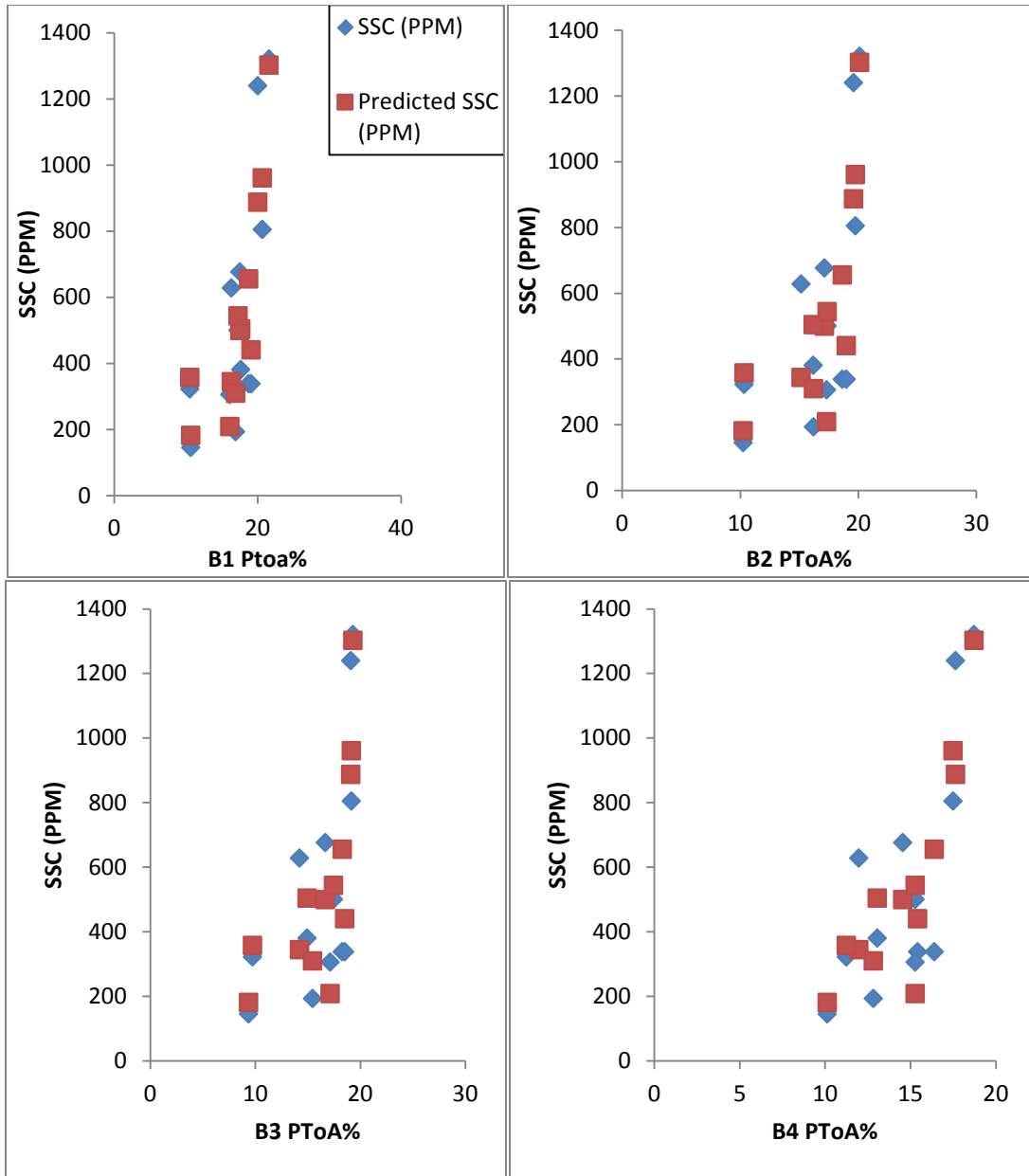


Fig. 6.11: Bands 1-4 ToA reflectance percentage plot

Multiple regression analysis allowed the investigation of how multiple independent variables were related to dependent variables. From the results of regression analyses, a robust model [4] can be derived.

$$SSC = -931.07 + 280.62B1 - 473.49B2 + 114.44B3 + 186.85B4 \quad [4]$$

Where, B1, B2, B3 and B4 are ToA reflectance percentage of respective bands. SSC can be estimated by inputting top of atmosphere reflectance percentage (PToA%) of corresponding four bands. However, the predictive values (P-value) of the Exoatmospheric reflectance percentage of bands 1, 2 and 3 were above 0.15; which are very insignificant and therefore can be omitted from the linear model (Lunt, 2015). Only band 4 reflectance percentage possessed P-value low enough to be significant in predicting SSC values. Sediment color is an integral factor when considering robust models for sediment mapping; due to lack of ground-based spectrometer and hyperspectral images, there are no reliable measured sediment color data available. Principle sources of uncertainty in these robust relationships, within a study area, are differences in mineralogy, grain sizes as well as color (Choubey, 1998; Novo et al., 1991). Considering the aforementioned facts, the robust model [4] was not considered for spatio-temporal mapping of SSC in the Padma River.

Chapter 7

Spatio-temporal Variation of SSC

7.1 Retrieval of Spatial Distribution of SSC

To demonstrate the spatial and temporal variations of SSC in the Padma River, the previously developed polynomial relationship (3) was applied. A sum of 18 Landsat ETM+ images from both monsoon and post-monsoon seasons, between years 2000 to 2010, were used for this purpose. Landsat 7 ETM+ data were initially acquired from USGS specified website, i.e. www.earthexplorer.usgs.gov as compressed files and then extracted to reveal the images corresponding different bands. Quantum GIS (QGIS) was used for processing the images. QGIS is an Open Source Geographic Information System (GIS) licensed under the General Public License. QGIS is an official project of the Open Source Geospatial Foundation (OSGeo). It runs on Linux, Unix, Mac OSX, Windows and Android and supports numerous vector, raster, and database formats and functionalities (www.qgis.org).

Raster images corresponding to band 4 (wavelength: 0.77-0.90 μ m) were imported into the QGIS software and cropped to magnify the area under focus. For each image, a vector layer was created and the water body of the Padma River, extending up to approximately 20 km upstream and 20 km downstream of BWDB Gauge Station Mawa 93.5L, was extracted. This interactive process, in which a segment map is shaped while a raster map is displayed in the background, is conventionally known as On-Screen Digitization. Using the extracted raster image, SSC spatial distribution maps were created. For this purpose, raster calculation was applied - where the raw digital number (DN) was first converted to spectral radiance using the appropriate conversion formula, and then to Top of Atmosphere (ToA) reflectance percentage. The resultant reflectance percentage values were input into the polynomial relationship (3) to reveal the SSC values for each pixel. For facilitating visualization, continuous Pseudocolor images were created. Sand bars and cloud patches were excluded from the maps since their presence would disrupt the actual representation of SSC distribution.

Landsat 7 ETM+ images were error free up to May 31, 2003. Since then, the Scan Line Corrector (SLC) which compensates for the forward motion of Landsat 7 ETM+ has failed, resulting in duplicated image area and width that increases towards the edge of the images. Therefore, all images acquired after May 2003 is accompanied by SLC error; this mode is also referred to as SLC-off mode. However, the SLC-off mode did not hamper the effective depiction of SSC distribution of the Padma River in this study. Coordinate Reference System (CRS) was set to WGS 84/ UTM Zone 46N for both layer and project files. There was particular difficulty in obtaining cloud-free Landsat images during monsoon season; and as a consequence, there were no suitable images for demonstrating SSC spatial distribution for the monsoon of 2003, 2009 and 2010. However, suitable post-monsoon images were available for all of the years between 2000 and 2010. The resultant maps have been shown in figures 7.1-7.18. Since coefficients of the polynomial relationship (3) is based on a single station and confined to monsoon and post monsoon seasons, some errors may be expected while computing Spatio-temporal distribution of SSC in the Padma River.

7.2 Spatial Distribution Maps of SSC in the Padma River

Spatial distribution maps of SSC in the Padma River, from the year 2000 to 2010 (Figures 7.1-7.18), and their respective discussions are given below.

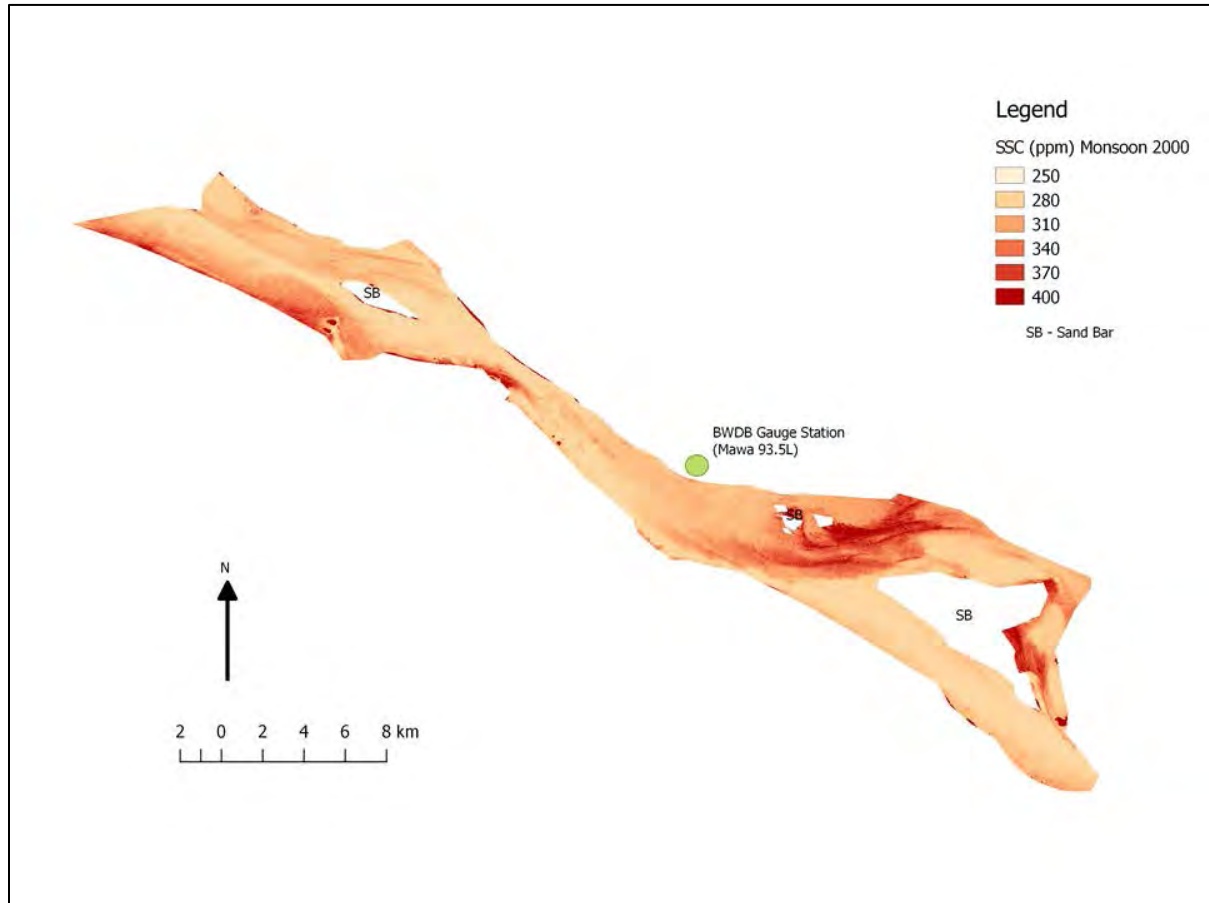


Fig. 7.1: Spatial distribution map of SSC in the Padma River for Monsoon of 2000

The Landsat scene identification number used for this spatial distribution map (Figure 7.1) was LE71370442000283SGS00 (Image courtesy of the U.S. Geological Survey). The SSC values ranged between 250-400 ppm. There was no significant cloud patch over the water body of the river. The sand bars excluded from the map have been marked appropriately. A notable rise of suspended sediment concentrations can be observed immediately downstream of sand bars; an observation which may be attributed to erosive effect of the river. Another interesting observation in this map is the sand bar, which apparently is situated at the margin where water flows from the Ganges and Brahmaputra conflate, was not subjected to the

erosive effect of the river, contrary to the observed behavior of sand bars downstream. The detailed processes responsible for the formation of a braided river are still poorly understood. Many published works deal specifically with the process of braiding, but little agreement can be found, and the hydraulic parameters of a braided stream are extremely complex (Coleman, 1969).

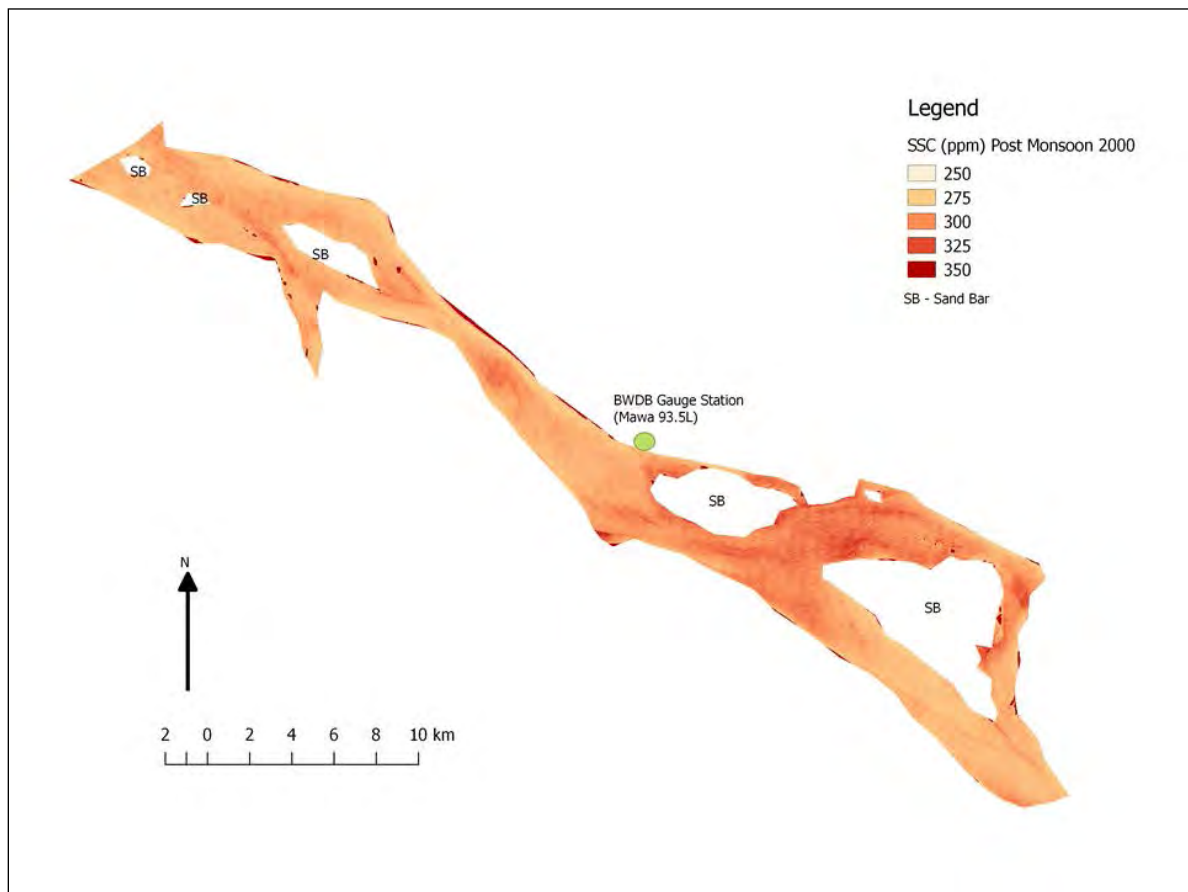


Fig. 7.2: Spatial distribution map of SSC in the Padma River for Post Monsoon of 2000

The Landsat scene identification number used for this spatial distribution map (Figure 7.2) was LE71370442000331SGS00 (Image courtesy of the U.S. Geological Survey). Compared to the monsoon image shown previously (Figure 7.1), slight decline in SSC levels can be observed; in this post-monsoon map, the SSC levels varied between 250-350 ppm. Also, in contrast with the previous map, the sand bars are not facing erosion apparently. The average measured discharge of Padma River at Mawa for monsoon season of 2000 was $63519 \text{ m}^3/\text{s}$, and the average measured discharge for the corresponding post-monsoon season was 38028

m³/s. The average water flow velocity declined from 3.06 m/s in monsoon to 2.30 m/s in post-monsoon season. These declines in discharge and flow velocity could be driving factors behind the decline of sand bar erosion. There was also a decline of measured average water level at Mawa 93.5L of more than 1 m between monsoon and post-monsoon seasons, also possibly influencing erosion. The decline of SSC levels may be attributed to declines in discharge, water level and flow velocity (Bogárdi and Szilvássy, 1974).

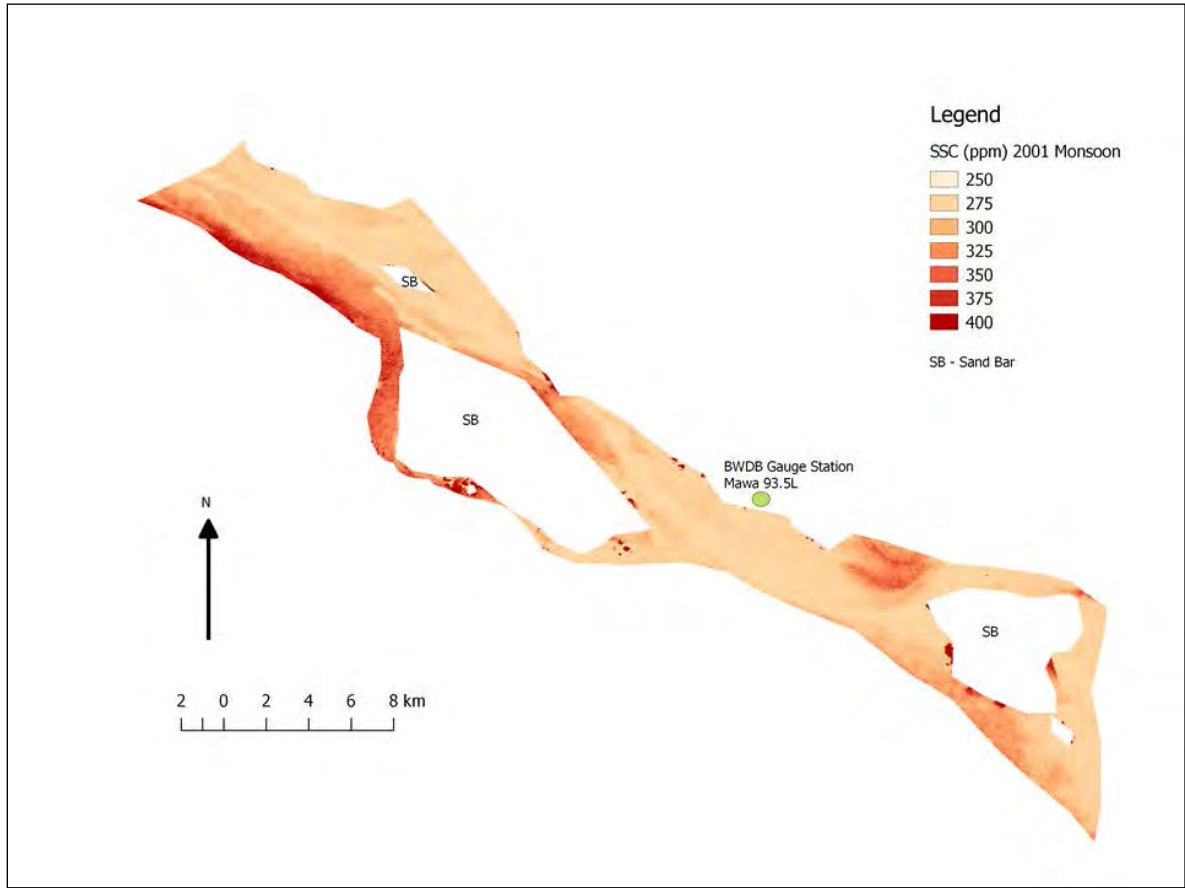


Fig. 7.3: Spatial distribution map of SSC in the Padma River for Monsoon of 2001

The Landsat scene identification number used for this spatial distribution map (Figure 7.3) was LE71370442001269SGS00 (Image courtesy of the U.S. Geological Survey). SSC values in this map varied between 250-400 ppm; quite similar to the SSC distribution of 2000 monsoon. Although some sporadic erosion of sand bars can be observed, they are not significantly visible like the monsoon map of previous year (Figure 7.1). This reduced erosion rate can again be attributed to reduced average monsoon discharge and flow velocity

– the average monsoon discharge and flow velocity for monsoon 2001 were 46784 m³/s and 2.41 m/s respectively. Suspended Sediment - Discharge relations are influenced by multiple factors - precipitation intensity and areal distribution, runoff amount and rate, floodwater travel rates and travel distances, spatial and temporal storage-mobilization-depletion processes of available sediment, and sediment travel rates and distances (Williams, 1989). The Ganges and Brahmaputra River flows combine to form the Padma River. Flow from the Ganges, adjacent to the left bank in the upstream (u/s) direction, seemed to be transporting greater concentration of suspended sediments compared to the flow from the Brahmaputra. The two flows can be delineated considering the stark difference between SSC levels of the Ganges and the Brahmaputra flows.

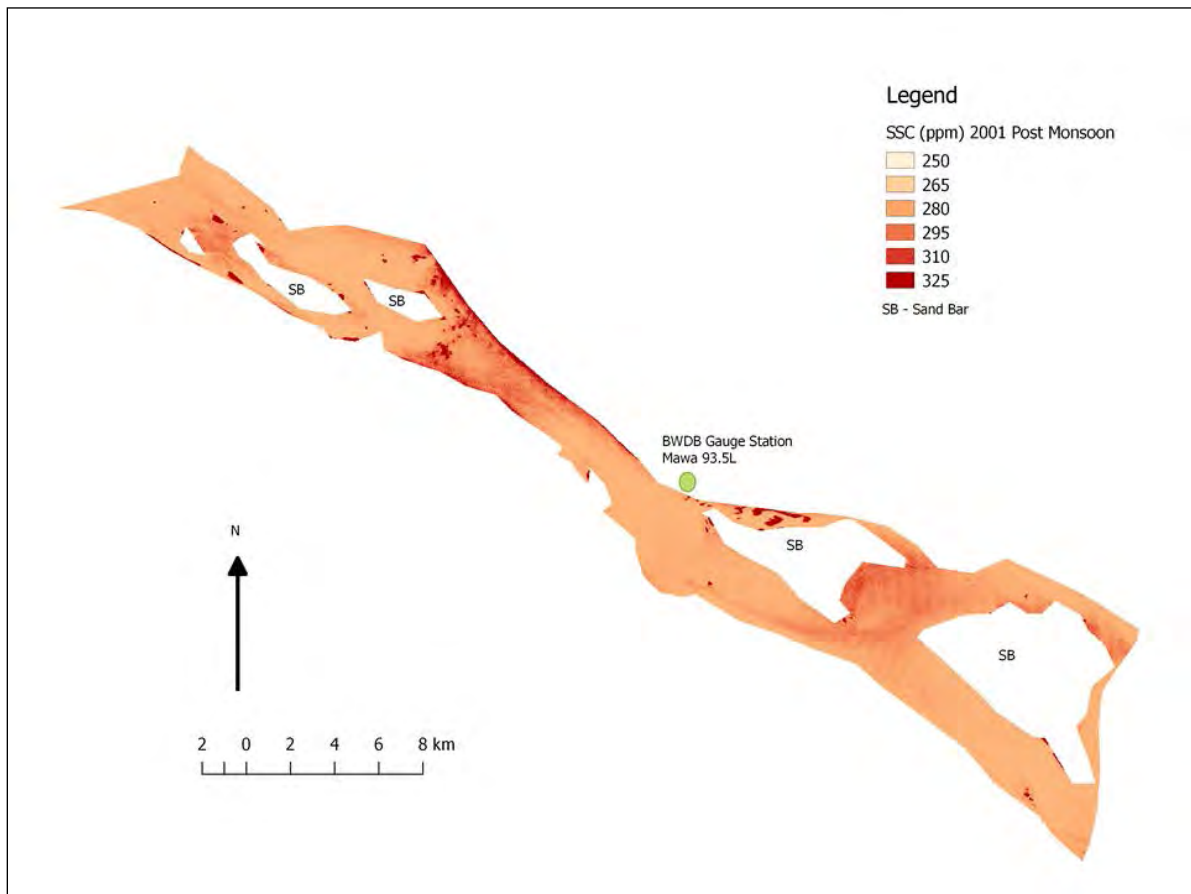


Fig. 7.4: Spatial Distribution Map of SSC in Padma River for Post Monsoon of 2001

The Landsat scene identification number used for this spatial distribution map (Figure 7.4) was LE71370442001333SGS00 (Image courtesy of the U.S. Geological Survey). SSC values

in this map varied between 250-325 ppm – slightly lower than the maximum SSC during the post-monsoon season of previous year (Figure 7.2). The average measured discharge and flow velocity for post-monsoon of 2001 were 42045 m³/s and 2.13 m/s respectively; slightly lower than the monsoon season (Figure 7.3). Although some bank erosion can be seen, significant sand bar erosion was not apparent; possibly due to the nearly unchanged average discharge and flow velocity (Bogárdi and Szilvássy, 1974). Also measured average water level did not change significantly between monsoon and post monsoon seasons of 2001.

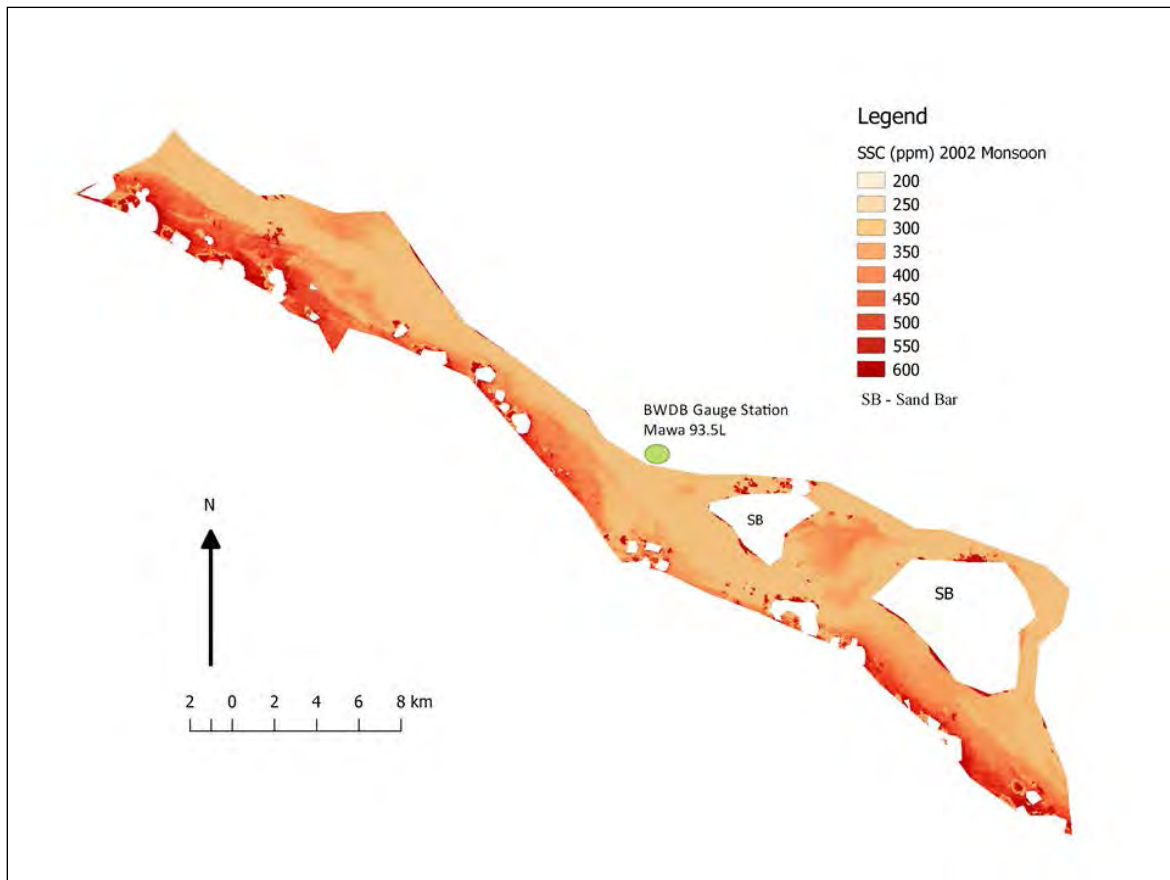


Fig. 7.5: Spatial distribution map of SSC in the Padma River for Monsoon of 2002

The Landsat scene identification number used for this spatial distribution map (Figure 7.5) was LE71370442002256SGS00 (Image courtesy of the U.S. Geological Survey). It must be noted that in this map, excluding the designated sand bars, the missing patches towards are bank are cloud covers. A significant rise of SSC level can be seen for 2002 monsoon. This rise may be due to increased discharge, water level or flow velocity considering the

prevalence of a monsoon flood in 2002. However, there is no definitive data available on the aforementioned parameters for this map. In this map again, the flow from the Ganges and the Brahmaputra can be delineated based on their sharp difference in SSC levels. The Ganges seemed to be contributing higher levels suspended sediment concentration into the Padma compared to the Brahmaputra.

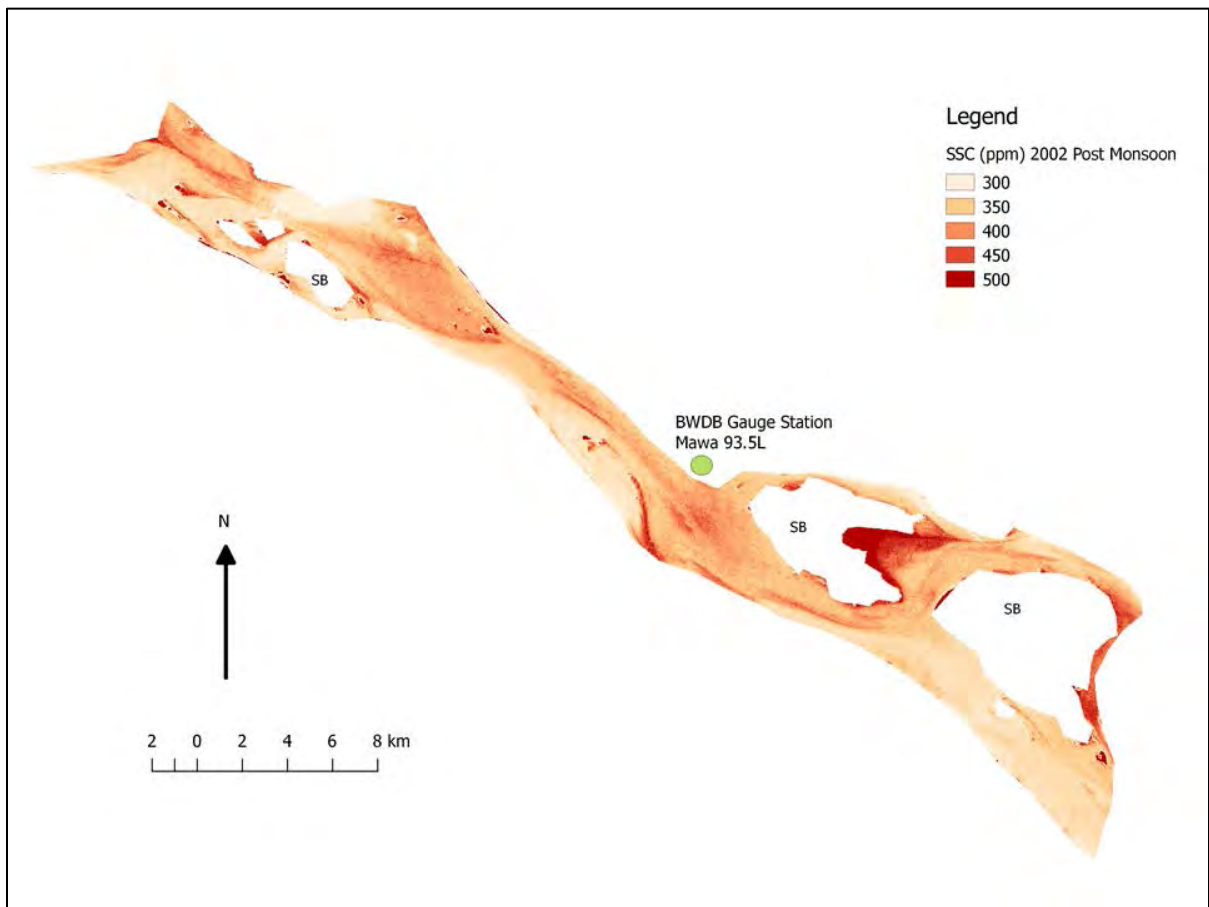


Fig. 7.6: Spatial distribution map of SSC in the Padma River for Post Monsoon of 2002

The Landsat scene identification number used for this spatial distribution map (Figure 7.6) was LE71370442002304SGS00 (Image courtesy of the U.S. Geological Survey). Although the SSC levels in this map are higher than the post monsoon seasons of previous years, a significant amount of sand bar erosion can be observed. Since there are no reliable in situ data available corresponding to this map, the erosive behavior cannot be exactly attributed to certain hydro-morphological aspects.

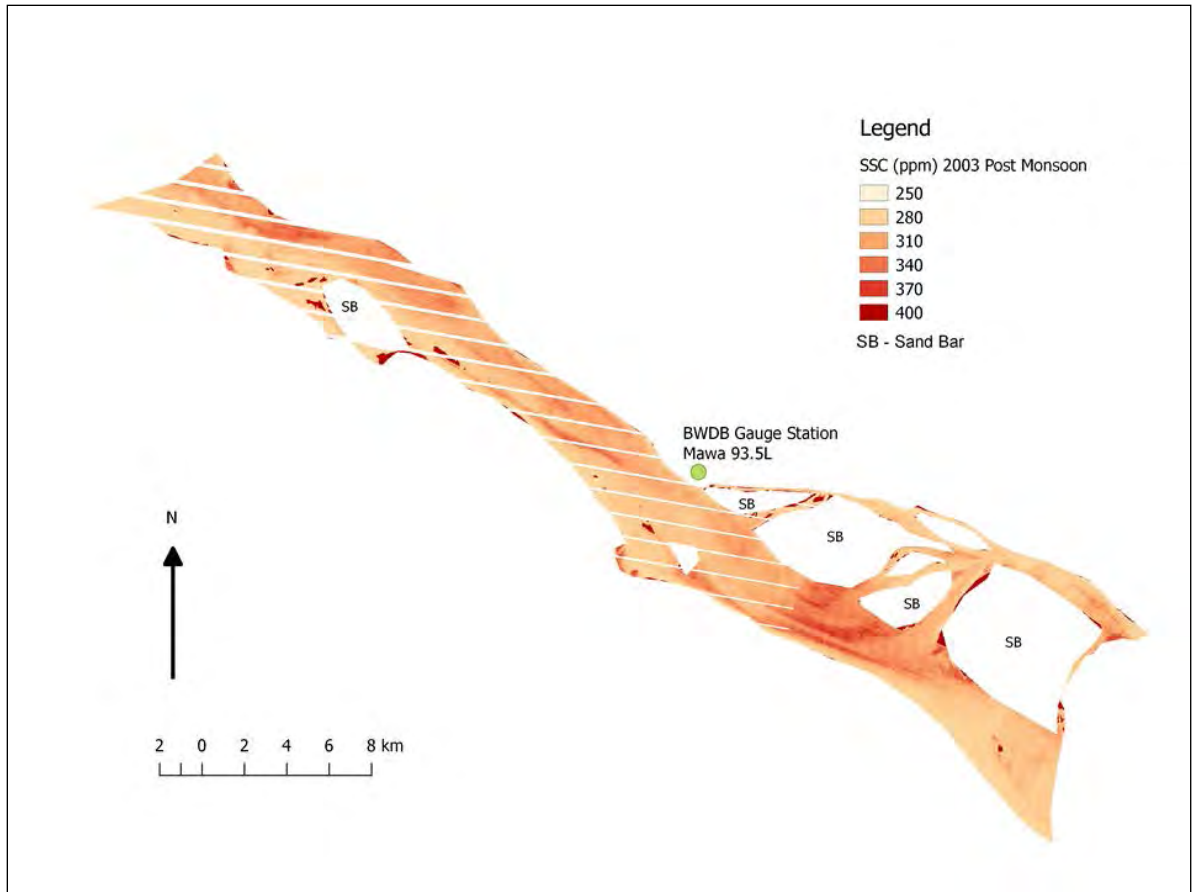


Fig. 7.7: Spatial distribution map of SSC in the Padma River for Post Monsoon of 2003

The Landsat scene identification number used for this spatial distribution map (Figure 7.7) was LE71370442003323ASN01 (Image courtesy of the U.S. Geological Survey). There was no suitable cloud-free monsoon image for appropriate depiction of SSC distribution, therefore only post-monsoon image was chosen. As mentioned earlier, SLC-off mode caused the line errors in the maps starting from 2003. Compared to the post monsoon SSC values of previous year, there was some decline noticeable for 2003. However, levels of SSC for post monsoon of 2003 seem to be higher compared to post monsoon of 2000 (Figure 7.2) and 2001 (Figure 7.4); again this may be because measured average water level, discharge and flow velocity were higher. Contrary to previous observations, flow contributed by the Brahmaputra had higher SSC compared to the flow contributed by the Ganges. There is appearance of aggradation of channel bars downstream of the image. Aggradation and degradation are generally influenced by river discharge, sediment load, morphological characteristics of river channel and human interventions; if the river water is unable to

transfer the bed load or the channel material then the same is deposited within the channel and channel height increases, aggradation occurs (Mugade and Sapkale, 2015).

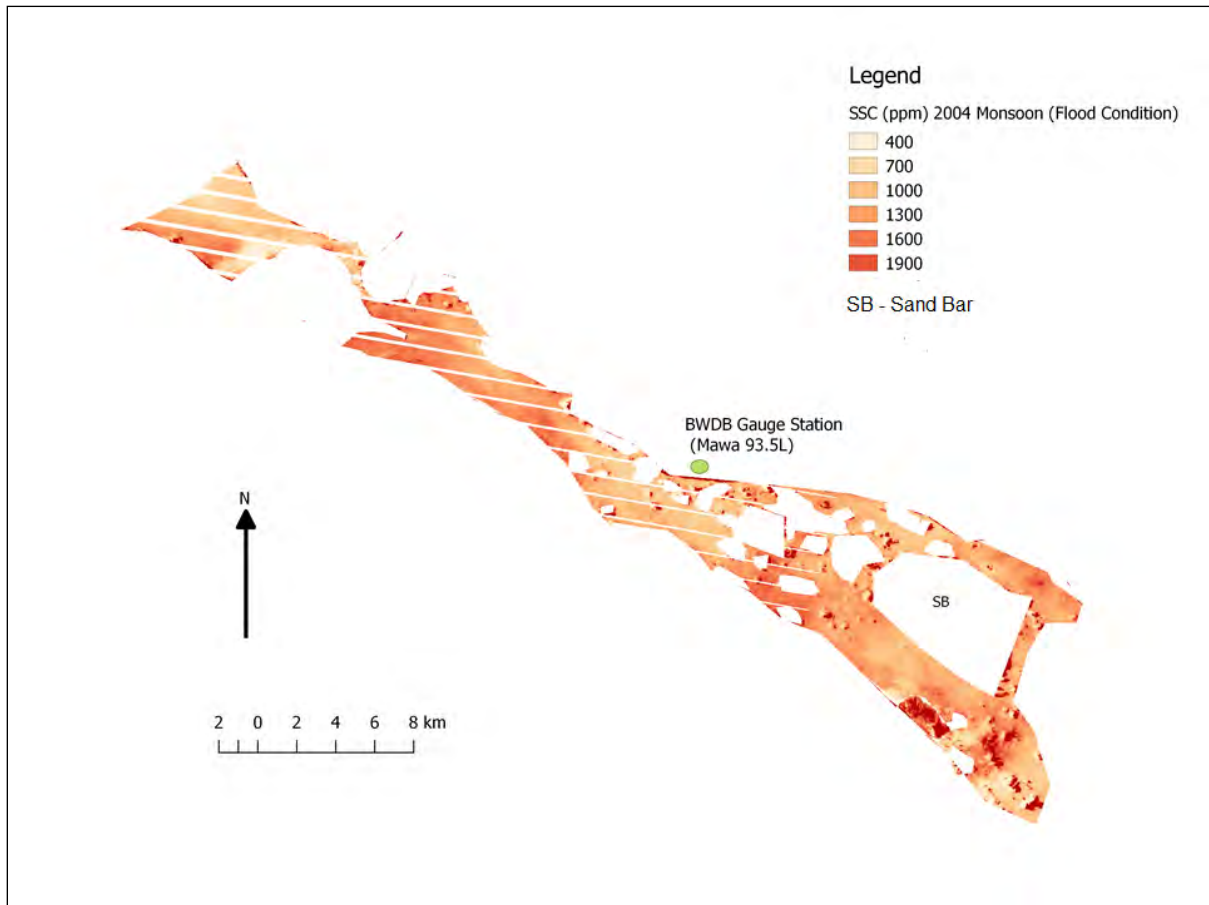


Fig. 7.8: Spatial distribution map of SSC in the Padma River for Monsoon of 2004

The Landsat scene identification number used for this spatial distribution map (Figure 7.8) was LE71370442004230PFS01 (Image courtesy of the U.S. Geological Survey). Although there were multiple patches of cloud over the body of the river, this image bared evidence of a sharp rise in SSC levels in the 2004 flood. This image in particular was acquired during flood condition. Minimum SSC in this map was about 400 ppm, but the highest SSC value was over 2000 ppm. The most intensive transport processes in rivers occur during the passage of a flood wave (Rowiński and Czernuszenko, 1998). Sediment transport is usually different in unsteady flow during flood events (Tabarestani and Zarrati, 2015). There was no in situ data acquired by BWDB during the flood season. The average monsoon water levels

of 5.20 m, discharge of 63414 m³/s and flow velocity of 2.64 m/s were not truly representative of the flood conditions.

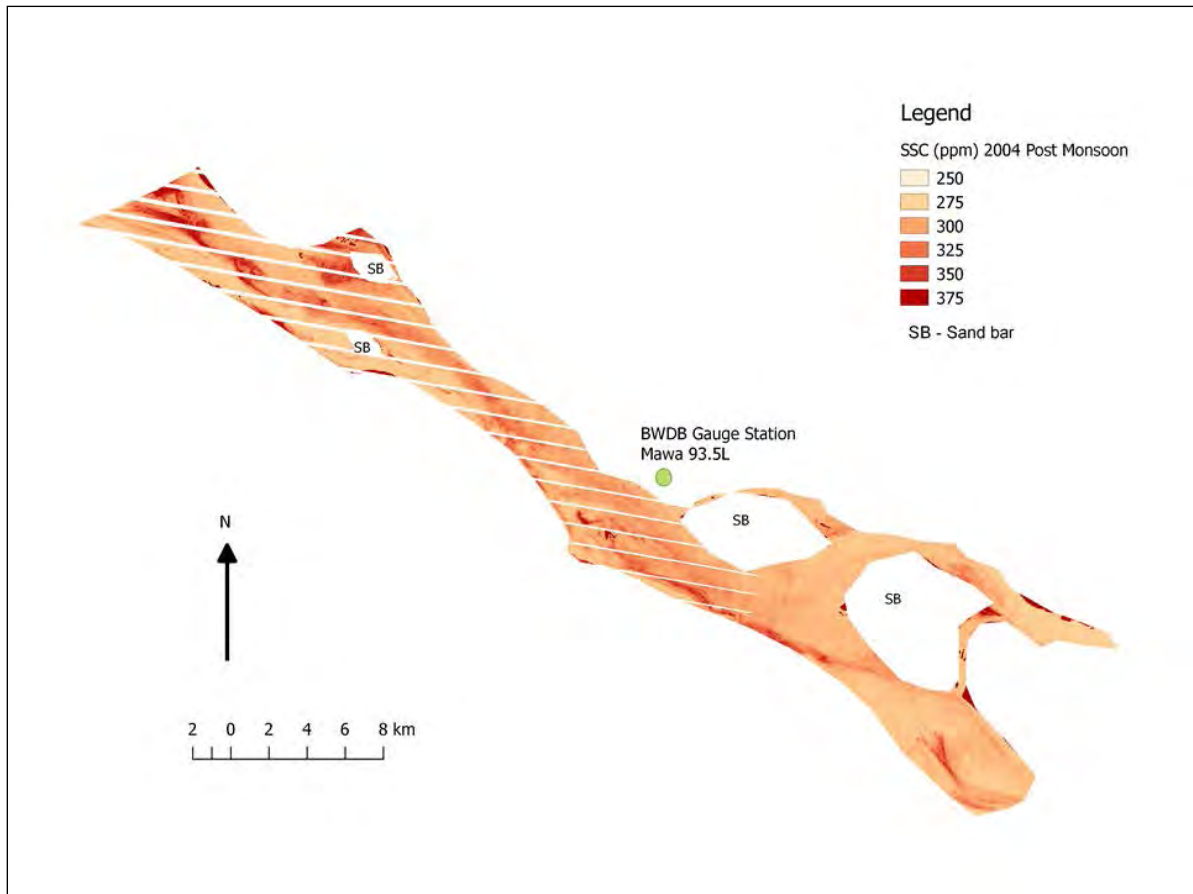


Fig. 7.9: Spatial distribution map of SSC in the Padma River for Post Monsoon of 2004

The Landsat scene identification number used for this spatial distribution map (Figure 7.9) was LE71370442004294PFS01 (Image courtesy of the U.S. Geological Survey). Compared to the SSC spatial distribution map during monsoon flood, the post monsoon map showed dramatic decrease in overall SSC. Sand bar erosion was not a prominent feature of this map and measured morphological parameters such as average water level, discharge and flow velocity, although attenuated a little, did not change notably compared to the post monsoon map of previous year (Figure 7.7).

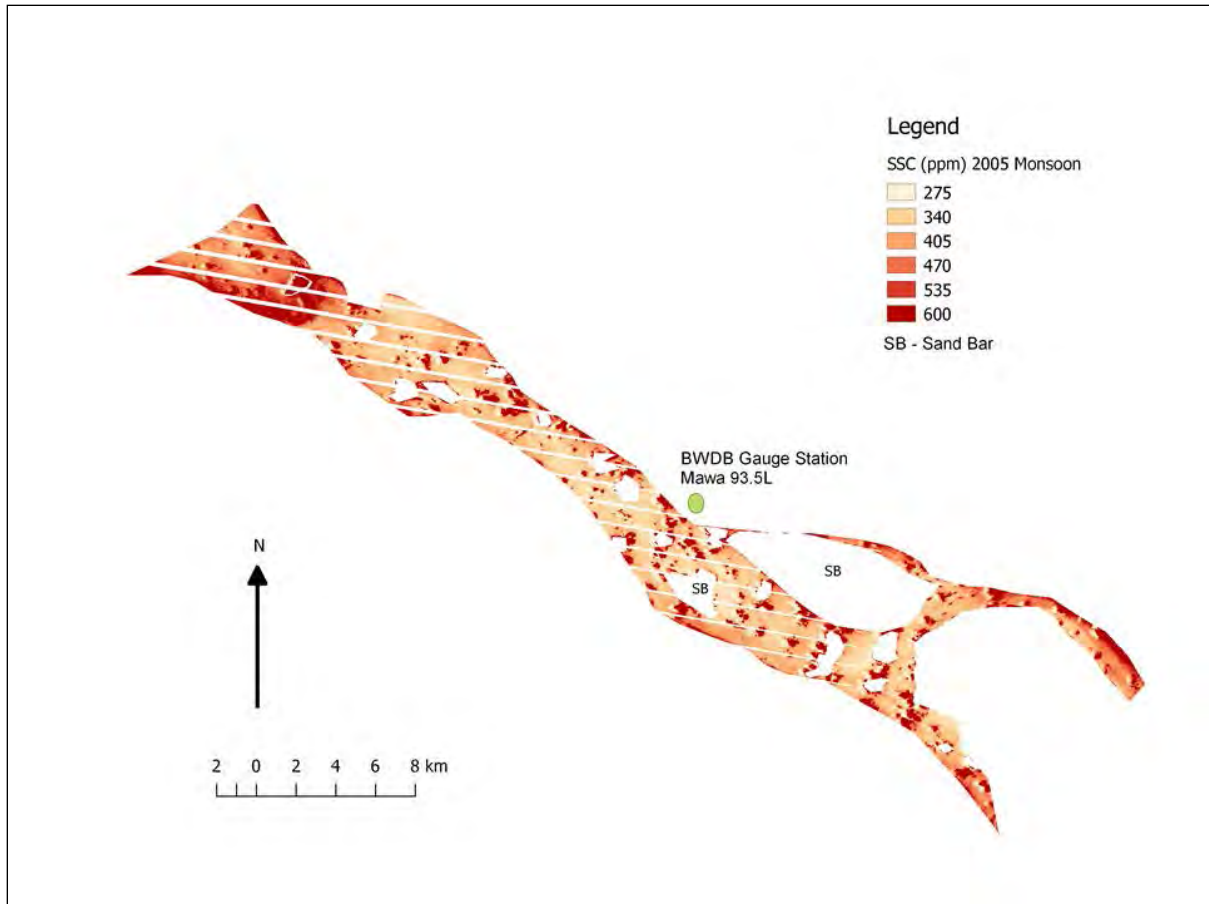


Fig. 7.10: Spatial distribution map of SSC in the Padma River for Monsoon of 2005

The Landsat scene identification number used for this spatial distribution map (Figure 7.10) was LE71370442005152PFS00 (Image courtesy of the U.S. Geological Survey). The maximum SSC level for this map was about 600 ppm. Owing to the presence of patches of clouds, this map does not depict the true variation of SSC on that day. Shadows cast by cloud patches also resulted in irregular variations of SSC in the map, which can be considered as errors or limitations while representing SSC variation through spatial maps.

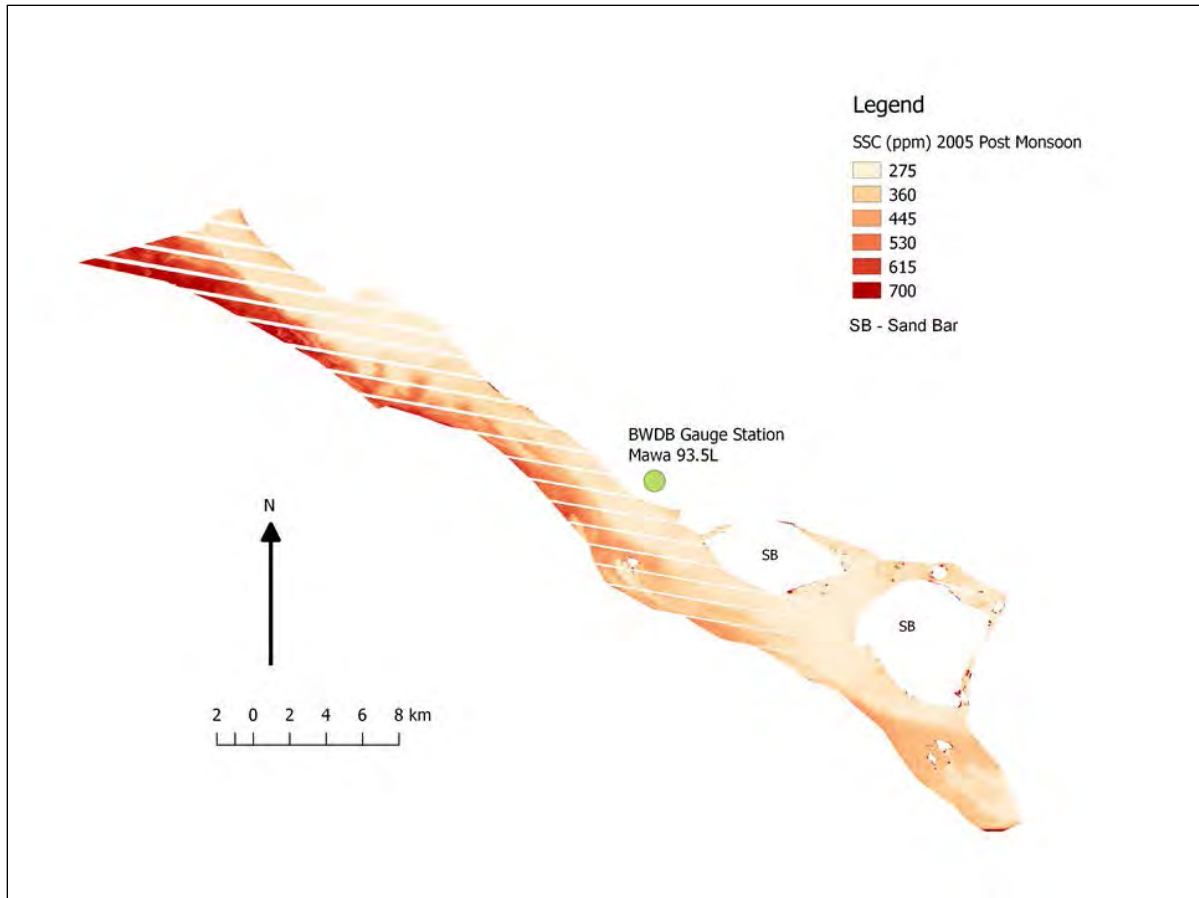


Fig. 7.11: Spatial distribution map of SSC in the Padma River for Post Monsoon of 2005

The Landsat scene identification number used for this spatial distribution map (Figure 7.11) was LE71370442005294PFS00 (Image courtesy of the U.S. Geological Survey). The most prominent feature of this map is the unusually different SSC levels between flow contributed by the Ganges and the Brahmaputra. The Ganges flow, which merges from the eastern upstream direction, is clearly higher in suspended sediments, and it is not till further downstream, the sediments diffuse. In a large alluvial river, like the Padma, the constraints imposed by the capacity of flow to transport sediments reflect upon suspended-sediment transport, sediment flux and the longitudinal profile of the channel (Dade and Friend, 1998).

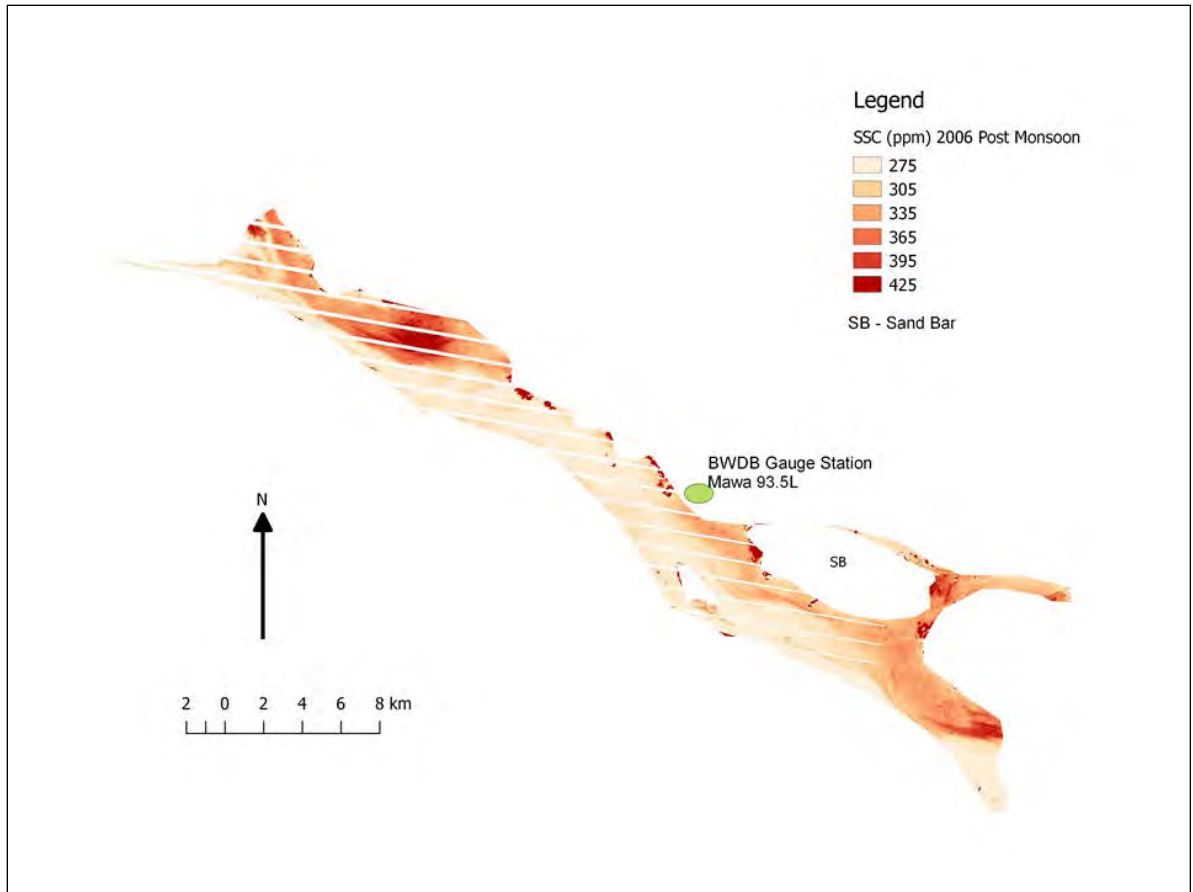


Fig. 7.12: Spatial distribution map of SSC in the Padma River for Post Monsoon of 2006

The Landsat scene identification number used for this spatial distribution map (Figure 7.12) was LE71370442006283PFS00 (Image courtesy of the U.S. Geological Survey). Compared to the post monsoon of 2005 (Figure 7.11), the maximum SSC value for this image decreased notably. Contrary to 2005, in this image, the Brahmaputra appears to be contributing higher suspended sediment concentration compared to flow from the Ganges. An interesting observation is a vortex-like secondary flow pattern at the upstream portion of the image. Such pattern of flow is a common phenomenon in alluvial rivers and associated with the complex process of scouring (Lagasse et al., 2012).

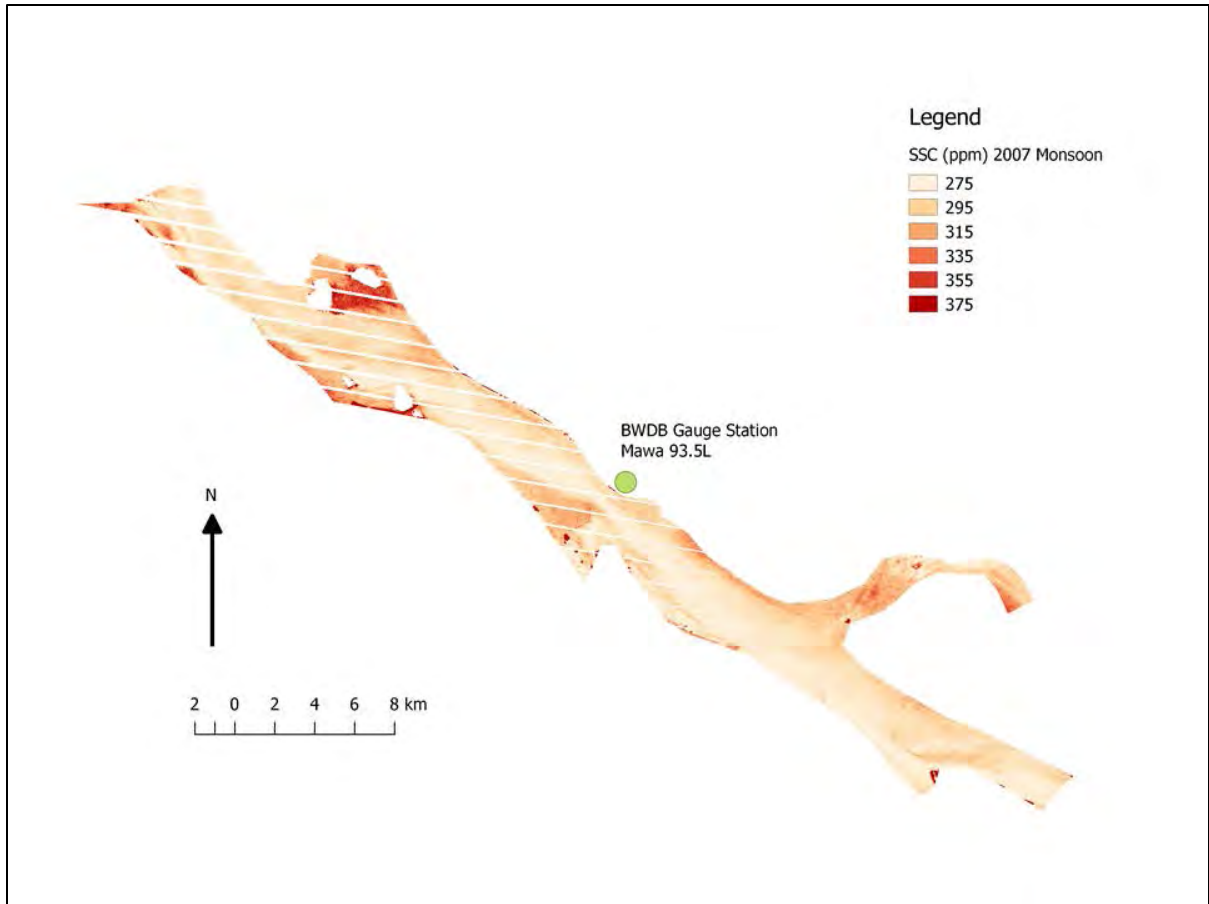


Fig. 7.13: Spatial distribution map of SSC in the Padma River for Monsoon of 2007

The Landsat scene identification number used for this spatial distribution map (Figure 7.13) was LE71370442007270PFS00 (Image courtesy of the U.S. Geological Survey). In this map, SSC values ranged between 275 to 375 ppm. There are no in situ data of corresponding water level, discharge or flow velocity data available for this image. However, compared to previous monsoons, SSC values were considerably lower for this particular image.

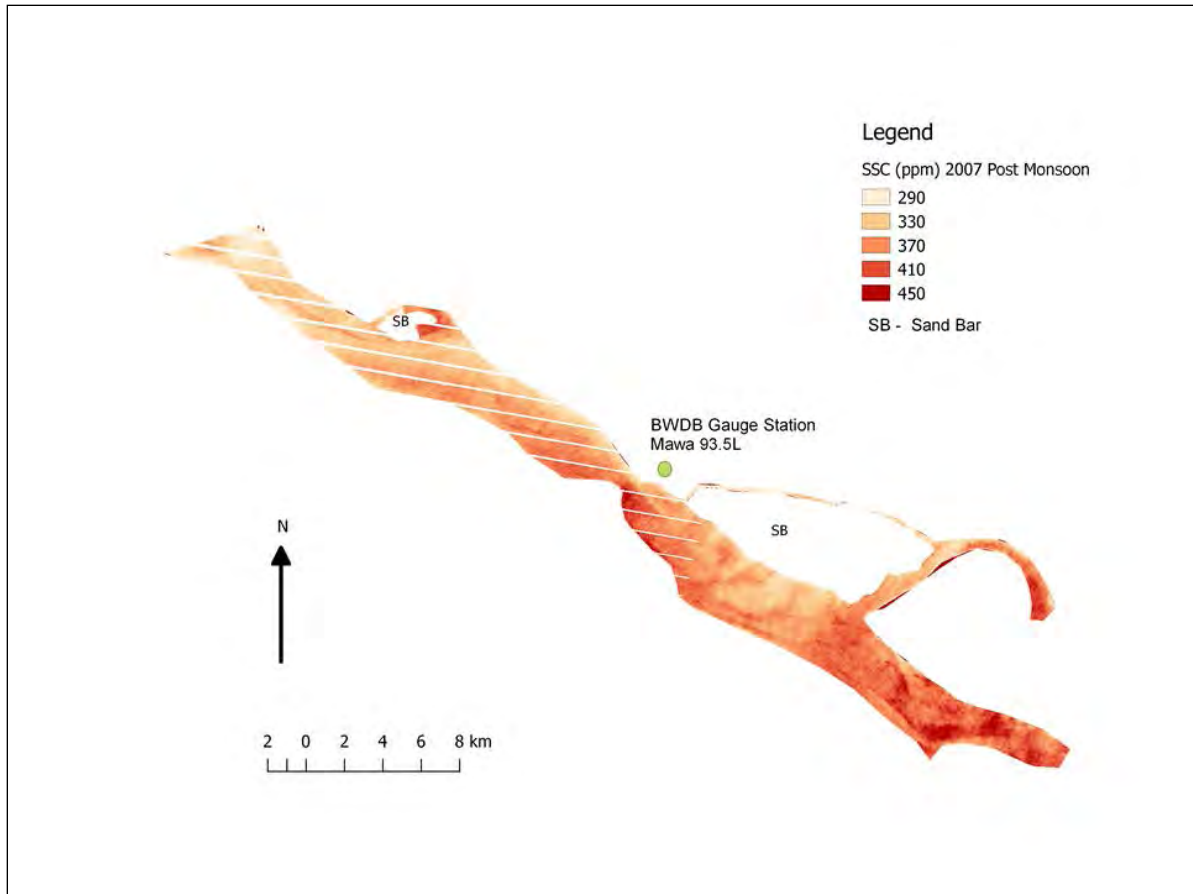


Fig. 7.14: Spatial distribution map of SSC in the Padma River for Post Monsoon of 2007

The Landsat scene identification number used for this spatial distribution map (Figure 7.14) was LE71370442007334PFS00 (Image courtesy of the U.S. Geological Survey). Conflicting previous observations, this post monsoon image has higher SSC range compared to the monsoon season. Even though there are no corresponding in situ discharge, water level and flow velocity data available for this image, the rise in post monsoon sediment transport may be possibly due to increased flow in delayed monsoon (Mirza, 2002).

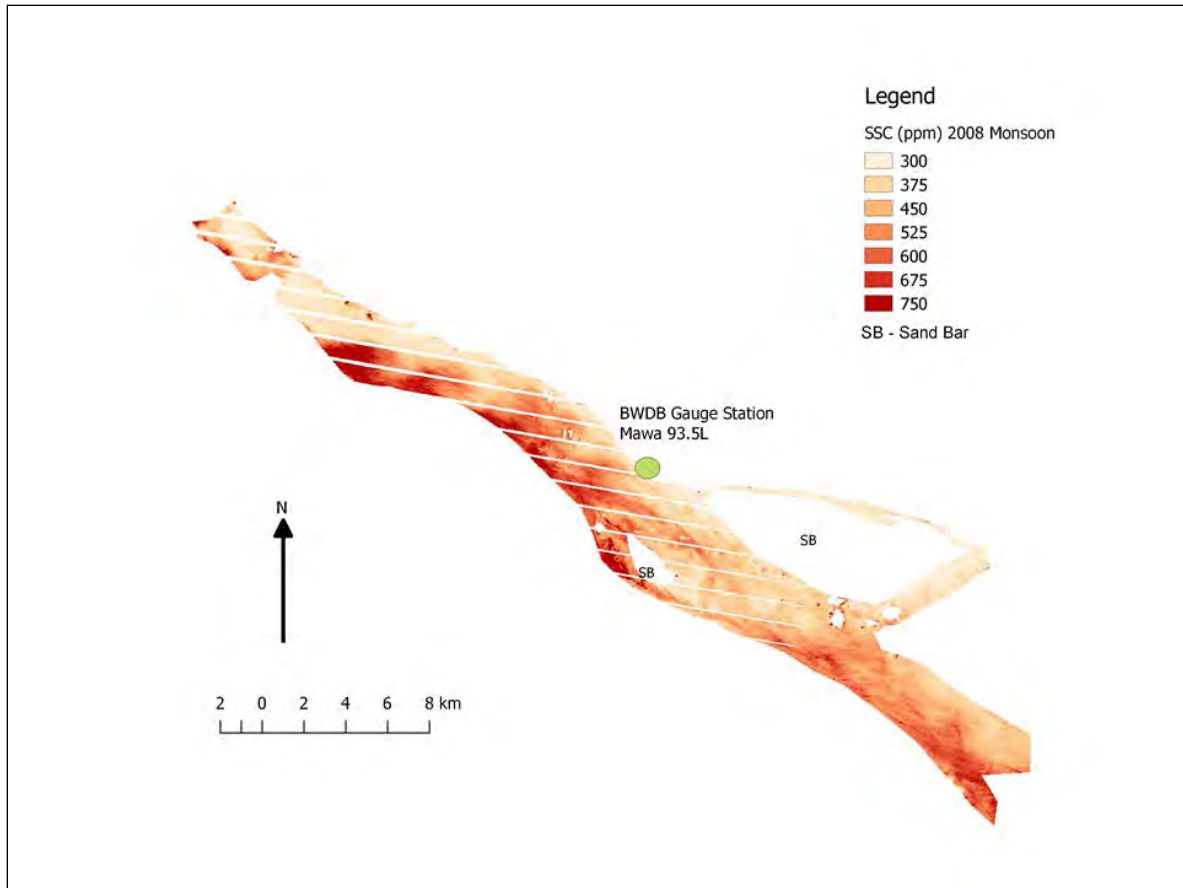


Fig. 7.15: Spatial distribution map of SSC in the Padma River for Monsoon of 2008

The Landsat scene identification number used for this spatial distribution map (Figure 7.15) was LE71370442008209SGS01 (Image courtesy of the U.S. Geological Survey). SSC range varied between 300 to 750 ppm for this image. This increase is expected due to increase in average discharge, flow velocity and water level compared to the previous monsoon (Bogárdi and Szilvássy, 1974).

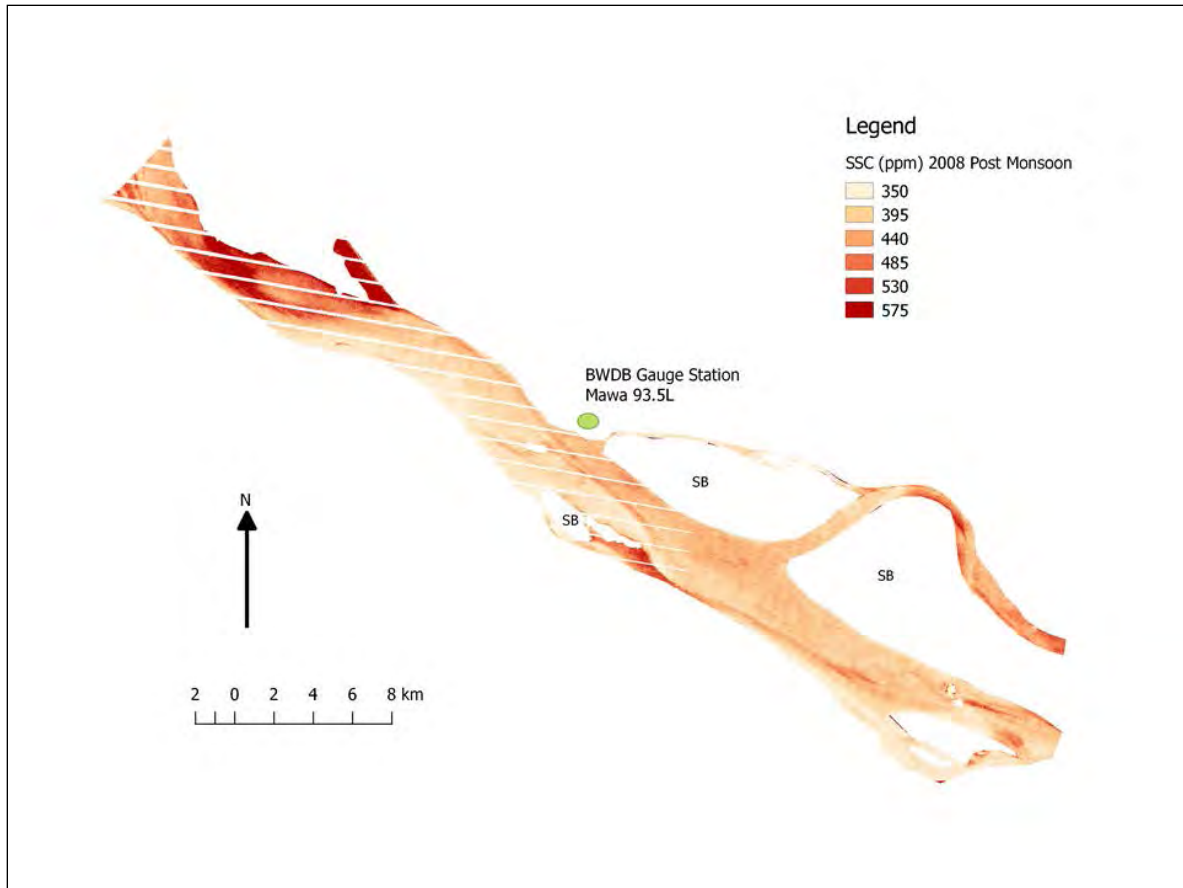


Fig. 7.16: Spatial distribution map of SSC in the Padma River for Post Monsoon of 2008

The Landsat scene identification number used for this spatial distribution map (Figure 7.16) was LE71370442008305SGS01 (Image courtesy of the U.S. Geological Survey). Owing to decreases in water level, discharge and flow velocity, the maximum SSC also declined compared to corresponding monsoon season (Bogárdi and Szilvássy, 1974). Some differences in upstream and downstream SSC levels can be seen. These observations may possibly be due to variations in sediment settling rate and boundary layer shear stress (Van Rijn, 1993).

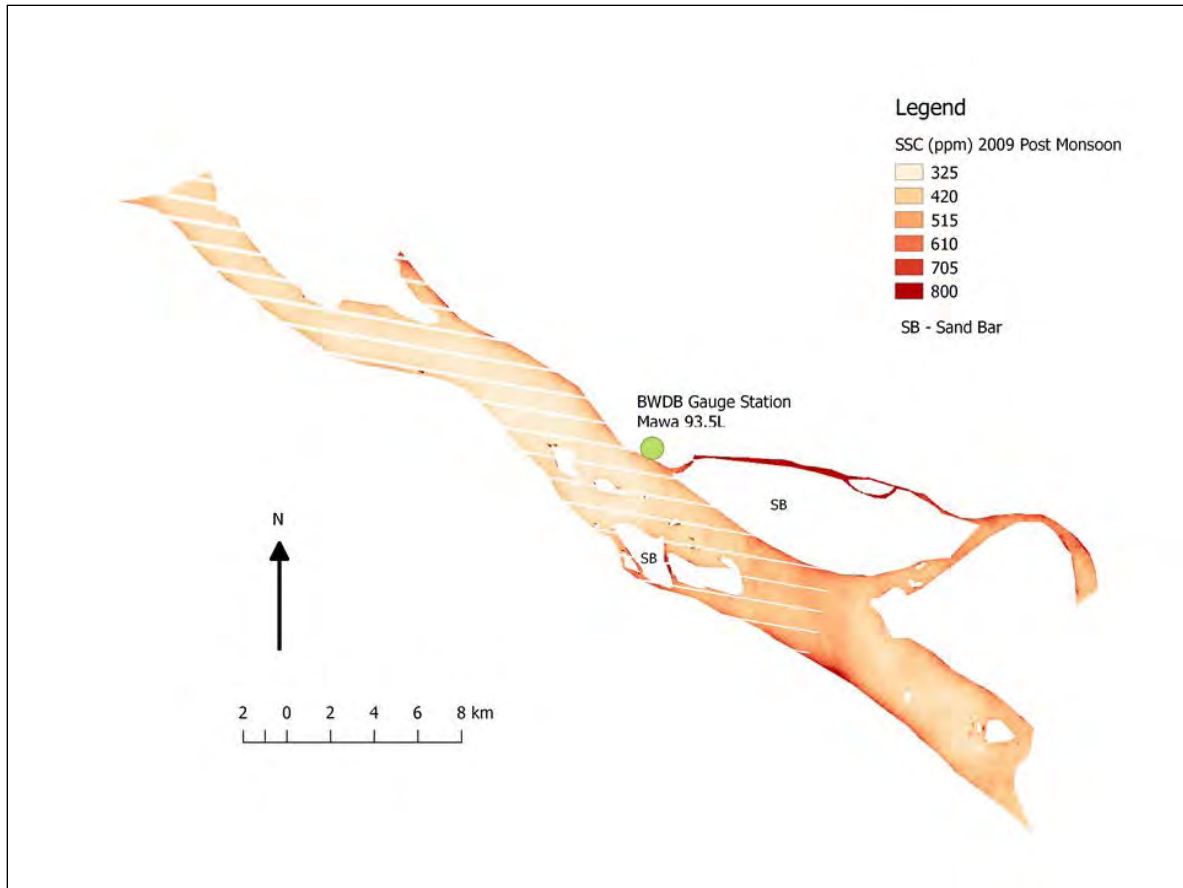


Fig. 7.17: Spatial distribution map of SSC in the Padma River for Post Monsoon of 2009

The Landsat scene identification number used for this spatial distribution map (Figure 7.17) was LE71370442009339SGS00 (Image courtesy of the U.S. Geological Survey). The post monsoon of 2009 saw an increase in average measured water level, discharge and flow velocity compared to the monsoon season. Therefore, the suspended sediment concentration rate was unexpectedly high as well, in agreement with known theories (Bogárdi and Szilvássy, 1974). The anomalous monsoon delay has become a noticeable observation in the advent of unnatural weather patterns in the face of climate change, and it is found to be responsible for unexpected rise of river flow and sediment transport in rivers (Bookhagen et al., 2005).

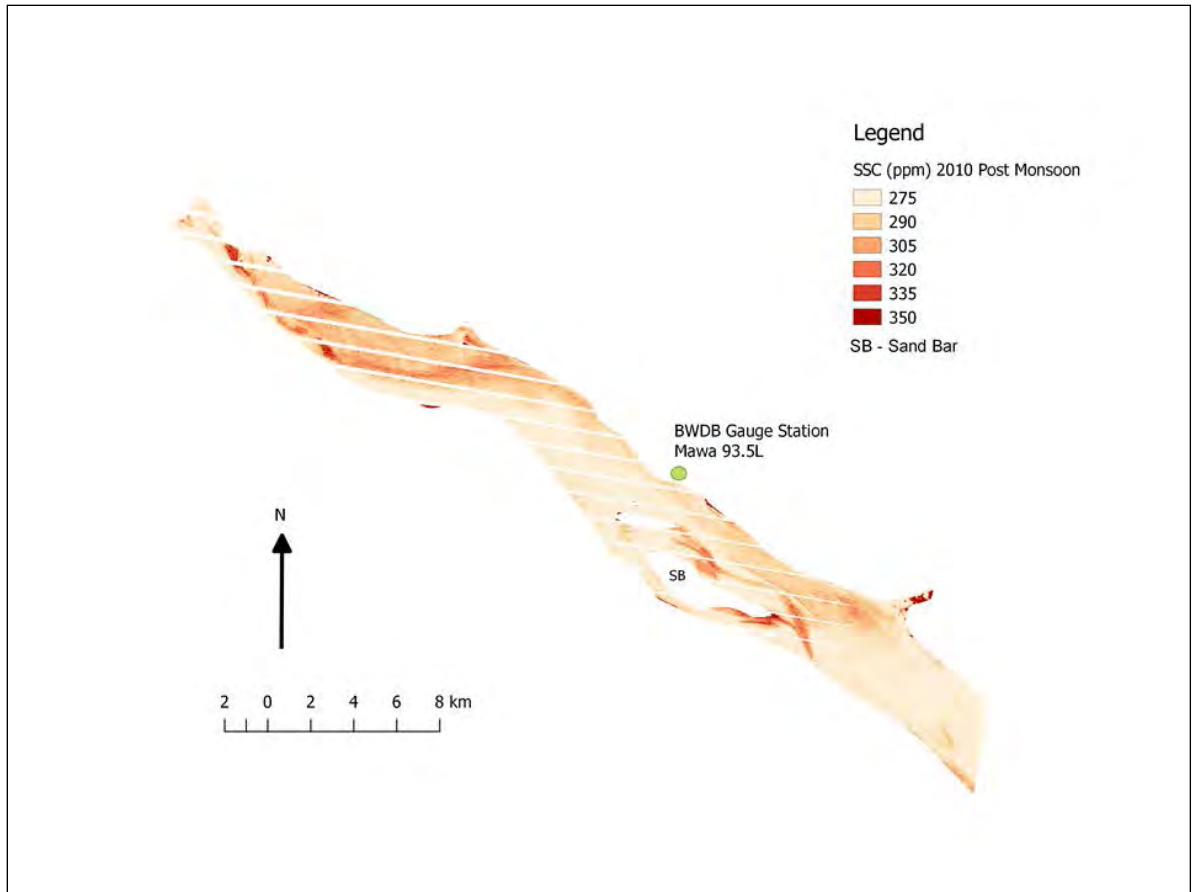


Fig. 7.18: Spatial distribution map of SSC in the Padma River for Post Monsoon of 2010

The Landsat scene identification number used for this spatial distribution map (Figure 7.18) was LE71370442010294SGS00 (Image courtesy of the U.S. Geological Survey). Compared to the monsoon of 2010 (Figure 7.17), the post monsoon levels of SSC declined with attenuating average discharge, water level and flow velocity. Suspended sediment transport patterns show erosion or degradation of sand bars in this image. These processes are complex (Middleton and Southard, 1984) and require more extensive analyses.

7.3 Temporal Variation of SSC at Mawa

To observe how average monsoon and post monsoon SSC values varied at the Mawa, SW 93.5L station at the Padma River, the temporal variation of SSC between the years 2000 and 2010 was plotted (Figure 7.19).

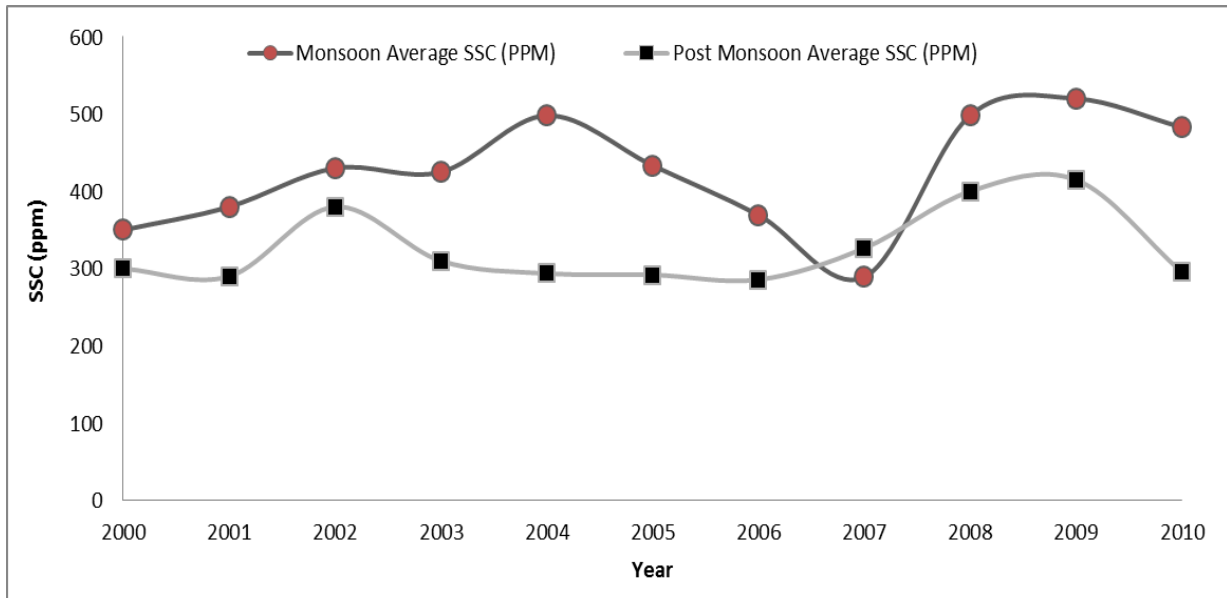


Fig. 7.19: Temporal variation of SSC

7.3 Relationship between SSC and Cross-section of River

To observe any existing relationship between spatial variations of SSC and measured cross section of the Padma River at Mawa, SSC values corresponding to cross sectional distance were recorded. The results have been shown in figures 7.20-7.23.

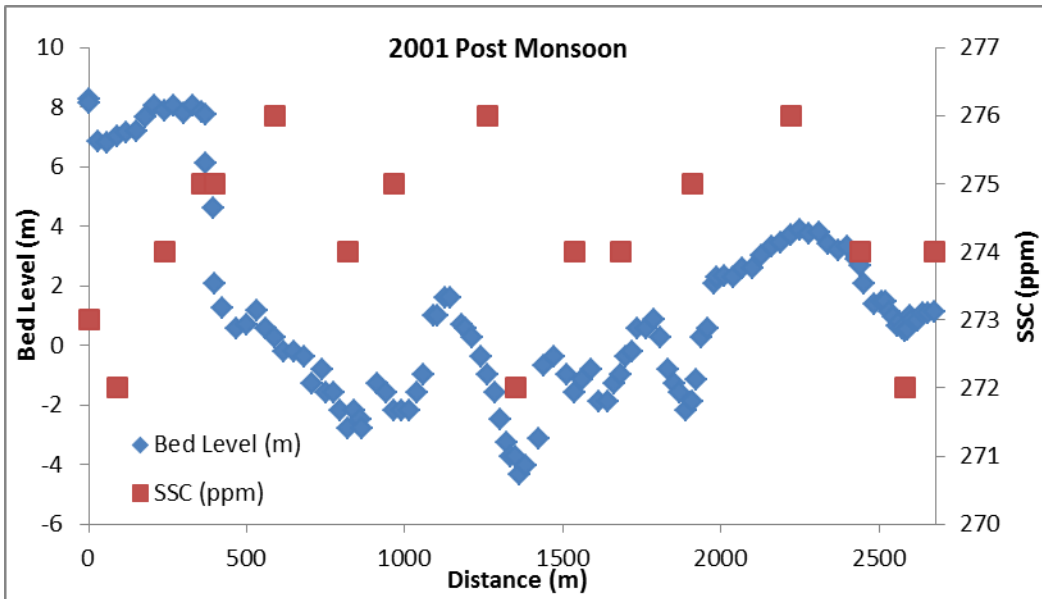


Fig. 7.20: Variation of cross section and corresponding SSC for Post Monsoon of 2001

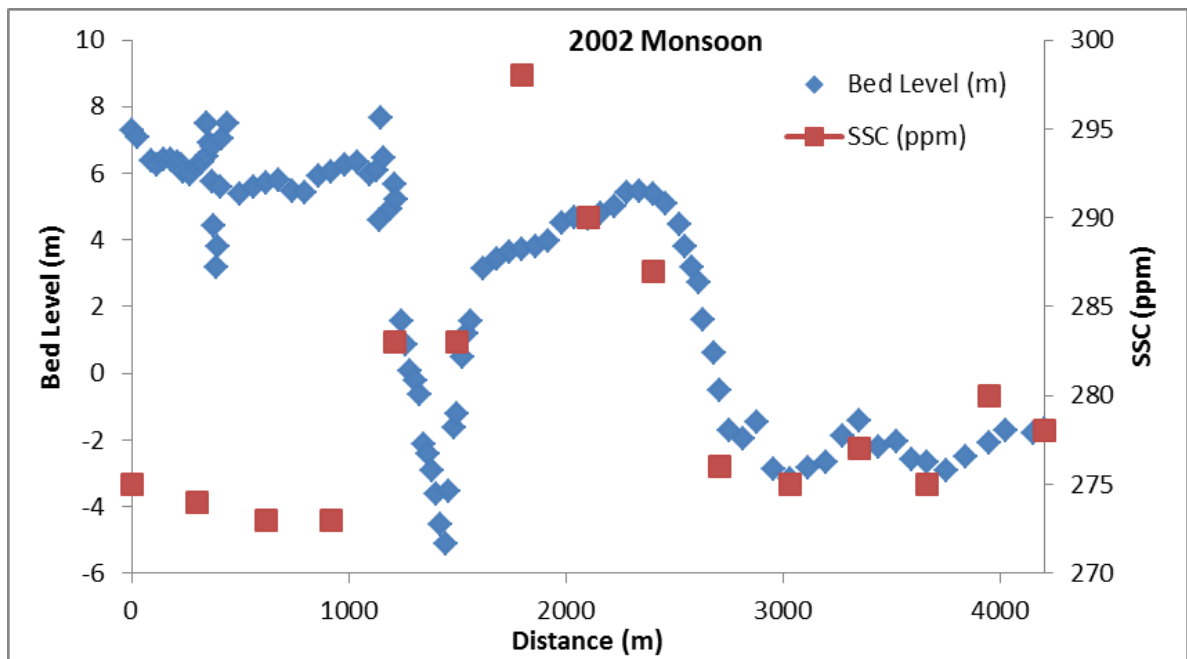


Fig. 7.21: Variation of cross section and corresponding SSC for Monsoon of 2002

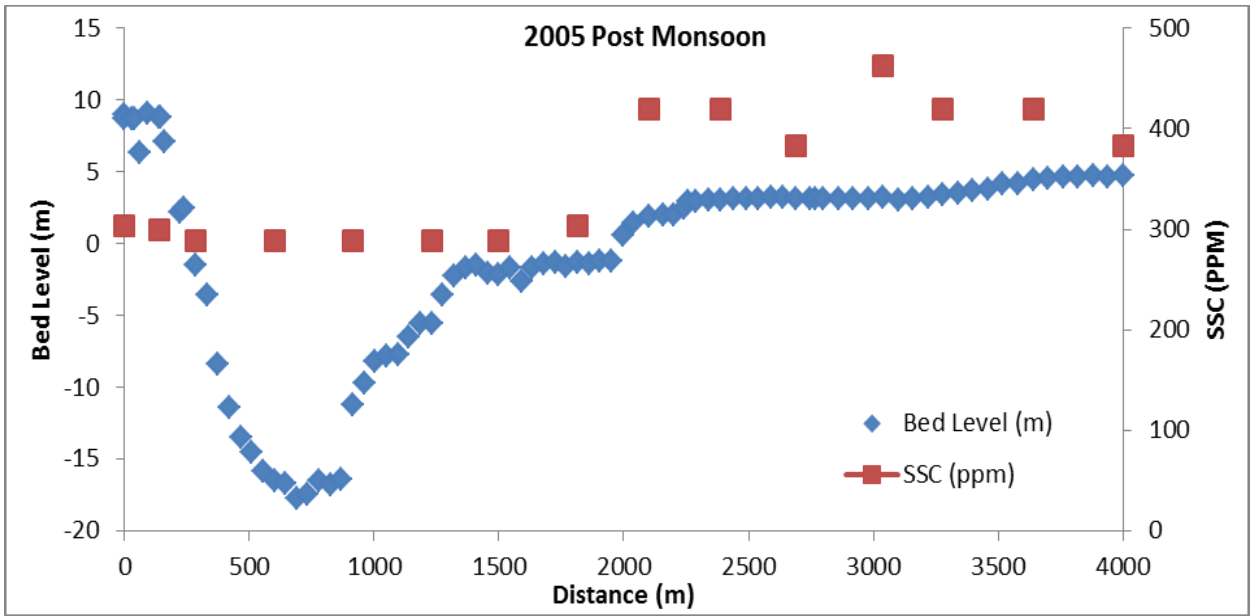


Fig. 7.22: Variation of cross section and corresponding SSC for Post Monsoon of 2005

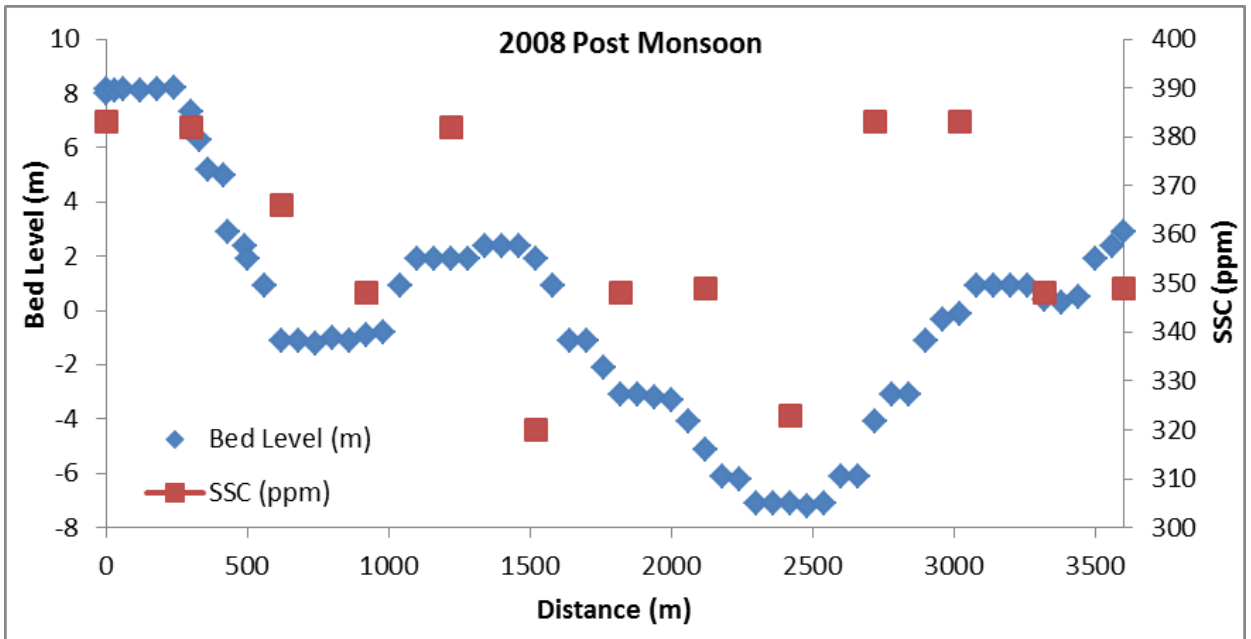


Fig. 7.23: Variation of cross section and corresponding SSC for Post Monsoon of 2008

The cross-sectional data acquired for 2001 Post Monsoon (Figure 7.20) is from BWDB's River Maintenance Project (RMP)-6. For 2002 Monsoon (Figure 7.21), the cross-sectional data was recorded during RMP-4, and for Post Monsoon of 2005 (Figure 7.22) and 2008 (Figure 7.23), cross sectional data was recorded during RMP-7. It can be observed from all the four plots that SSC rises, albeit through variable range, whenever the Reduced Level (RL) value rises. SSC tends to increase with depth, and when bed level rises, the corresponding SSC also tends to increase (Okada, 2016). Although near-infrared wavelengths of band 4 of Landsat 7 ETM+ is less susceptible to be influenced by shallow water environments (Tolk et al., 2000), there may still be some degree of influence during changes in water depth. This phenomenon maybe a limitation when remotely sensed SSC is used to assess changes in water depth (Gao, 2009).

7.4 Measured Average Discharge, Water Level and Flow Velocity at Mawa 93.5L

The measured average monsoon and post monsoon data of discharge, water level (WL) and flow velocity at Mawa 93.5L gauging station, used for interpretation of spatial distribution maps of SSC have been represented in figures 7.24-7.26. Historical data sets provided by BWDB have been included in the appendix section (Appendix-B).

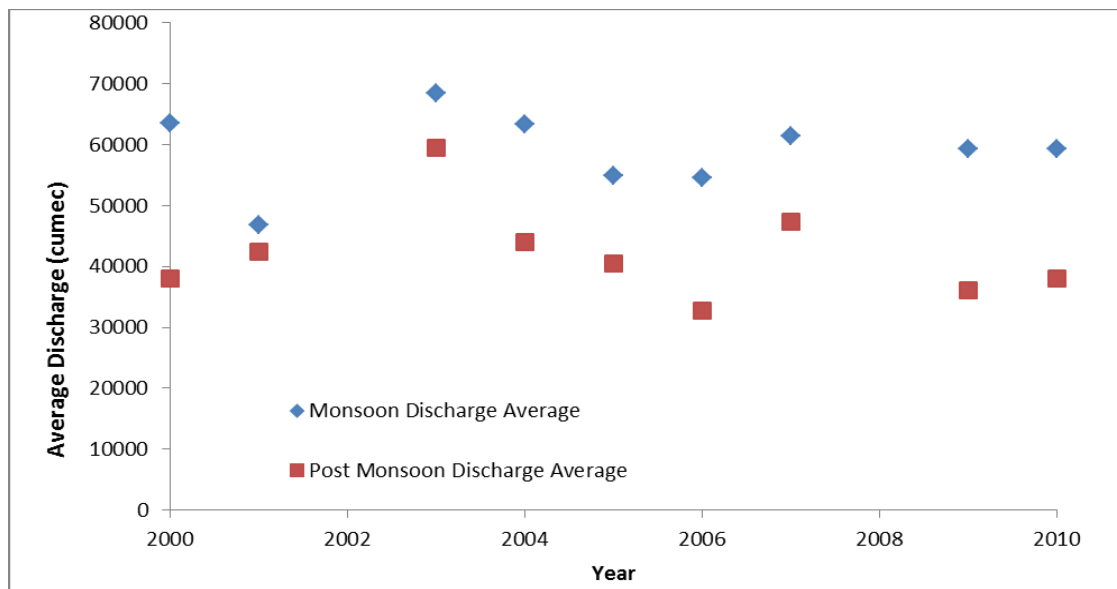


Fig. 7.24: Measured average yearly discharge at Mawa 93.5L

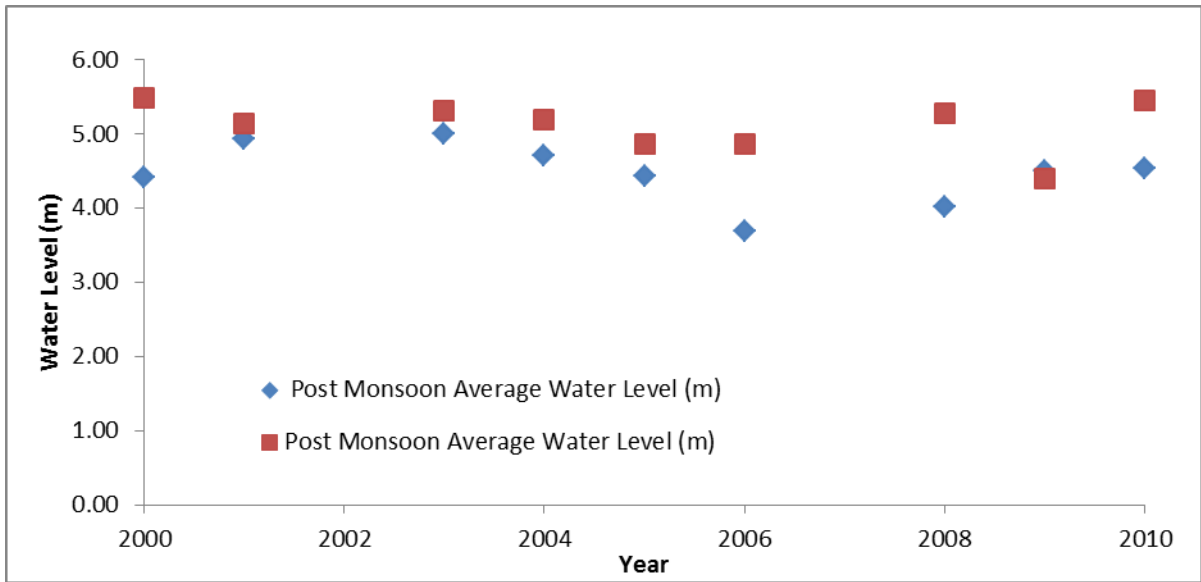


Fig. 7.25: Measured average yearly water level at Mawa 93.5L

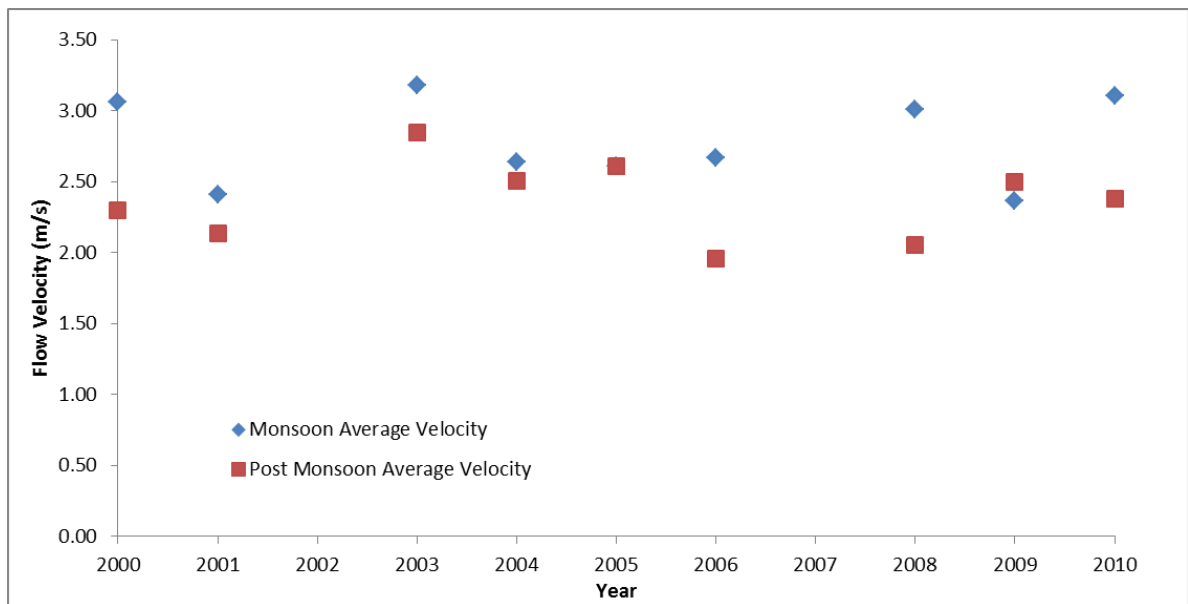


Fig. 7.26: Measured average yearly flow velocity at Mawa 93.5L

7.5 Relationship between Measured SSC and Flow Velocity

To investigate whether measured values of flow velocity have any statistical relationship with in situ values of SSC, a correlation analysis (Figure 7.29) was carried out. The result has been depicted below.

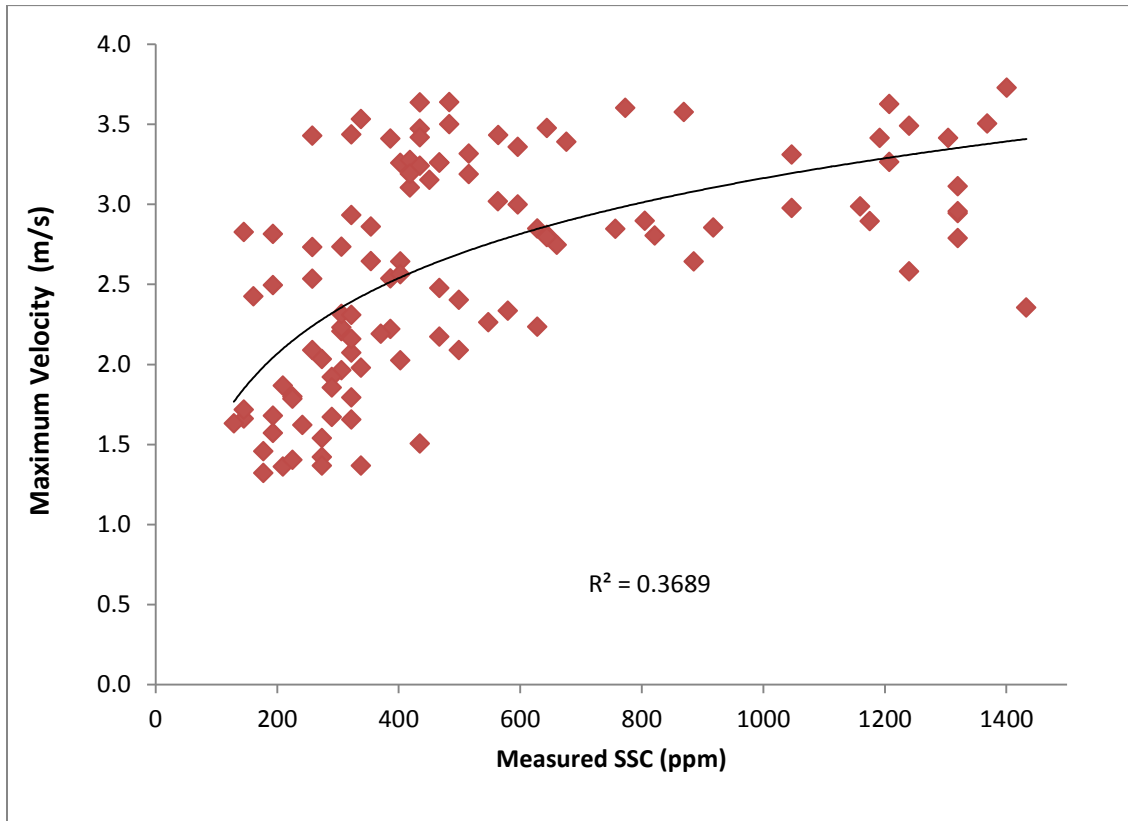


Fig. 7.27: Scatter plot of maximum flow velocity and measured SSC

A logarithmic trendline generated moderate coefficient of determination of 0.3689. The following logarithmic model [6] was derived.

$$\text{Flow Velocity} = 0.6814\ln(\text{SSC}) - 1.5434 \quad [6]$$

Using the logarithmic model [6], measured values of SSC were used to estimate corresponding flow velocity. The estimated values were then compared with actual values to assess this model's accuracy. The average relative error between estimated and observed values was found to be $\pm 14.93\%$. Results have been represented in table 7.1.

Table 7.1: Relative error assessment of estimated flow velocity using [6]

| Measured SSC (ppm) | Measured Velocity (m/s) | Estimated Velocity (m/s) | Residuals | Relative Error % |
|--------------------|-------------------------|--------------------------|-----------|------------------|
| 225.4 | 1.8 | 2.1 | -0.4 | -20.8 |
| 257.6 | 1.9 | 2.2 | -0.4 | -18.5 |
| 450.8 | 3.0 | 2.6 | 0.4 | 12.8 |
| 563.5 | 2.9 | 2.8 | 0.1 | 4.0 |
| 579.6 | 3.0 | 2.8 | 0.2 | 7.5 |
| 627.9 | 3.2 | 2.8 | 0.4 | 11.4 |
| 595.7 | 3.5 | 2.8 | 0.6 | 18.7 |
| 644.0 | 3.5 | 2.9 | 0.6 | 17.7 |
| 885.5 | 2.7 | 3.1 | -0.4 | -15.9 |
| 805.0 | 2.6 | 3.0 | -0.4 | -15.2 |
| 837.2 | 3.0 | 3.0 | 0.0 | -0.9 |
| 788.9 | 2.7 | 3.0 | -0.3 | -9.4 |
| 724.5 | 2.7 | 2.9 | -0.3 | -10.5 |
| 644.0 | 2.2 | 2.9 | -0.7 | -32.7 |
| 483.0 | 1.8 | 2.7 | -0.9 | -51.8 |
| 273.7 | 1.6 | 2.3 | -0.7 | -41.7 |
| 241.5 | 1.6 | 2.2 | -0.5 | -33.2 |
| 354.2 | 2.1 | 2.5 | -0.4 | -17.4 |
| 483.0 | 2.7 | 2.7 | 0.1 | 1.9 |
| 563.5 | 3.2 | 2.8 | 0.4 | 13.1 |
| 547.4 | 2.8 | 2.8 | 0.0 | 1.5 |
| 466.9 | 2.7 | 2.6 | 0.0 | 1.1 |
| 547.4 | 2.6 | 2.8 | -0.1 | -4.2 |
| 579.6 | 2.5 | 2.8 | -0.3 | -11.8 |

As the average relative error was less than 15%, the model [6] was used to generate spatial distribution maps from corresponding spatial variation maps of SSC. The two maps chosen were 2000 Monsoon and 2002 Post Monsoon. After appropriate conversions using raster calculation in GIS software, the two maps (Figure 7.28 and 7.29) were rendered. This practice may be considered an example on the application of Landsat images to observe spatial variation of flow velocity in large alluvial rivers.

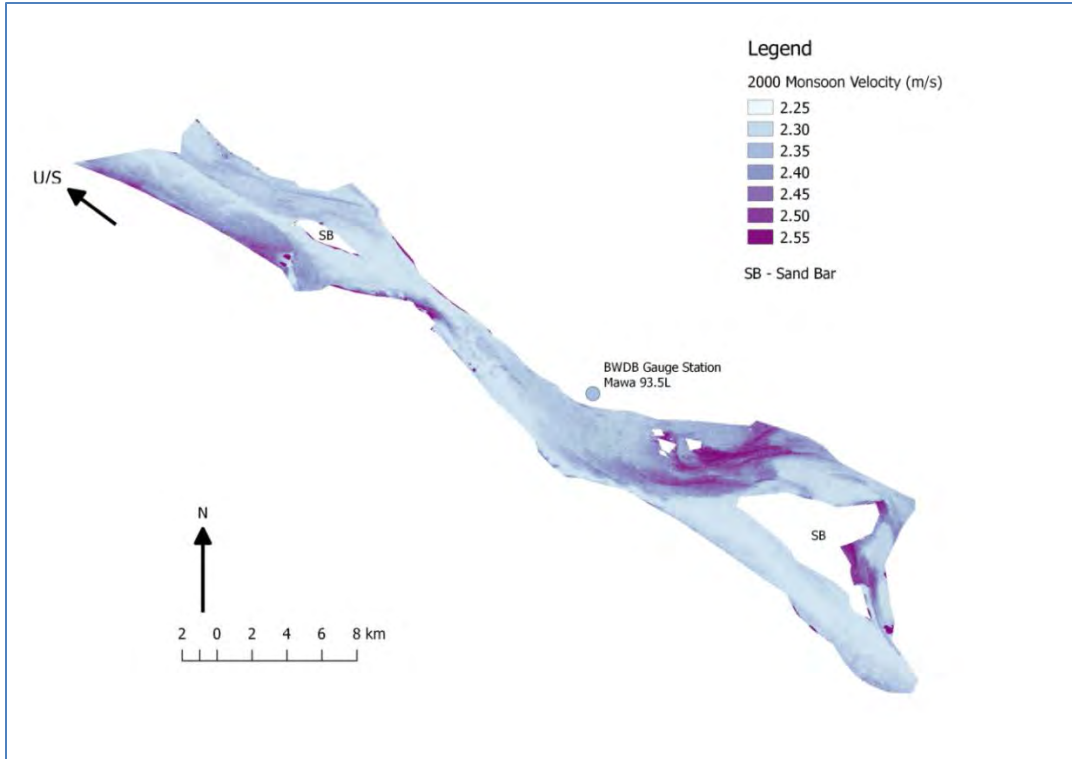


Fig 7.28: Spatial variation of flow velocity for monsoon of year 2000

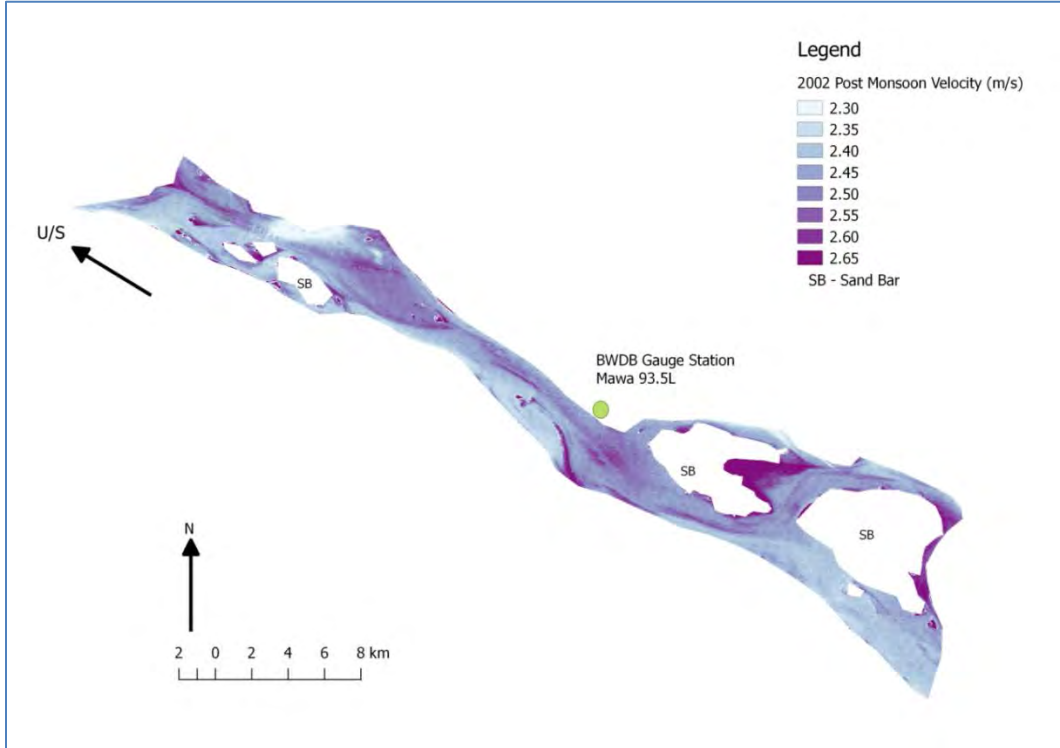


Fig 7.29: Spatial variation of flow velocity for post monsoon of year 2002

Chapter 8

Conclusions and Recommendations

8.1 Conclusions

Landsat ETM+ images were used in combination with available in situ values of SSC to develop a model for retrieving temporal values of SSC at the Padma River in Bangladesh. The analysis saw extraction of DN from Landsat data and their conversion to spectral radiance values. The radiance values were then transformed into ToA Reflectance or Exoatmospheric Reflectance values using appropriate conversion formulae. Thereafter regression methods were applied to investigate statistical relationship between ToA reflectance percentage and corresponding in situ values of SSC; Band 4 (0.76-0.90 μm) ToA reflectance % values proved to be the most sensitive and suitable indicator of SSC for the Padma River.

For validation of the polynomial model involving SSC and Band 4 Reflectance Percentage values, scatter plot of predicted values of SSC from the model versus measured values of SSC was drawn and the Root Mean Square Error (RMSE) was extracted. Scatter plot of predicted SSC values from the polynomial equation (3) against in situ values of SSC with 1:1 fit line generated strong positive coefficient of determination (R^2) of 0.89 and Root Mean Square Error (RMSE) of 88.3 ppm. Because predicted values and measured values of SSC were in strong statistical agreement, polynomial model based on the band 4 data was selected to estimate monsoon and post-monsoon spatial variations of SSC for the years 2000 to 2010.

Assessment of applicability of a robust relationship, combining bands 1-4, through multiple regression analysis was also carried out. However, the predictive values (P-value) of the ToA Reflectance percentage of bands 1, 2 and 3 were very insignificant; only band 4 reflectance percentage possessed P-value low enough to be significant in predicting SSC values. The robust model was therefore not considered further on.

Spatial distribution maps of SSC, between years 2000 and 2010 were observed. Among the notable observations, overall SSC levels appeared to be generally higher in monsoon and flood seasons compared to post-monsoon season. However, there were exceptions in this

observation too. Rise in discharge, water level and flow velocity increased the overall SSC. During cross-section analysis, it was generally observed that rise in bed level also caused small jumps in SSC levels.

Using statistical correlation analysis of measured values of SSC and corresponding in situ values of maximum flow velocity, a logarithmic relationship model were derived. Using this model and spatial distribution maps of SSC, spatial variation maps of maximum flow velocity was created. This exercise was conducted as an example on application of satellite remote sensing.

The task of obtaining and reliable and constant spatial and temporal SSC data of rivers in Bangladesh is severely constrained. These limitations include size and extent of rivers, financial and economic constraints; lack of experienced personnel. Although in situ measurement techniques of suspended sediment are continually changing, it is generally accepted that they do not completely satisfy requirements. This study has shown a way in which these problems can be alleviated with the help of satellite remote sensing. The polynomial relationship developed in this study is the first of its kind for the large alluvial Padma River, and it presents room for further development of such relations for the other rivers of Bangladesh.

8.2 Recommendations

It may be recommended to further augment the applicability of this study by integrating similar models for the Ganges and Brahmaputra Rivers. It is also recommended that more data measurement points be introduced along the Padma River to know the spatial variability of coefficients of the polynomial relationship [3]. In situ atmospheric data at the data point is expected to further bolster the validity of such models. Spatial distribution maps of SSC can be useful tools of improving the understanding of sediment transport patterns in the Padma River. It is recommended that further in situ studies be carried out in conjunction with spatio-temporal mapping of SSC to better understand hydro-morphological process in the Padma River and the greater GBM delta.

References

- Alam, M., Alam, M.M., Curray, J.R., Chowdhury, M.L.R. and Gani, M.R., 2003. An overview of the sedimentary geology of the Bengal Basin in relation to the regional tectonic framework and basin-fill history. *Sedimentary Geology*, 155(3): 179-208.
- Allison, M.A., 1998. Historical Changes in the Ganges-Brahmaputra Delta Front. *Journal of Coastal Research*, 14(4): 1269-1275.
- Aranuvachapun, S. and LeBlond, P.H., 1981. Turbidity of coastal water determined from Landsat. *Remote Sensing of Environment*, 11: 113-132.
- Aranuvachapun, S. and Walling, D., 1988. Landsat-MSS radiance as a measure of suspended sediment in the Lower Yellow River (Hwang Ho). *Remote Sensing of Environment*, 25(2): 145-165.
- Bogárdi, J. and Szilvássy, Z., 1974. Sediment transport in alluvial streams, Akadémiai Kiadó Budapest, Hungary.
- Bookhagen, B., Thiede, R.C. and Strecker, M.R., 2005. Abnormal monsoon years and their control on erosion and sediment flux in the high, arid northwest Himalaya. *Earth and Planetary Science Letters*, 231(1-2): 131-146.
- Choubey, V., 1998. Laboratory experiment, field and remotely sensed data analysis for the assessment of suspended solids concentration and secchi depth of the reservoir surface water. *International Journal of Remote Sensing*, 19(17): 3349-3360.
- Coleman, J.M., 1969. Brahmaputra River: channel processes and sedimentation. *Sedimentary Geology*, 3(2-3): 129-239.
- Coleman, J.M., 1976. Deltas: processes of deposition & models for exploration. Continuing Education Publication Co.
- Collins, A.L. and Walling, D.E., 2004. Documenting catchment suspended sediment sources: problems, approaches and prospects. *Progress in Physical Geography*, 28(2): 159-196.
- Cózar, A., García, C.M., Gálvez, J.A., Loiselle, S.A., Bracchini, L. and Cagnetta, A., 2005. Remote sensing imagery analysis of the lacustrine system of Ibera wetland (Argentina). *Ecological Modelling*, 186(1): 29-41.

- Crawford, A.M. and Hay, A.E., 1993. Determining suspended sand size and concentration from multifrequency acoustic backscatter. *The Journal of the Acoustical Society of America*, 94(6): 3312-3324.
- Curran, P., 1987. AIRBORNE MULTISPECTRAL SCANNER DATA FOR ESTIMATION OF DYE DISPERSION FROM SEA OUTFALLS. *Proceedings of the Institution of Civil Engineers*, 83(1): 213-241.
- Curran, P. and Hay, A., 1986. The importance of measurement error for certain procedures in remote sensing at optical wavelengths. *Photogrammetric Engineering and Remote Sensing*, 52(2): 229-241.
- Curran, P. and Novo, E., 1988. The relationship between suspended sediment concentration and remotely sensed spectral radiance: a review. *Journal of Coastal Research*: 351-368.
- Cyrus, D. and Blaber, S., 1987. The influence of turbidity on juvenile marine fish in the estuaries of Natal, South Africa. *Continental Shelf Research*, 7(11): 1411-1416.
- Dade, W.B. and Friend, P.F., 1998. Grain Size, Sediment Transport Regime, and Channel Slope in Alluvial Rivers. *The Journal of Geology*, 106(6): 661-676.
- Darby, S.E., Dunn, F.E., Nicholls, R.J., Rahman, M. and Riddy, L., 2015. A first look at the influence of anthropogenic climate change on the future delivery of fluvial sediment to the Ganges–Brahmaputra–Meghna delta. *Environmental Science: Processes & Impacts*, 17(9): 1587-1600.
- Dekker, A., Vos, R. and Peters, S., 2001. Comparison of remote sensing data, model results and in situ data for total suspended matter (TSM) in the southern Frisian lakes. *Science of the Total Environment*, 268(1): 197-214.
- Doxaran, D., Froidefond, J.-M., Lavender, S. and Castaing, P., 2002. Spectral signature of highly turbid waters: Application with SPOT data to quantify suspended particulate matter concentrations. *Remote sensing of Environment*, 81(1): 149-161.
- Ekerin, S., 2007. Water Quality Retrievals from High Resolution Ikonos Multispectral Imagery: A Case Study in Istanbul, Turkey. *Water, Air, and Soil Pollution*, 183(1): 239-251.

- Fleiflea, A.E., 2013. Suspended Sediment Load Monitoring Along the Mekong River from Satellite Images. *Journal of Earth Science & Climatic Change*, 2013.
- Gao, J., 2009. Bathymetric mapping by means of remote sensing: methods, accuracy and limitations. *Progress in Physical Geography*, 33(1): 103-116.
- Goodbred Jr, S.L. and Kuehl, S.A., 1998. Floodplain processes in the Bengal Basin and the storage of Ganges–Brahmaputra river sediment: an accretion study using Cs-137 and Pb-210 geochronology. *Sedimentary Geology*, 121(3): 239-258.
- Goodbred, S.L. and Kuehl, S.A., 1999. Holocene and modern sediment budgets for the Ganges-Brahmaputra river system: Evidence for highstand dispersal to flood-plain, shelf, and deep-sea depocenters. *Geology*, 27(6): 559-562.
- Goodbred, S.L. and Kuehl, S.A., 2000. The significance of large sediment supply, active tectonism, and eustasy on margin sequence development: Late Quaternary stratigraphy and evolution of the Ganges–Brahmaputra delta. *Sedimentary Geology*, 133(3-4): 227-248.
- Gray, J.R. and Gartner, J.W., 2009. Technological advances in suspended-sediment surrogate monitoring. *Water resources research*, 45(4).
- Han, Z., Jin, Y.Q. and Yun, C.X., 2006. Suspended sediment concentrations in the Yangtze River estuary retrieved from the CMODIS data. *International Journal of Remote Sensing*, 27(19): 4329-4336.
- Hellweger, F.L., Miller, W. and Oshodi, K.S., 2007. Mapping turbidity in the Charles River, Boston using a high-resolution satellite. *Environmental monitoring and assessment*, 132(1-3): 311-320.
- Heroy, D.C., Kuehl, S.A. and Goodbred, S.L., 2003. Mineralogy of the Ganges and Brahmaputra Rivers: implications for river switching and Late Quaternary climate change. *Sedimentary Geology*, 155(3): 343-359.
- Holyer, R.J., 1978. Toward universal multispectral suspended sediment algorithms. *Remote Sensing of Environment*, 7(4): 323-338.
- Islam, G.M.T. and Jaman, S., 2006. Modelling sediment loads in the Lower Ganges, Bangladesh, *Proceedings of the Institution of Civil Engineers-Water Management*. Thomas Telford Ltd, pp. 87-94.

- Islam, M.R., Begum, S.F., Yamaguchi, Y. and Ogawa, K., 2002. Distribution of suspended sediment in the coastal sea off the Ganges–Brahmaputra River mouth: observation from TM data. *Journal of Marine Systems*, 32(4): 307-321.
- Islam, M.R., Yamaguchi, Y. and Ogawa, K., 2001. Suspended sediment in the Ganges and Brahmaputra Rivers in Bangladesh: observation from TM and AVHRR data. *Hydrological Processes*, 15(3): 493-509.
- Keiner, L.E. and Yan, X.-H., 1998. A Neural Network Model for Estimating Sea Surface Chlorophyll and Sediments from Thematic Mapper Imagery. *Remote Sensing of Environment*, 66(2): 153-165.
- Kirk, J.T., 1994. *Light and photosynthesis in aquatic ecosystems*. Cambridge university press.
- Kuehl, S.A., Hariu, T.M. and Moore, W.S., 1989. Shelf sedimentation off the Ganges-Brahmaputra river system: Evidence for sediment bypassing to the Bengal fan. *Geology*, 17(12): 1132-1135.
- Lagasse, P.F., Zevenbergen, L., Spitz, W. and Arneson, L., 2012. Stream stability at highway structures.
- Lathrop, R.G., Lillesand, T.M. and Yandell, B.S., 1991. Testing the utility of simple multi-date Thematic Mapper calibration algorithms for monitoring turbid inland waters. *Remote Sensing*, 12(10): 2045-2063.
- Lunt, M., 2015. Introduction to statistical modelling: linear regression. *Rheumatology*, 54(7): 1137-1140.
- Matsushita, B. and Fukushima, T., 2009. Methods for retrieving hydrologically significant surface parameters from remote sensing: a review for applications to east Asia region. *Hydrological Processes*, 23(4): 524-533.
- Mertes, L.A.K., Smith, M.O. and Adams, J.B., 1993. Estimating suspended sediment concentrations in surface waters of the Amazon River wetlands from Landsat images. *Remote Sensing of Environment*, 43(3): 281-301.
- Michels, K.H., Suckow, A., Breitzke, M., Kudrass, H.R. and Kottke, B., 2003. Sediment transport in the shelf canyon “Swatch of No Ground” (Bay of Bengal). *Deep Sea Research Part II: Topical Studies in Oceanography*, 50(5): 1003-1022.
- Middleton, G.V. and Southard, J.B., 1984. *Mechanics of sediment movement*. SEPM.

- Miller, R.L. and McKee, B.A., 2004. Using MODIS Terra 250 m imagery to map concentrations of total suspended matter in coastal waters. *Remote sensing of Environment*, 93(1): 259-266.
- Milliman, J.D. and Meade, R.H., 1983. World-Wide Delivery of River Sediment to the Oceans. *The Journal of Geology*, 91(1): 1-21.
- Milliman, J.D. and Syvitski, J.P., 1992a. Geomorphic/tectonic control of sediment discharge to the ocean: the importance of small mountainous rivers. *The Journal of Geology*: 525-544.
- Milliman, J.D. and Syvitski, J.P.M., 1992b. Geomorphic/Tectonic Control of Sediment Discharge to the Ocean: The Importance of Small Mountainous Rivers. *The Journal of Geology*, 100(5): 525-544.
- Mirza, M.M.Q., 2002. Global warming and changes in the probability of occurrence of floods in Bangladesh and implications. *Global environmental change*, 12(2): 127-138.
- Mugade, U.R. and Sapkale, J.B., 2015. Influence of Aggradation and Degradation on River Channels: A Review. *International Journal of Engineering and Technical Research (IJETR)*, 3(6): 209-212.
- Mukherjee, A., Fryar, A.E. and Thomas, W.A., 2009. Geologic, geomorphic and hydrologic framework and evolution of the Bengal basin, India and Bangladesh. *Journal of Asian Earth Sciences*, 34(3): 227-244.
- Munday, J.C. and Alföldi, T.T., 1979. Landsat test of diffuse reflectance models for aquatic suspended solids measurement. *Remote sensing of environment*, 8(2): 169-183.
- Novo, E., Hansom, J. and CURRAN†, P., 1989. The effect of sediment type on the relationship between reflectance and suspended sediment concentration. *Remote Sensing*, 10(7): 1283-1289.
- Novo, E.M.L.M., Steffen, C.A. and Braga, C.Z.F., 1991. Results of a laboratory experiment relating spectral reflectance to total suspended solids. *Remote Sensing of Environment*, 36(1): 67-72.
- Okada, A.Y., H Koseki., S. Kudo., K. Muraoka, 2016. Comprehensive measurement techniques of water flow, bedload and suspended sediment in large river using Acoustic Doppler Current Profiler. *River Sedimentation – Wieprecht et al. (Eds): 1274-1280.*

- Ouillon, S., Douillet, P. and Andréfouët, S., 2004. Coupling satellite data with in situ measurements and numerical modeling to study fine suspended-sediment transport: a study for the lagoon of New Caledonia. *Coral Reefs*, 23(1): 109-122.
- Pavelsky, T.M. and Smith, L.C., 2009. Remote sensing of suspended sediment concentration, flow velocity, and lake recharge in the Peace-Athabasca Delta, Canada. *Water Resources Research*, 45(11).
- Poonawala, I., Ranade, S., Selvan, S., Gnanaseelan, C. and Rajagopalan, A., 2006. Detection of shallow water depth using remotely sensed data.
- Rasul, G., 2015. Water for growth and development in the Ganges, Brahmaputra, and Meghna basins: an economic perspective. *International Journal of River Basin Management*, 13(3): 387-400.
- Reddy and Srinivasulu, S., 1994. Comparison of IRS-IB LISS-IIA pixel array sizes for estimating suspended solids concentration in Hussain Sagar Lake, Hyderabad, India—a statistical approach. *International Journal of Remote Sensing*, 15(18): 3693-3706.
- Rice, S.K., 2007. *Suspended Sediment Transport in the Ganges-Brahmaputra River System, Bangladesh*, Texas A&M University, Texas, United States of America.
- Rimmer, J., Collins, M. and Pattiaratchi, C., 1987. Mapping of water quality in coastal waters using Airborne Thematic Mapper data. *International Journal of Remote Sensing*, 8(1): 85-102.
- Ritchie, J.C., Cooper, C.M. and Yongqing, J., 1987. Using Landsat multispectral scanner data to estimate suspended sediments in Moon Lake, Mississippi. *Remote Sensing of Environment*, 23(1): 65-81.
- Ritchie, J.C. and Schiebe, F.R., 2000. *Water quality, Remote Sensing in Hydrology and Water Management*. Springer, pp. 287-303.
- Ritchie, J.C., Schiebe, F.R. and McHENRY, J., 1976. Remote sensing of suspended sediments in surface waters. *American Society of Photogrammetry, Journal of*, 42(12).
- Ritchie, J.C., Zimba, P.V. and Everitt, J.H., 2003. Remote sensing techniques to assess water quality. *Photogrammetric Engineering & Remote Sensing*, 69(6): 695-704.

- Rowiński, P. and Czernuszenko, W., 1998. Experimental study of river turbulence under unsteady conditions. *Acta Geophysica Polonica*, 46(4): 461-480.
- Scherz, J.P., 1972. Development of a practical remote sensing water quality monitoring system, *Remote Sensing of Environment*, VIII, pp. 35.
- Schiebe, F., Harrington Jr, J. and Ritchie, J., 1992. Remote sensing of suspended sediments: the Lake Chicot, Arkansas project. *International Journal of Remote Sensing*, 13(8): 1487-1509.
- Sheng, J. and Hay, A.E., 1988. An examination of the spherical scatterer approximation in aqueous suspensions of sand. *The Journal of the Acoustical Society of America*, 83(2): 598-610.
- Shi, W. and Wang, M., 2009. Satellite observations of flood-driven Mississippi River plume in the spring of 2008. *Geophysical Research Letters*, 36(7).
- Sood, A. and Mathukumalli, B.K.P., 2011. Managing international river basins: reviewing India–Bangladesh transboundary water issues. *Intl. J. River Basin Management*, 9(1): 43-52.
- Sterckx, S., Knaeps, E., Bollen, M., Trouw, K. and Houthuys, R., 2007. Retrieval of suspended sediment from advanced hyperspectral sensor data in the Scheldt estuary at different stages in the tidal cycle. *Marine Geodesy*, 30(1-2): 97-108.
- Tabarestani, M.K. and Zarrati, A., 2015. Sediment transport during flood event: a review. *International Journal of Environmental Science and Technology*, 12(2): 775-788.
- Tassan, S., 1987. Evaluation of the potential of the Thematic Mapper for marine application. *International Journal of Remote Sensing*, 8(10): 1455-1478.
- Taylor, R., 1990. Interpretation of the correlation coefficient: a basic review. *Journal of diagnostic medical sonography*, 6(1): 35-39.
- Thorne, P.D. and Hardcastle, P.J., 1997. Acoustic measurements of suspended sediments in turbulent currents and comparison with in-situ samples. *The Journal of the Acoustical Society of America*, 101(5): 2603-2614.
- Thorne, P.D., Hardcastle, P.J. and Soulsby, R.L., 1993. Analysis of acoustic measurements of suspended sediments. *Journal of Geophysical Research: Oceans*, 98(C1): 899-910.

- Tolk, B.L., Han, L. and Rundquist, D., 2000. The impact of bottom brightness on spectral reflectance of suspended sediments. *International Journal of Remote Sensing*, 21(11): 2259-2268.
- Topliss, B., Almos, C. and Hill, P., 1990. Algorithms for remote sensing of high concentration, inorganic suspended sediment. *International Journal of Remote Sensing*, 11(6): 947-966.
- USGS, 2013. Landsat—A Global Land-Imaging Mission.
- Van Rijn, L.C., 1993. Principles of sediment transport in rivers, estuaries and coastal seas, 1006. Aqua publications Amsterdam.
- Wang, J.-J. and Lu, X., 2010. Estimation of suspended sediment concentrations using Terra MODIS: An example from the Lower Yangtze River, China. *Science of the Total Environment*, 408(5): 1131-1138.
- Wang, J.-J., Lu, X.X., Liew, S.C. and Zhou, Y., 2009. Retrieval of suspended sediment concentrations in large turbid rivers using Landsat ETM+: an example from the Yangtze River, China. *Earth Surface Processes and Landforms*, 34(8): 1082-1092.
- Wass, P.D., Marks, S.D., Finch, J.W., Leeks, G.J.L. and Ingram, J.K., 1997. U.K. Fluxes to the North Sea, Land Ocean Interaction Study (LOIS) Rivers Basins Research, the First Two Years Monitoring and preliminary interpretation of in-river turbidity and remote sensed imagery for suspended sediment transport studies in the Humber catchment. *Science of The Total Environment*, 194: 263-283.
- Wilber, D.H. and Clarke, D.G., 2001. Biological Effects of Suspended Sediments: A Review of Suspended Sediment Impacts on Fish and Shellfish with Relation to Dredging Activities in Estuaries. *North American Journal of Fisheries Management*, 21(4): 855-875.
- Williams, G.P., 1989. Sediment concentration versus water discharge during single hydrologic events in rivers. *Journal of Hydrology*, 111(1): 89-106.
- Woodruff, D.L., Stumpf, R.P., Scope, J.A. and Paerl, H.W., 1999. Remote Estimation of Water Clarity in Optically Complex Estuarine Waters. *Remote Sensing of Environment*, 68(1): 41-52.

- Wu, G., de Leeuw, J., Skidmore, A.K., Prins, H.H. and Liu, Y., 2007. Concurrent monitoring of vessels and water turbidity enhances the strength of evidence in remotely sensed dredging impact assessment. *Water Research*, 41(15): 3271-3280.
- Xia, L., 1993. A united model for quantitative remote sensing of suspended sediment concentration. *International Journal of Remote Sensing*, 14(14): 2665-2676.
- Zhang, X., Zhang, Y., Wen, A. and Feng, M., 2003. Assessment of soil losses on cultivated land by using the ^{137}Cs technique in the Upper Yangtze River Basin of China. *Soil and Tillage Research*, 69(1): 99-106.

Appendix-A

Historical sediment data corresponding to Mawa SW 93.5L - provided by Bangladesh Water Development Board

| RiverName | Station ID | StationName | Date | Sand kg/s | Fine kg/s | Maximum Sand Concentration (PPM) |
|--------------|------------|-------------|------------|-----------|-----------|----------------------------------|
| Ganges-Padma | SW93.5L | Mawa | 06/06/2001 | 1.49 | | 177.10 |
| Ganges-Padma | SW93.5L | Mawa | 13/06/2001 | 2.17 | | 273.70 |
| Ganges-Padma | SW93.5L | Mawa | 20/06/2001 | 2.57 | | 322.00 |
| Ganges-Padma | SW93.5L | Mawa | 27/06/2001 | 3.93 | | 305.90 |
| Ganges-Padma | SW93.5L | Mawa | 08/07/2001 | 4.35 | | 338.10 |
| Ganges-Padma | SW93.5L | Mawa | 11/07/2001 | 5.78 | | 499.10 |
| Ganges-Padma | SW93.5L | Mawa | 18/07/2001 | 6.19 | | 386.40 |
| Ganges-Padma | SW93.5L | Mawa | 25/07/2001 | 9.14 | | 499.10 |
| Ganges-Padma | SW93.5L | Mawa | 01/08/2001 | 15.40 | | 821.10 |
| Ganges-Padma | SW93.5L | Mawa | 08/08/2001 | 17.12 | | 676.20 |
| Ganges-Padma | SW93.5L | Mawa | 15/08/2001 | 7.71 | | 386.40 |
| Ganges-Padma | SW93.5L | Mawa | 22/08/2001 | 7.11 | | 466.90 |
| Ganges-Padma | SW93.5L | Mawa | 29/08/2001 | 29.40 | | 1175.30 |
| Ganges-Padma | SW93.5L | Mawa | 05/09/2001 | 42.04 | | 1159.20 |
| Ganges-Padma | SW93.5L | Mawa | 12/09/2001 | 21.99 | | 869.40 |
| Ganges-Padma | SW93.5L | Mawa | 19/09/2001 | 14.69 | | 756.70 |
| Ganges-Padma | SW93.5L | Mawa | 26/09/2001 | 9.91 | | 627.90 |
| Ganges-Padma | SW93.5L | Mawa | 03/10/2001 | 8.65 | | 676.20 |
| Ganges-Padma | SW93.5L | Mawa | 10/10/2001 | 8.15 | | 547.40 |
| Ganges-Padma | SW93.5L | Mawa | 17/10/2001 | 5.66 | | 305.90 |

| RiverName | Station ID | StationName | Date | Sand kg/s | Fine kg/s | Maximum Sand Concentration (PPM) |
|--------------|------------|-------------|------------|-----------|-----------|----------------------------------|
| Ganges-Padma | SW93.5L | Mawa | 24/10/2001 | 3.21 | | 209.30 |
| Ganges-Padma | SW93.5L | Mawa | 31/10/2001 | 2.27 | | 370.30 |
| Ganges-Padma | SW93.5L | Mawa | 02/06/2004 | 0.27 | | 144.90 |
| Ganges-Padma | SW93.5L | Mawa | 09/06/2004 | 0.19 | | 209.30 |
| Ganges-Padma | SW93.5L | Mawa | 16/06/2004 | 0.26 | | 128.80 |
| Ganges-Padma | SW93.5L | Mawa | 23/06/2004 | 0.46 | | 289.80 |
| Ganges-Padma | SW93.5L | Mawa | 30/06/2004 | 2.18 | | 805.00 |
| Ganges-Padma | SW93.5L | Mawa | 07/07/2004 | 0.95 | | 627.90 |
| Ganges-Padma | SW93.5L | Mawa | 14/07/2004 | 2.91 | | 1304.10 |
| Ganges-Padma | SW93.5L | Mawa | 21/07/2004 | 4.07 | | 1400.70 |
| Ganges-Padma | SW93.5L | Mawa | 28/07/2004 | 2.40 | | 1368.50 |
| Ganges-Padma | SW93.5L | Mawa | 01/08/2004 | | 25769.30 | 1320.20 |
| Ganges-Padma | SW93.5L | Mawa | 04/08/2004 | | 30430.49 | 1320.20 |
| Ganges-Padma | SW93.5L | Mawa | 11/08/2004 | | 27602.01 | 1320.20 |
| Ganges-Padma | SW93.5L | Mawa | 18/08/2004 | | 24760.34 | 1239.70 |
| Ganges-Padma | SW93.5L | Mawa | 25/08/2004 | | 16472.45 | 644.00 |
| Ganges-Padma | SW93.5L | Mawa | 01/09/2004 | | 25769.30 | 1320.20 |
| Ganges-Padma | SW93.5L | Mawa | 08/09/2004 | | 13322.04 | 660.10 |
| Ganges-Padma | SW93.5L | Mawa | 15/09/2004 | | 27652.28 | 1432.90 |
| Ganges-Padma | SW93.5L | Mawa | 21/09/2004 | | 5692.68 | 305.90 |
| Ganges-Padma | SW93.5L | Mawa | 29/09/2004 | | 5419.19 | 305.90 |
| Ganges-Padma | SW93.5L | Mawa | 06/10/2004 | | 6244.08 | 354.20 |
| Ganges-Padma | SW93.5L | Mawa | 13/10/2004 | | 10307.84 | 402.50 |

| RiverName | Station ID | StationName | Date | Sand kg/s | Fine kg/s | Maximum Sand Concentration (PPM) |
|--------------|------------|-------------|------------|-----------|-----------|----------------------------------|
| Ganges-Padma | SW93.5L | Mawa | 20/10/2004 | | 5232.62 | 322.00 |
| Ganges-Padma | SW93.5L | Mawa | 27/10/2004 | | 3297.84 | 273.70 |
| Ganges-Padma | SW93.5L | Mawa | 01/06/2005 | | 2074.75 | 193.20 |
| Ganges-Padma | SW93.5L | Mawa | 08/06/2005 | | 3044.83 | 241.50 |
| Ganges-Padma | SW93.5L | Mawa | 22/06/2005 | | 3526.34 | 289.80 |
| Ganges-Padma | SW93.5L | Mawa | 29/06/2005 | | 4960.11 | 289.80 |
| Ganges-Padma | SW93.5L | Mawa | 06/07/2005 | | 6032.76 | 322.00 |
| Ganges-Padma | SW93.5L | Mawa | 15/07/2005 | | 15499.77 | 563.50 |
| Ganges-Padma | SW93.5L | Mawa | 20/07/2005 | | 31829.59 | 772.80 |
| Ganges-Padma | SW93.5L | Mawa | 27/07/2005 | | 38939.32 | 1207.50 |
| Ganges-Padma | SW93.5L | Mawa | 03/08/2005 | | 30532.96 | 1046.50 |
| Ganges-Padma | SW93.5L | Mawa | 10/08/2005 | | 26088.11 | 917.70 |
| Ganges-Padma | SW93.5L | Mawa | 17/08/2005 | | 35840.29 | 1207.50 |
| Ganges-Padma | SW93.5L | Mawa | 24/08/2005 | | 32782.84 | 1046.50 |
| Ganges-Padma | SW93.5L | Mawa | 31/08/2005 | | 40517.22 | 1239.70 |
| Ganges-Padma | SW93.5L | Mawa | 07/09/2005 | | 33000.66 | 1191.40 |
| Ganges-Padma | SW93.5L | Mawa | 14/09/2005 | | 16679.02 | 885.50 |
| Ganges-Padma | SW93.5L | Mawa | 21/09/2005 | | 8264.07 | 579.60 |
| Ganges-Padma | SW93.5L | Mawa | 28/09/2005 | | 5913.88 | 322.00 |
| Ganges-Padma | SW93.5L | Mawa | 05/10/2005 | | 8953.33 | 402.50 |
| Ganges-Padma | SW93.5L | Mawa | 12/10/2005 | | 6663.10 | 322.00 |
| Ganges-Padma | SW93.5L | Mawa | 29/10/2005 | | 3999.54 | 257.60 |
| Ganges-Padma | SW93.5L | Mawa | 11/06/2008 | | 3548.14 | 225.40 |

| RiverName | Station ID | StationName | Date | Sand kg/s | Fine kg/s | Maximum Sand Concentration (PPM) |
|--------------|------------|-------------|------------|-----------|-----------|----------------------------------|
| Ganges-Padma | SW93.5L | Mawa | 15/06/2008 | | 2486.91 | 225.40 |
| Ganges-Padma | SW93.5L | Mawa | 25/06/2008 | | 6284.12 | 338.10 |
| Ganges-Padma | SW93.5L | Mawa | 09/07/2008 | | 9833.62 | 402.50 |
| Ganges-Padma | SW93.5L | Mawa | 16/07/2008 | | 12557.46 | 418.60 |
| Ganges-Padma | SW93.5L | Mawa | 23/07/2008 | | 13665.12 | 515.20 |
| Ganges-Padma | SW93.5L | Mawa | 30/07/2008 | | 16545.26 | 434.70 |
| Ganges-Padma | SW93.5L | Mawa | 06/08/2008 | 14264.73 | | 483.00 |
| Ganges-Padma | SW93.5L | Mawa | 13/08/2008 | 12268.52 | | 466.90 |
| Ganges-Padma | SW93.5L | Mawa | 20/08/2008 | 18034.34 | | 466.90 |
| Ganges-Padma | SW93.5L | Mawa | 27/08/2008 | 19558.23 | | 418.60 |
| Ganges-Padma | SW93.5L | Mawa | 03/09/2008 | 30575.73 | | 644.00 |
| Ganges-Padma | SW93.5L | Mawa | 10/09/2008 | 19557.42 | | 434.70 |
| Ganges-Padma | SW93.5L | Mawa | 17/09/2008 | 11169.52 | | 338.10 |
| Ganges-Padma | SW93.5L | Mawa | 24/09/2008 | 6881.52 | | 305.90 |
| Ganges-Padma | SW93.5L | Mawa | 08/10/2008 | 5276.67 | | 257.60 |
| Ganges-Padma | SW93.5L | Mawa | 15/10/2008 | 3791.83 | | 193.20 |
| Ganges-Padma | SW93.5L | Mawa | 22/10/2008 | 2303.16 | | 161.00 |
| Ganges-Padma | SW93.5L | Mawa | 29/10/2008 | 1918.71 | | 144.90 |
| Ganges-Padma | SW93.5L | Mawa | 03/06/2009 | 2176.07 | | 193.20 |
| Ganges-Padma | SW93.5L | Mawa | 10/06/2009 | 2186.35 | | 225.40 |
| Ganges-Padma | SW93.5L | Mawa | 17/06/2009 | 1909.26 | | 177.10 |
| Ganges-Padma | SW93.5L | Mawa | 01/07/2009 | 3798.06 | | 273.70 |
| Ganges-Padma | SW93.5L | Mawa | 08/07/2009 | 11082.77 | | 434.70 |

| RiverName | Station ID | StationName | Date | Sand kg/s | Fine kg/s | Maximum Sand Concentration (PPM) |
|--------------|------------|-------------|------------|-----------|-----------|----------------------------------|
| Ganges-Padma | SW93.5L | Mawa | 15/07/2009 | 8188.37 | | 322.00 |
| Ganges-Padma | SW93.5L | Mawa | 22/07/2009 | 5871.72 | | 257.60 |
| Ganges-Padma | SW93.5L | Mawa | 29/07/2009 | 4433.88 | | 273.70 |
| Ganges-Padma | SW93.5L | Mawa | 05/08/2009 | | 10636.93 | 402.50 |
| Ganges-Padma | SW93.5L | Mawa | 12/08/2009 | | 12557.26 | 450.80 |
| Ganges-Padma | SW93.5L | Mawa | 19/08/2009 | | 17432.00 | 515.20 |
| Ganges-Padma | SW93.5L | Mawa | 09/09/2009 | | 8113.38 | 322.00 |
| Ganges-Padma | SW93.5L | Mawa | 30/09/2009 | | 6303.20 | 354.20 |
| Ganges-Padma | SW93.5L | Mawa | 14/10/2009 | | 4111.98 | 193.20 |
| Ganges-Padma | SW93.5L | Mawa | 28/10/2009 | | 2325.68 | 144.90 |
| Ganges-Padma | SW93.5L | Mawa | 27/01/2010 | 3053.87 | | 193.20 |
| Ganges-Padma | SW93.5L | Mawa | 07/07/2010 | 1508.00 | 15079.00 | 466.90 |
| Ganges-Padma | SW93.5L | Mawa | 14/07/2010 | 19058.34 | 19058.34 | 483.00 |
| Ganges-Padma | SW93.5L | Mawa | 21/07/2010 | 16726.56 | 16726.56 | 434.70 |
| Ganges-Padma | SW93.5L | Mawa | 28/07/2010 | 22932.86 | 22932.86 | 595.70 |
| Ganges-Padma | SW93.5L | Mawa | 04/08/2010 | 15373.13 | 15373.13 | 563.90 |
| Ganges-Padma | SW93.5L | Mawa | 18/08/2010 | 11909.90 | 11909.90 | 418.60 |
| Ganges-Padma | SW93.5L | Mawa | 25/08/2010 | 21415.40 | 21415.40 | 644.00 |
| Ganges-Padma | SW93.5L | Mawa | 08/09/2010 | 24585.59 | | 595.70 |
| Ganges-Padma | SW93.5L | Mawa | 22/09/2010 | 18933.65 | | 434.70 |
| Ganges-Padma | SW93.5L | Mawa | 29/09/2010 | 13562.00 | | 386.40 |
| Ganges-Padma | SW93.5L | Mawa | 13/10/2010 | 5701.05 | | 257.60 |
| Ganges-Padma | SW93.5L | Mawa | 19/05/2011 | | | 32.20 |

| RiverName | Station ID | StationName | Date | Sand kg/s | Fine kg/s | Maximum Sand Concentration (PPM) |
|--------------|------------|-------------|------------|-----------|-----------|----------------------------------|
| Ganges-Padma | SW93.5L | Mawa | 25/05/2011 | | | 48.30 |
| Ganges-Padma | SW93.5L | Mawa | 08/06/2011 | | 3343.99 | 225.40 |
| Ganges-Padma | SW93.5L | Mawa | 22/06/2011 | | 3975.70 | 257.60 |
| Ganges-Padma | SW93.5L | Mawa | 13/07/2011 | | 15053.91 | 450.80 |
| Ganges-Padma | SW93.5L | Mawa | 27/07/2011 | | 18769.74 | 563.50 |
| Ganges-Padma | SW93.5L | Mawa | 03/08/2011 | | 26632.21 | 579.60 |
| Ganges-Padma | SW93.5L | Mawa | 10/08/2011 | | 22563.01 | 627.90 |
| Ganges-Padma | SW93.5L | Mawa | 17/08/2011 | | 25085.89 | 595.70 |
| Ganges-Padma | SW93.5L | Mawa | 24/08/2011 | | 26813.46 | 644.00 |
| Ganges-Padma | SW93.5L | Mawa | 07/09/2011 | | 23354.82 | 885.50 |
| Ganges-Padma | SW93.5L | Mawa | 14/09/2011 | | 19254.03 | 805.00 |
| Ganges-Padma | SW93.5L | Mawa | 21/09/2011 | | 24317.93 | 837.20 |
| Ganges-Padma | SW93.5L | Mawa | 28/09/2011 | | 22098.44 | 788.90 |
| Ganges-Padma | SW93.5L | Mawa | 05/10/2011 | | 18936.34 | 724.50 |
| Ganges-Padma | SW93.5L | Mawa | 12/10/2011 | | 11503.30 | 644.00 |
| Ganges-Padma | SW93.5L | Mawa | 19/10/2011 | | 6565.72 | 483.00 |
| Ganges-Padma | SW93.5L | Mawa | 26/10/2011 | | 4027.59 | 273.70 |
| Ganges-Padma | SW93.5L | Mawa | 08/02/2012 | | | 24.15 |
| Ganges-Padma | SW93.5L | Mawa | 11/03/2012 | | | 24.15 |
| Ganges-Padma | SW93.5L | Mawa | 17/03/2012 | | | 24.15 |
| Ganges-Padma | SW93.5L | Mawa | 08/06/2012 | | 2779.48 | 241.50 |
| Ganges-Padma | SW93.5L | Mawa | 20/06/2012 | | 6455.85 | 354.20 |
| Ganges-Padma | SW93.5L | Mawa | 11/07/2012 | | 12784.47 | 483.00 |

| RiverName | Station ID | StationName | Date | Sand kg/s | Fine kg/s | Maximum Sand Concentration (PPM) |
|--------------|------------|-------------|------------|-----------|-----------|----------------------------------|
| Ganges-Padma | SW93.5L | Mawa | 25/07/2012 | | 19733.13 | 563.50 |
| Ganges-Padma | SW93.5L | Mawa | 08/08/2012 | | 16288.16 | 547.40 |
| Ganges-Padma | SW93.5L | Mawa | 15/08/2012 | | 14715.67 | 466.90 |
| Ganges-Padma | SW93.5L | Mawa | 22/08/2012 | | 13600.67 | 547.40 |
| Ganges-Padma | SW93.5L | Mawa | 29/08/2012 | | 13178.00 | 579.60 |
| Ganges-Padma | SW93.5L | Mawa | 14/11/2012 | | | 64.40 |
| Ganges-Padma | SW93.5L | Mawa | 21/11/2012 | | | 32.20 |

Appendix-B

Water Level, discharge and flow velocity data sets, as provided by BWDB, are given below.

| StationID | StationName | Date | Water Level (m) | Discharge (cumec) | Maximum Velocity (m/s) |
|-----------|-------------|------------|-----------------|-------------------|------------------------|
| SW93.5L | Mawa | 11/06/1997 | 3.23 | 19151.28 | 1.83 |
| SW93.5L | Mawa | 18/06/1997 | 4.30 | 40511.25 | 2.66 |
| SW93.5L | Mawa | 25/06/1997 | 4.49 | 43641.45 | 2.66 |
| SW93.5L | Mawa | 02/07/1997 | 4.48 | 36786.67 | 2.64 |
| SW93.5L | Mawa | 09/07/1997 | 4.92 | 49173.77 | 3.07 |
| SW93.5L | Mawa | 16/07/1997 | 5.78 | 82324.20 | 3.22 |
| SW93.5L | Mawa | 23/07/1997 | 5.65 | 76351.83 | 2.96 |
| SW93.5L | Mawa | 31/07/1997 | 5.15 | 50222.16 | 2.45 |
| SW93.5L | Mawa | 06/08/1997 | 5.11 | 43089.77 | 2.58 |
| SW93.5L | Mawa | 13/08/1997 | 5.30 | 63029.74 | 2.91 |
| SW93.5L | Mawa | 20/08/1997 | 5.76 | 58218.85 | 2.78 |
| SW93.5L | Mawa | 27/08/1997 | 5.12 | 49034.07 | 2.91 |
| SW93.5L | Mawa | 03/09/1997 | 4.85 | 37368.77 | 2.82 |
| SW93.5L | Mawa | 10/09/1997 | 5.23 | 52228.49 | 3.17 |
| SW93.5L | Mawa | 25/09/1997 | 5.22 | 51094.51 | 3.27 |
| SW93.5L | Mawa | 03/10/1997 | 5.03 | 38961.94 | 2.86 |
| SW93.5L | Mawa | 08/10/1997 | 4.53 | 33486.16 | 2.47 |
| SW93.5L | Mawa | 17/10/1997 | 3.86 | 23641.94 | 1.79 |
| SW93.5L | Mawa | 22/10/1997 | 3.37 | 17921.40 | 1.48 |
| SW93.5L | Mawa | 29/10/1997 | 2.87 | 16464.51 | 1.58 |
| SW93.5L | Mawa | 03/06/1998 | 3.56 | 16826.69 | 1.31 |
| SW93.5L | Mawa | 12/06/1998 | 4.26 | 30621.83 | 1.96 |
| SW93.5L | Mawa | 17/06/1998 | 4.92 | 38660.55 | 2.62 |
| SW93.5L | Mawa | 24/06/1998 | 5.00 | 47859.72 | 2.69 |
| SW93.5L | Mawa | 01/07/1998 | 5.22 | 52201.07 | 2.69 |
| SW93.5L | Mawa | 08/07/1998 | 5.38 | 59413.67 | 3.36 |
| SW93.5L | Mawa | 22/07/1998 | 6.02 | 70585.65 | 3.57 |
| SW93.5L | Mawa | 29/07/1998 | 6.44 | 86318.52 | 3.77 |
| SW93.5L | Mawa | 06/08/1998 | 6.19 | 79239.09 | 3.51 |
| SW93.5L | Mawa | 12/08/1998 | 6.25 | 73152.51 | 3.23 |
| SW93.5L | Mawa | 19/08/1998 | 6.50 | 85162.81 | 3.34 |
| SW93.5L | Mawa | 02/09/1998 | 6.56 | 87839.94 | 3.81 |
| SW93.5L | Mawa | 10/09/1998 | 7.07 | 116011.20 | 4.35 |
| SW93.5L | Mawa | 23/09/1998 | 5.28 | 61772.40 | 2.84 |
| SW93.5L | Mawa | 30/09/1998 | 4.78 | 46542.10 | 2.14 |
| SW93.5L | Mawa | 07/10/1998 | 4.86 | 44855.99 | 2.60 |
| SW93.5L | Mawa | 14/10/1998 | 4.15 | 27333.16 | 1.84 |
| SW93.5L | Mawa | 21/10/1998 | 4.21 | 26478.87 | 1.61 |
| SW93.5L | Mawa | 02/06/1999 | 3.61 | 26236.16 | 1.74 |

| StationID | StationName | Date | Water Level (m) | Discharge (cumec) | Maximum Velocity (m/s) |
|-----------|-------------|------------|-----------------|-------------------|------------------------|
| SW93.5L | Mawa | 10/06/1999 | 3.95 | 27974.95 | 1.62 |
| SW93.5L | Mawa | 18/06/1999 | 3.69 | 19533.55 | 1.54 |
| SW93.5L | Mawa | 24/06/1999 | 4.18 | 31438.59 | 2.06 |
| SW93.5L | Mawa | 30/06/1999 | 5.02 | 54444.07 | 2.91 |
| SW93.5L | Mawa | 21/07/1999 | 5.45 | 61094.30 | 1.66 |
| SW93.5L | Mawa | 28/07/1999 | 5.44 | 53346.25 | 3.10 |
| SW93.5L | Mawa | 05/08/1999 | 5.46 | 64899.91 | 2.94 |
| SW93.5L | Mawa | 11/08/1999 | 5.22 | 60432.22 | 2.84 |
| SW93.5L | Mawa | 18/08/1999 | 5.53 | 70166.57 | 3.72 |
| SW93.5L | Mawa | 25/08/1999 | 5.64 | 77350.76 | 3.07 |
| SW93.5L | Mawa | 01/09/1999 | 6.18 | 96490.83 | 3.50 |
| SW93.5L | Mawa | 08/09/1999 | 5.83 | 86337.01 | 3.17 |
| SW93.5L | Mawa | 15/09/1999 | 5.80 | 94118.52 | 3.67 |
| SW93.5L | Mawa | 19/09/1999 | 5.48 | 82975.45 | 3.43 |
| SW93.5L | Mawa | 24/09/1999 | 5.47 | 84014.41 | 3.62 |
| SW93.5L | Mawa | 25/09/1999 | 5.45 | 84913.73 | 3.62 |
| SW93.5L | Mawa | 29/09/1999 | 5.56 | 92322.04 | 3.69 |
| SW93.5L | Mawa | 02/10/1999 | 5.25 | 74547.86 | 3.42 |
| SW93.5L | Mawa | 05/10/1999 | 4.97 | 61422.66 | 3.38 |
| SW93.5L | Mawa | 13/10/1999 | 4.83 | 58914.55 | 3.57 |
| SW93.5L | Mawa | 19/10/1999 | 4.85 | 57704.75 | 3.40 |
| SW93.5L | Mawa | 27/10/1999 | 4.71 | 49915.02 | 2.89 |
| SW93.5L | Mawa | 07/06/2000 | 4.25 | 33956.77 | 2.14 |
| SW93.5L | Mawa | 14/06/2000 | 4.29 | 40500.99 | 2.56 |
| SW93.5L | Mawa | 21/06/2000 | 4.93 | 41775.65 | 2.68 |
| SW93.5L | Mawa | 28/06/2000 | 5.53 | 62736.79 | 3.22 |
| SW93.5L | Mawa | 05/07/2000 | 5.35 | 56732.86 | 2.96 |
| SW93.5L | Mawa | 12/07/2000 | 5.35 | 55108.39 | 2.88 |
| SW93.5L | Mawa | 19/07/2000 | 5.56 | 70497.98 | 3.29 |
| SW93.5L | Mawa | 26/07/2000 | 5.23 | 60061.86 | 3.24 |
| SW93.5L | Mawa | 02/08/2000 | 5.61 | 74176.84 | 3.54 |
| SW93.5L | Mawa | 09/08/2000 | 6.15 | 85597.38 | 3.45 |
| SW93.5L | Mawa | 17/08/2000 | 5.90 | 68759.84 | 3.58 |
| SW93.5L | Mawa | 23/08/2000 | 5.76 | 70305.74 | 2.97 |
| SW93.5L | Mawa | 31/08/2000 | 5.77 | 68056.48 | 3.18 |
| SW93.5L | Mawa | 06/09/2000 | 5.71 | 63760.10 | 2.72 |
| SW93.5L | Mawa | 13/09/2000 | 5.82 | 66285.97 | 2.92 |
| SW93.5L | Mawa | 20/09/2000 | 6.14 | 77487.04 | 3.56 |
| SW93.5L | Mawa | 27/09/2000 | 5.96 | 84025.47 | 3.16 |
| SW93.5L | Mawa | 04/10/2000 | 5.27 | 60222.75 | 2.95 |
| SW93.5L | Mawa | 11/10/2000 | 4.51 | 41289.23 | 2.63 |
| SW93.5L | Mawa | 18/10/2000 | 4.22 | 27431.14 | 1.79 |
| SW93.5L | Mawa | 25/10/2000 | 3.67 | 23172.75 | 1.81 |

| StationID | StationName | Date | Water Level (m) | Discharge (cumec) | Maximum Velocity (m/s) |
|-----------|-------------|------------|-----------------|-------------------|------------------------|
| SW93.5L | Mawa | 06/06/2001 | 3.60 | 19907.74 | 1.32 |
| SW93.5L | Mawa | 13/06/2001 | 4.35 | 23376.89 | 1.54 |
| SW93.5L | Mawa | 20/06/2001 | 4.23 | 24182.56 | 1.65 |
| SW93.5L | Mawa | 27/06/2001 | 4.66 | 32540.54 | 1.96 |
| SW93.5L | Mawa | 04/07/2001 | 4.84 | 32871.98 | 1.98 |
| SW93.5L | Mawa | 11/07/2001 | 4.81 | 36158.81 | 2.09 |
| SW93.5L | Mawa | 18/07/2001 | 4.88 | 38100.92 | 2.22 |
| SW93.5L | Mawa | 25/07/2001 | 5.33 | 50032.63 | 2.40 |
| SW93.5L | Mawa | 01/08/2001 | 5.63 | 58009.71 | 2.80 |
| SW93.5L | Mawa | 08/08/2001 | 6.02 | 70030.43 | 3.39 |
| SW93.5L | Mawa | 15/08/2001 | 5.30 | 48810.14 | 2.54 |
| SW93.5L | Mawa | 22/08/2001 | 5.34 | 44446.73 | 2.48 |
| SW93.5L | Mawa | 29/08/2001 | 5.83 | 64215.65 | 2.89 |
| SW93.5L | Mawa | 05/09/2001 | 5.87 | 71962.10 | 2.99 |
| SW93.5L | Mawa | 12/09/2001 | 5.79 | 71758.00 | 3.58 |
| SW93.5L | Mawa | 19/09/2001 | 5.74 | 63182.83 | 2.85 |
| SW93.5L | Mawa | 26/09/2001 | 5.10 | 45744.65 | 2.23 |
| SW93.5L | Mawa | 10/10/2001 | 5.26 | 46555.25 | 2.26 |
| SW93.5L | Mawa | 17/10/2001 | 5.15 | 41347.70 | 2.21 |
| SW93.5L | Mawa | 24/10/2001 | 4.49 | 39349.60 | 1.87 |
| SW93.5L | Mawa | 31/10/2001 | 4.86 | 42368.78 | 2.19 |
| SW93.5L | Mawa | 04/06/2003 | 3.01 | 21175.44 | 1.14 |
| SW93.5L | Mawa | 11/06/2003 | 3.43 | 27422.81 | 1.65 |
| SW93.5L | Mawa | 18/06/2003 | 4.49 | 40172.08 | 2.17 |
| SW93.5L | Mawa | 25/06/2003 | 4.65 | 44846.79 | 2.37 |
| SW93.5L | Mawa | 02/07/2003 | 5.48 | 63862.52 | 2.92 |
| SW93.5L | Mawa | 09/07/2003 | 5.96 | 81832.91 | 3.54 |
| SW93.5L | Mawa | 16/07/2003 | 6.45 | 105301.00 | 3.93 |
| SW93.5L | Mawa | 23/07/2003 | 6.00 | 81640.75 | 3.58 |
| SW93.5L | Mawa | 30/07/2003 | 5.77 | 65414.64 | 3.35 |
| SW93.5L | Mawa | 06/08/2003 | 5.71 | 70599.89 | 3.47 |
| SW93.5L | Mawa | 13/08/2003 | 5.48 | 80475.68 | 3.87 |
| SW93.5L | Mawa | 20/08/2003 | 5.33 | 72196.73 | 3.41 |
| SW93.5L | Mawa | 27/08/2003 | 5.78 | 77111.47 | 3.43 |
| SW93.5L | Mawa | 03/09/2003 | 5.61 | 74843.84 | 3.61 |
| SW93.5L | Mawa | 10/09/2003 | 5.72 | 80835.71 | 3.90 |
| SW93.5L | Mawa | 17/09/2003 | 5.81 | 89206.88 | 3.74 |
| SW93.5L | Mawa | 24/09/2003 | 5.82 | 86082.18 | 3.95 |
| SW93.5L | Mawa | 03/10/2003 | 5.50 | 82709.33 | 3.36 |
| SW93.5L | Mawa | 10/10/2003 | 5.48 | 75520.43 | 3.33 |
| SW93.5L | Mawa | 15/10/2003 | 5.17 | 61613.79 | 3.10 |
| SW93.5L | Mawa | 22/10/2003 | 4.49 | 44068.22 | 2.44 |
| SW93.5L | Mawa | 29/10/2003 | 4.39 | 33408.48 | 1.99 |

| StationID | StationName | Date | Water Level (m) | Discharge (cumec) | Maximum Velocity (m/s) |
|-----------|-------------|------------|-----------------|-------------------|------------------------|
| SW93.5L | Mawa | 02/06/2004 | 3.97 | 38209.20 | 1.66 |
| SW93.5L | Mawa | 09/06/2004 | 3.70 | 24809.30 | 1.36 |
| SW93.5L | Mawa | 16/06/2004 | 3.90 | 36797.90 | 1.63 |
| SW93.5L | Mawa | 23/06/2004 | 4.40 | 48746.10 | 1.92 |
| SW93.5L | Mawa | 30/06/2004 | 5.44 | 72288.90 | 2.90 |
| SW93.5L | Mawa | 07/07/2004 | 4.93 | 59801.50 | 2.85 |
| SW93.5L | Mawa | 14/07/2004 | 6.09 | 82364.67 | 3.41 |
| SW93.5L | Mawa | 21/07/2004 | 6.62 | 103358.60 | 3.73 |
| SW93.5L | Mawa | 28/07/2004 | 6.66 | 84256.11 | 3.50 |
| SW93.5L | Mawa | 04/08/2004 | 6.05 | 78193.55 | 3.11 |
| SW93.5L | Mawa | 11/08/2004 | 5.54 | 74496.31 | 2.94 |
| SW93.5L | Mawa | 18/08/2004 | 5.32 | 68971.02 | 2.79 |
| SW93.5L | Mawa | 25/08/2004 | 5.29 | 65560.77 | 2.58 |
| SW93.5L | Mawa | 01/09/2004 | 5.48 | 74759.72 | 2.81 |
| SW93.5L | Mawa | 08/09/2004 | 5.23 | 60869.19 | 2.96 |
| SW93.5L | Mawa | 15/09/2004 | 5.57 | 77061.63 | 2.75 |
| SW93.5L | Mawa | 21/09/2004 | 4.88 | 46460.76 | 2.35 |
| SW93.5L | Mawa | 29/09/2004 | 4.63 | 44449.06 | 2.23 |
| SW93.5L | Mawa | 06/10/2004 | 4.70 | 45964.29 | 2.31 |
| SW93.5L | Mawa | 13/10/2004 | 5.41 | 58058.40 | 2.64 |
| SW93.5L | Mawa | 20/10/2004 | 4.66 | 42241.77 | 3.26 |
| SW93.5L | Mawa | 27/10/2004 | 4.10 | 29532.54 | 1.79 |
| SW93.5L | Mawa | 01/06/2005 | 3.10 | 22862.83 | 1.42 |
| SW93.5L | Mawa | 08/06/2005 | 3.62 | 27924.44 | 1.68 |
| SW93.5L | Mawa | 15/06/2005 | 3.41 | 26491.62 | 1.62 |
| SW93.5L | Mawa | 22/06/2005 | 3.80 | 28026.92 | 1.67 |
| SW93.5L | Mawa | 29/06/2005 | 4.63 | 37852.32 | 1.86 |
| SW93.5L | Mawa | 06/07/2005 | 4.70 | 40290.91 | 2.07 |
| SW93.5L | Mawa | 15/07/2005 | 5.50 | 62344.53 | 3.02 |
| SW93.5L | Mawa | 20/07/2005 | 5.75 | 77928.59 | 3.60 |
| SW93.5L | Mawa | 27/07/2005 | 5.88 | 86074.66 | 3.63 |
| SW93.5L | Mawa | 03/08/2005 | 5.23 | 72857.53 | 2.98 |
| SW93.5L | Mawa | 10/08/2005 | 5.27 | 69470.86 | 2.85 |
| SW93.5L | Mawa | 17/08/2005 | 5.57 | 82241.10 | 3.26 |
| SW93.5L | Mawa | 24/08/2005 | 5.52 | 77976.71 | 3.31 |
| SW93.5L | Mawa | 31/08/2005 | 5.86 | 85301.73 | 3.49 |
| SW93.5L | Mawa | 07/09/2005 | 5.56 | 58896.08 | 3.41 |
| SW93.5L | Mawa | 14/09/2005 | 5.04 | 52008.72 | 2.64 |
| SW93.5L | Mawa | 21/09/2005 | 4.65 | 42136.30 | 2.33 |
| SW93.5L | Mawa | 28/09/2005 | 4.38 | 37464.96 | 2.16 |
| SW93.5L | Mawa | 05/10/2005 | 4.85 | 51281.52 | 2.64 |
| SW93.5L | Mawa | 12/10/2005 | 4.48 | 42135.04 | 2.31 |
| SW93.5L | Mawa | 19/10/2005 | 4.19 | 36030.95 | 2.09 |

| StationID | StationName | Date | Water Level (m) | Discharge (cumec) | Maximum Velocity (m/s) |
|-----------|-------------|------------|-----------------|-------------------|------------------------|
| SW93.5L | Mawa | 26/10/2005 | 4.23 | 32728.62 | 1.80 |
| SW93.5L | Mawa | 14/06/2006 | 4.63 | 40927.10 | 2.07 |
| SW93.5L | Mawa | 28/06/2006 | 4.44 | 39046.58 | 1.95 |
| SW93.5L | Mawa | 19/07/2006 | 5.25 | 70984.08 | 3.23 |
| SW93.5L | Mawa | 16/08/2006 | 4.94 | 63105.23 | 3.11 |
| SW93.5L | Mawa | 13/09/2006 | 5.06 | 58263.95 | 2.91 |
| SW93.5L | Mawa | 27/09/2006 | 4.94 | 55110.04 | 2.74 |
| SW93.5L | Mawa | 14/10/2006 | 4.02 | 40097.03 | 2.29 |
| SW93.5L | Mawa | 28/10/2006 | 3.36 | 25329.74 | 1.63 |
| SW93.5L | Mawa | 11/06/2008 | 3.57 | 30747.55 | 1.78 |
| SW93.5L | Mawa | 17/06/2008 | 3.08 | 19604.96 | 1.37 |
| SW93.5L | Mawa | 25/06/2008 | 4.67 | 44577.00 | 2.56 |
| SW93.5L | Mawa | 09/07/2008 | 5.29 | 64340.04 | 3.10 |
| SW93.5L | Mawa | 16/07/2008 | 5.23 | 70440.44 | 3.32 |
| SW93.5L | Mawa | 23/07/2008 | 5.63 | 74500.02 | 3.47 |
| SW93.5L | Mawa | 30/07/2008 | 5.94 | 83699.92 | 3.64 |
| SW93.5L | Mawa | 06/08/2008 | 5.81 | 71640.36 | 3.26 |
| SW93.5L | Mawa | 13/08/2008 | 5.63 | 67002.48 | 3.26 |
| SW93.5L | Mawa | 20/08/2008 | 5.97 | 77640.59 | 3.28 |
| SW93.5L | Mawa | 27/08/2008 | 5.99 | 87821.29 | 3.48 |
| SW93.5L | Mawa | 03/09/2008 | 6.26 | 108723.80 | 3.64 |
| SW93.5L | Mawa | 10/09/2008 | 6.10 | 91711.75 | 3.53 |
| SW93.5L | Mawa | 17/09/2008 | 5.56 | 67993.77 | 2.73 |
| SW93.5L | Mawa | 24/09/2008 | 4.62 | 46721.32 | 2.73 |
| SW93.5L | Mawa | 08/10/2008 | 4.51 | 42316.21 | 2.49 |
| SW93.5L | Mawa | 15/10/2008 | 4.27 | 37159.04 | 2.42 |
| SW93.5L | Mawa | 22/10/2008 | 3.72 | 27711.06 | 1.72 |
| SW93.5L | Mawa | 29/10/2008 | 3.58 | 25605.32 | 1.57 |
| SW93.5L | Mawa | 03/06/2009 | 3.17 | 20774.62 | 1.40 |
| SW93.5L | Mawa | 10/06/2009 | 3.14 | 20815.36 | 1.46 |
| SW93.5L | Mawa | 17/06/2009 | 3.08 | 19604.96 | 1.37 |
| SW93.5L | Mawa | 01/07/2009 | 3.61 | 25400.36 | 1.51 |
| SW93.5L | Mawa | 08/07/2009 | 5.12 | 56427.94 | 2.93 |
| SW93.5L | Mawa | 15/07/2009 | 4.92 | 49045.01 | 2.53 |
| SW93.5L | Mawa | 22/07/2009 | 4.55 | 39720.69 | 2.03 |
| SW93.5L | Mawa | 29/07/2009 | 4.38 | 32390.01 | 2.02 |
| SW93.5L | Mawa | 05/08/2009 | 5.06 | 51810.59 | 3.15 |
| SW93.5L | Mawa | 12/08/2009 | 5.10 | 56527.71 | 3.19 |
| SW93.5L | Mawa | 19/08/2009 | 5.48 | 69797.57 | 3.44 |
| SW93.5L | Mawa | 09/09/2009 | 5.15 | 54618.75 | 2.86 |
| SW93.5L | Mawa | 30/09/2009 | 4.52 | 43603.20 | 2.81 |
| SW93.5L | Mawa | 14/10/2009 | 4.50 | 43458.18 | 2.83 |
| SW93.5L | Mawa | 28/10/2009 | 4.51 | 28628.66 | 2.17 |

| StationID | StationName | Date | Water Level (m) | Discharge (cumec) | Maximum Velocity (m/s) |
|-----------|-------------|------------|-----------------|-------------------|------------------------|
| SW93.5L | Mawa | 02/06/2010 | 4.24 | 34004.65 | 1.88 |
| SW93.5L | Mawa | 23/06/2010 | 4.90 | 41786.51 | 2.66 |
| SW93.5L | Mawa | 07/07/2010 | 5.39 | 64011.02 | 3.50 |
| SW93.5L | Mawa | 14/07/2010 | 5.55 | 68728.23 | 3.24 |
| SW93.5L | Mawa | 21/07/2010 | 5.56 | 67254.48 | 3.36 |
| SW93.5L | Mawa | 28/07/2010 | 5.80 | 73134.33 | 3.43 |
| SW93.5L | Mawa | 04/08/2010 | 5.52 | 63957.75 | 3.19 |

Appendix-C

DN values extracted from Landsat ETM+ images, between years 2000-2010, for conversion to spectral reflectance.

Bands 1, 2, 3 and 4 are represented by B1-B4 respectively. The italicized rows depict the average DN corresponding to each band.

| Day of Year 2000: 235 | | | | Day of Year 2000: 283 | | | |
|-----------------------|--------------|------------|-----------|-----------------------|-------------|-------------|-------------|
| B1 | B2 | B3 | B4 | B1 | B2 | B3 | B4 |
| 118 | 101 | 103 | 39 | 99 | 84 | 84 | 27 |
| 117 | 102 | 106 | 39 | 101 | 84 | 83 | 27 |
| 121 | 103 | 106 | 39 | 101 | 83 | 83 | 27 |
| 123 | 107 | 106 | 41 | 102 | 85 | 86 | 28 |
| 125 | 111 | 112 | 42 | 103 | 87 | 88 | 28 |
| <i>120.8</i> | <i>104.8</i> | <i>117</i> | <i>40</i> | <i>101.2</i> | <i>84.6</i> | <i>84.8</i> | <i>27.4</i> |

| Day of Year 2000: 299 | | | | Day of Year 2000: 331 | | | |
|-----------------------|-----------|-----------|-------------|-----------------------|-----------|-------------|-------------|
| B1 | B2 | B3 | B4 | B1 | B2 | B3 | B4 |
| 107 | 87 | 82 | 28 | 97 | 78 | 72 | 34 |
| 106 | 86 | 84 | 28 | 98 | 78 | 71 | 33 |
| 104 | 86 | 84 | 27 | 98 | 78 | 74 | 34 |
| 102 | 85 | 83 | 27 | 98 | 77 | 76 | 34 |
| 103 | 86 | 87 | 26 | 97 | 79 | 73 | 34 |
| <i>104.4</i> | <i>86</i> | <i>84</i> | <i>27.2</i> | <i>97.6</i> | <i>78</i> | <i>73.2</i> | <i>33.8</i> |

| Day of Year 2001: 189 | | | | Day of Year 2001: 221 | | | |
|-----------------------|--------------|--------------|-----------|-----------------------|--------------|------------|-------------|
| B1 | B2 | B3 | B4 | B1 | B2 | B3 | B4 |
| 130 | 118 | 126 | 45 | 121 | 110 | 120 | 45 |
| 132 | 117 | 125 | 45 | 123 | 108 | 111 | 42 |
| 130 | 119 | 125 | 46 | 124 | 108 | 115 | 38 |
| 138 | 123 | 131 | 47 | 122 | 106 | 111 | 38 |
| 135 | 122 | 129 | 47 | 122 | 109 | 113 | 36 |
| <i>133</i> | <i>119.8</i> | <i>127.2</i> | <i>46</i> | <i>122.4</i> | <i>108.2</i> | <i>114</i> | <i>39.8</i> |

Day of Year 2001: 269

| B1 | B2 | B3 | B4 |
|--------------|-------------|-------------|-----------|
| 104 | 87 | 88 | 29 |
| 104 | 85 | 86 | 29 |
| 107 | 89 | 90 | 29 |
| 106 | 89 | 88 | 29 |
| 107 | 89 | 90 | 29 |
| <i>105.6</i> | <i>87.8</i> | <i>88.4</i> | <i>29</i> |

| Day of Year 2002: 256 | | | | Day of Year 2002: 304 | | | |
|-----------------------|-------------|--------------|-------------|-----------------------|-----------|-------------|-------------|
| B1 | B2 | B3 | B4 | B1 | B2 | B3 | B4 |
| 114 | 103 | 108 | 33 | 90 | 75 | 71 | 21 |
| 110 | 99 | 98 | 30 | 92 | 76 | 73 | 22 |
| 107 | 90 | 92 | 31 | 90 | 77 | 73 | 22 |
| 112 | 103 | 110 | 32 | 92 | 76 | 72 | 21 |
| 108 | 91 | 93 | 31 | 90 | 76 | 73 | 22 |
| <i>110.2</i> | <i>97.2</i> | <i>100.2</i> | <i>31.4</i> | <i>90.8</i> | <i>76</i> | <i>72.4</i> | <i>21.6</i> |

| Day of Year 2003: 227 | | | | Day of Year 2003: 307 | | | |
|-----------------------|--------------|--------------|-------------|-----------------------|-------------|-------------|-------------|
| B1 | B2 | B3 | B4 | B1 | B2 | B3 | B4 |
| 122 | 105 | 115 | 36 | 101 | 82 | 81 | 26 |
| 124 | 103 | 112 | 35 | 102 | 83 | 85 | 27 |
| 125 | 102 | 114 | 39 | 101 | 85 | 85 | 29 |
| 126 | 101 | 112 | 32 | 103 | 85 | 90 | 28 |
| 123 | 106 | 116 | 34 | 100 | 84 | 85 | 28 |
| <i>122</i> | <i>103.4</i> | <i>113.8</i> | <i>35.2</i> | <i>101.4</i> | <i>83.8</i> | <i>85.2</i> | <i>27.6</i> |

Day of Year 2003: 323

| B1 | B2 | B3 | B4 |
|-------------|-----------|-----------|-------------|
| 91 | 75 | 74 | 34 |
| 94 | 76 | 73 | 34 |
| 92 | 77 | 77 | 34 |
| 93 | 75 | 75 | 34 |
| 94 | 77 | 76 | 36 |
| <i>92.8</i> | <i>76</i> | <i>75</i> | <i>34.4</i> |

Day of Year 2004: 182

| B1 | B2 | B3 | B4 |
|--------------|--------------|------------|-------------|
| 141 | 128 | 133 | 49 |
| 151 | 127 | 135 | 50 |
| 148 | 128 | 134 | 50 |
| 147 | 128 | 133 | 49 |
| 151 | 128 | 135 | 50 |
| <i>147.6</i> | <i>127.8</i> | <i>134</i> | <i>49.6</i> |

Day of Year 2004: 230

| B1 | B2 | B3 | B4 |
|--------------|--------------|--------------|-------------|
| 140 | 124 | 130 | 50 |
| 142 | 125 | 133 | 49 |
| 141 | 125 | 132 | 49 |
| 141 | 124 | 131 | 49 |
| 139 | 125 | 132 | 49 |
| <i>140.6</i> | <i>124.6</i> | <i>131.6</i> | <i>49.2</i> |

| Day of Year 2004: 246 | | | | Day of Year 2004: 294 | | | |
|-----------------------|--------------|--------------|-----------|-----------------------|-----------|-------------|-------------|
| B1 | B2 | B3 | B4 | B1 | B2 | B3 | B4 |
| 149 | 126 | 130 | 53 | 62 | 56 | 57 | 25 |
| 150 | 127 | 131 | 52 | 62 | 54 | 56 | 27 |
| 152 | 127 | 131 | 52 | 62 | 54 | 54 | 26 |
| 150 | 127 | 133 | 51 | 60 | 52 | 54 | 25 |
| 152 | 127 | 133 | 52 | 62 | 54 | 55 | 25 |
| <i>150.6</i> | <i>126.8</i> | <i>131.6</i> | <i>52</i> | <i>61.6</i> | <i>54</i> | <i>55.2</i> | <i>25.6</i> |

| Day of Year 2005: 280 | | | |
|-----------------------|-------------|-------------|-------------|
| B1 | B2 | B3 | B4 |
| 113 | 96 | 94 | 32 |
| 112 | 92 | 92 | 32 |
| 115 | 93 | 94 | 32 |
| 115 | 95 | 94 | 33 |
| 114 | 93 | 93 | 32 |
| <i>113.8</i> | <i>93.8</i> | <i>93.4</i> | <i>32.2</i> |

| Day of Year 2006: 139 | | | | Day of Year 2006: 299 | | | |
|-----------------------|-------------|-----------|-----------|-----------------------|-----------|-----------|-------------|
| B1 | B2 | B3 | B4 | B1 | B2 | B3 | B4 |
| 115 | 97 | 96 | 28 | 99 | 88 | 88 | 25 |
| 113 | 94 | 91 | 27 | 99 | 88 | 87 | 25 |
| 112 | 94 | 91 | 28 | 100 | 90 | 92 | 26 |
| 112 | 95 | 91 | 26 | 99 | 88 | 88 | 25 |
| 113 | 94 | 91 | 26 | 98 | 86 | 85 | 27 |
| <i>113</i> | <i>94.8</i> | <i>92</i> | <i>27</i> | <i>99</i> | <i>88</i> | <i>88</i> | <i>25.6</i> |

| Day of Year 2007: 270 | | | | Day of Year 2007: 302 | | | |
|-----------------------|-------------|--------------|-----------|-----------------------|-------------|-----------|-------------|
| B1 | B2 | B3 | B4 | B1 | B2 | B3 | B4 |
| 106 | 96 | 102 | 30 | 64 | 57 | 57 | 26 |
| 107 | 95 | 102 | 33 | 63 | 56 | 56 | 26 |
| 107 | 96 | 105 | 35 | 65 | 56 | 58 | 26 |
| 106 | 95 | 103 | 34 | 65 | 57 | 60 | 27 |
| 107 | 95 | 102 | 33 | 65 | 57 | 59 | 28 |
| <i>106.6</i> | <i>95.4</i> | <i>102.8</i> | <i>33</i> | <i>64.4</i> | <i>56.6</i> | <i>58</i> | <i>26.6</i> |

Day of Year 2007: 334

| B1 | B2 | B3 | B4 |
|-----------|-------------|-------------|-------------|
| 90 | 72 | 66 | 31 |
| 90 | 73 | 68 | 29 |
| 90 | 76 | 70 | 27 |
| 89 | 76 | 69 | 27 |
| 91 | 77 | 70 | 28 |
| <i>90</i> | <i>74.8</i> | <i>68.6</i> | <i>28.4</i> |

Day of Year 2008: 209

| B1 | B2 | B3 | B4 |
|------------|--------------|--------------|-------------|
| 124 | 111 | 122 | 41 |
| 120 | 108 | 116 | 40 |
| 118 | 111 | 120 | 41 |
| 123 | 112 | 125 | 45 |
| 120 | 109 | 118 | 44 |
| <i>121</i> | <i>110.2</i> | <i>120.2</i> | <i>42.2</i> |

Day of Year 2008: 273

| B1 | B2 | B3 | B4 |
|--------------|-------------|-------------|-------------|
| 115 | 98 | 97 | 31 |
| 118 | 96 | 101 | 31 |
| 117 | 96 | 94 | 32 |
| 115 | 97 | 97 | 32 |
| 116 | 96 | 97 | 31 |
| <i>116.2</i> | <i>96.6</i> | <i>97.2</i> | <i>31.4</i> |

| Day of Year 2008: 289 | | | | Day of Year 2008: 305 | | | |
|-----------------------|-------------|-------------|-------------|-----------------------|-----------|-------------|-------------|
| B1 | B2 | B3 | B4 | B1 | B2 | B3 | B4 |
| 105 | 89 | 91 | 29 | 59 | 50 | 47 | 21 |
| 103 | 90 | 93 | 31 | 60 | 51 | 52 | 21 |
| 106 | 91 | 95 | 30 | 60 | 51 | 51 | 21 |
| 109 | 94 | 97 | 32 | 60 | 52 | 51 | 22 |
| 107 | 93 | 95 | 31 | 59 | 51 | 50 | 22 |
| <i>106</i> | <i>91.4</i> | <i>94.2</i> | <i>30.6</i> | <i>59.6</i> | <i>51</i> | <i>50.2</i> | <i>21.4</i> |

| Day of Year 2009: 163 | | | | Day of Year 2009: 291 | | | |
|-----------------------|--------------|--------------|-------------|-----------------------|-----------|-------------|-------------|
| B1 | B2 | B3 | B4 | B1 | B2 | B3 | B4 |
| 150 | 130 | 130 | 42 | 76 | 61 | 58 | 35 |
| 151 | 127 | 130 | 41 | 79 | 66 | 66 | 34 |
| 148 | 128 | 128 | 42 | 82 | 70 | 76 | 35 |
| 148 | 127 | 127 | 42 | 76 | 65 | 71 | 35 |
| 149 | 130 | 131 | 42 | 79 | 68 | 73 | 33 |
| <i>149.2</i> | <i>128.4</i> | <i>129.2</i> | <i>41.8</i> | <i>78.4</i> | <i>66</i> | <i>68.8</i> | <i>34.4</i> |

Day of Year 2010: 182

| B1 | B2 | B3 | B4 |
|--------------|--------------|--------------|-----------|
| 138 | 124 | 132 | 45 |
| 133 | 117 | 121 | 44 |
| 131 | 114 | 118 | 43 |
| 133 | 114 | 120 | 44 |
| 133 | 115 | 122 | 44 |
| <i>133.6</i> | <i>116.8</i> | <i>122.6</i> | <i>44</i> |

Day of Year 2010: 294

| B1 | B2 | B3 | B4 |
|--------------|-------------|-----------|-----------|
| 100 | 87 | 86 | 28 |
| 100 | 87 | 92 | 29 |
| 101 | 89 | 91 | 29 |
| 100 | 87 | 92 | 30 |
| 100 | 88 | 94 | 29 |
| <i>100.2</i> | <i>87.6</i> | <i>91</i> | <i>29</i> |

Appendix-D

Earth-sun distance correction coefficient (d) table provided by NASA/USGS in astronomical units for Day of Year (DOY)

Part (i) Day of Year (DOY): 1-180

| DOY | d | DOY | d | DOY | d |
|------------|----------|------------|----------|------------|----------|
| 1 | 0.98331 | 61 | 0.99108 | 121 | 1.00756 |
| 2 | 0.98330 | 62 | 0.99133 | 122 | 1.00781 |
| 3 | 0.98330 | 63 | 0.99158 | 123 | 1.00806 |
| 4 | 0.98330 | 64 | 0.99183 | 124 | 1.00831 |
| 5 | 0.98330 | 65 | 0.99208 | 125 | 1.00856 |
| 6 | 0.98332 | 66 | 0.99234 | 126 | 1.00880 |
| 7 | 0.98333 | 67 | 0.99260 | 127 | 1.00904 |
| 8 | 0.98335 | 68 | 0.99286 | 128 | 1.00928 |
| 9 | 0.98338 | 69 | 0.99312 | 129 | 1.00952 |
| 10 | 0.98341 | 70 | 0.99339 | 130 | 1.00975 |
| 11 | 0.98345 | 71 | 0.99365 | 131 | 1.00998 |
| 12 | 0.98349 | 72 | 0.99392 | 132 | 1.01020 |
| 13 | 0.98354 | 73 | 0.99419 | 133 | 1.01043 |
| 14 | 0.98359 | 74 | 0.99446 | 134 | 1.01065 |
| 15 | 0.98365 | 75 | 0.99474 | 135 | 1.01087 |
| 16 | 0.98371 | 76 | 0.99501 | 136 | 1.01108 |
| 17 | 0.98378 | 77 | 0.99529 | 137 | 1.01129 |
| 18 | 0.98385 | 78 | 0.99556 | 138 | 1.01150 |
| 19 | 0.98393 | 79 | 0.99584 | 139 | 1.01170 |
| 20 | 0.98401 | 80 | 0.99612 | 140 | 1.01191 |
| 21 | 0.98410 | 81 | 0.99640 | 141 | 1.01210 |
| 22 | 0.98419 | 82 | 0.99669 | 142 | 1.01230 |
| 23 | 0.98428 | 83 | 0.99697 | 143 | 1.01249 |
| 24 | 0.98439 | 84 | 0.99725 | 144 | 1.01267 |
| 25 | 0.98449 | 85 | 0.99754 | 145 | 1.01286 |
| 26 | 0.98460 | 86 | 0.99782 | 146 | 1.01304 |
| 27 | 0.98472 | 87 | 0.99811 | 147 | 1.01321 |
| 28 | 0.98484 | 88 | 0.99840 | 148 | 1.01338 |
| 29 | 0.98496 | 89 | 0.99868 | 149 | 1.01355 |
| 30 | 0.98509 | 90 | 0.99897 | 150 | 1.01371 |
| 31 | 0.98523 | 91 | 0.99926 | 151 | 1.01387 |
| 32 | 0.98536 | 92 | 0.99954 | 152 | 1.01403 |
| 33 | 0.98551 | 93 | 0.99983 | 153 | 1.01418 |

| DOY | d | DOY | d | DOY | d |
|------------|----------|------------|----------|------------|----------|
| 34 | 0.98565 | 94 | 1.00012 | 154 | 1.01433 |
| 35 | 0.98580 | 95 | 1.00041 | 155 | 1.01447 |
| 36 | 0.98596 | 96 | 1.00069 | 156 | 1.01461 |
| 37 | 0.98612 | 97 | 1.00098 | 157 | 1.01475 |
| 38 | 0.98628 | 98 | 1.00127 | 158 | 1.01488 |
| 39 | 0.98645 | 99 | 1.00155 | 159 | 1.01500 |
| 40 | 0.98662 | 100 | 1.00184 | 160 | 1.01513 |
| 41 | 0.98680 | 101 | 1.00212 | 161 | 1.01524 |
| 42 | 0.98698 | 102 | 1.00240 | 162 | 1.01536 |
| 43 | 0.98717 | 103 | 1.00269 | 163 | 1.01547 |
| 44 | 0.98735 | 104 | 1.00297 | 164 | 1.01557 |
| 45 | 0.98755 | 105 | 1.00325 | 165 | 1.01567 |
| 46 | 0.98774 | 106 | 1.00353 | 166 | 1.01577 |
| 47 | 0.98794 | 107 | 1.00381 | 167 | 1.01586 |
| 48 | 0.98814 | 108 | 1.00409 | 168 | 1.01595 |
| 49 | 0.98835 | 109 | 1.00437 | 169 | 1.01603 |
| 50 | 0.98856 | 110 | 1.00464 | 170 | 1.01610 |
| 51 | 0.98877 | 111 | 1.00492 | 171 | 1.01618 |
| 52 | 0.98899 | 112 | 1.00519 | 172 | 1.01625 |
| 53 | 0.98921 | 113 | 1.00546 | 173 | 1.01631 |
| 54 | 0.98944 | 114 | 1.00573 | 174 | 1.01637 |
| 55 | 0.98966 | 115 | 1.00600 | 175 | 1.01642 |
| 56 | 0.98989 | 116 | 1.00626 | 176 | 1.01647 |
| 57 | 0.99012 | 117 | 1.00653 | 177 | 1.01652 |
| 58 | 0.99036 | 118 | 1.00679 | 178 | 1.01656 |
| 59 | 0.99060 | 119 | 1.00705 | 179 | 1.01659 |
| 60 | 0.99084 | 120 | 1.00731 | 180 | 1.01662 |

Part (ii) Day of Year (DOY): 180-360

| DOY | d | DOY | d | DOY | d |
|------------|----------|------------|----------|------------|----------|
| 181 | 1.01665 | 241 | 1.00992 | 301 | 0.99359 |
| 182 | 1.01667 | 242 | 1.00969 | 302 | 0.99332 |
| 183 | 1.01668 | 243 | 1.00946 | 303 | 0.99306 |
| 184 | 1.01670 | 244 | 1.00922 | 304 | 0.99279 |
| 185 | 1.01670 | 245 | 1.00898 | 305 | 0.99253 |
| 186 | 1.01670 | 246 | 1.00874 | 306 | 0.99228 |
| 187 | 1.01670 | 247 | 1.00850 | 307 | 0.99202 |
| 188 | 1.01669 | 248 | 1.00825 | 308 | 0.99177 |
| 189 | 1.01668 | 249 | 1.00800 | 309 | 0.99152 |
| 190 | 1.01666 | 250 | 1.00775 | 310 | 0.99127 |
| 191 | 1.01664 | 251 | 1.00750 | 311 | 0.99102 |
| 192 | 1.01661 | 252 | 1.00724 | 312 | 0.99078 |
| 193 | 1.01658 | 253 | 1.00698 | 313 | 0.99054 |
| 194 | 1.01655 | 254 | 1.00672 | 314 | 0.99030 |
| 195 | 1.01650 | 255 | 1.00646 | 315 | 0.99007 |
| 196 | 1.01646 | 256 | 1.00620 | 316 | 0.98983 |
| 197 | 1.01641 | 257 | 1.00593 | 317 | 0.98961 |
| 198 | 1.01635 | 258 | 1.00566 | 318 | 0.98938 |
| 199 | 1.01629 | 259 | 1.00539 | 319 | 0.98916 |
| 200 | 1.01623 | 260 | 1.00512 | 320 | 0.98894 |
| 201 | 1.01616 | 261 | 1.00485 | 321 | 0.98872 |
| 202 | 1.01609 | 262 | 1.00457 | 322 | 0.98851 |
| 203 | 1.01601 | 263 | 1.00430 | 323 | 0.98830 |
| 204 | 1.01592 | 264 | 1.00402 | 324 | 0.98809 |
| 205 | 1.01584 | 265 | 1.00374 | 325 | 0.98789 |
| 206 | 1.01575 | 266 | 1.00346 | 326 | 0.98769 |
| 207 | 1.01565 | 267 | 1.00318 | 327 | 0.98750 |
| 208 | 1.01555 | 268 | 1.00290 | 328 | 0.98731 |
| 209 | 1.01544 | 269 | 1.00262 | 329 | 0.98712 |
| 210 | 1.01533 | 270 | 1.00234 | 330 | 0.98694 |
| 211 | 1.01522 | 271 | 1.00205 | 331 | 0.98676 |
| 212 | 1.01510 | 272 | 1.00177 | 332 | 0.98658 |
| 213 | 1.01497 | 273 | 1.00148 | 333 | 0.98641 |
| 214 | 1.01485 | 274 | 1.00119 | 334 | 0.98624 |
| 215 | 1.01471 | 275 | 1.00091 | 335 | 0.98608 |
| 216 | 1.01458 | 276 | 1.00062 | 336 | 0.98592 |
| 217 | 1.01444 | 277 | 1.00033 | 337 | 0.98577 |
| 218 | 1.01429 | 278 | 1.00005 | 338 | 0.98562 |
| 219 | 1.01414 | 279 | 0.99976 | 339 | 0.98547 |

| DOY | d | DOY | d | DOY | d |
|------------|----------|------------|----------|------------|----------|
| 220 | 1.01399 | 280 | 0.99947 | 340 | 0.98533 |
| 221 | 1.01383 | 281 | 0.99918 | 341 | 0.98519 |
| 222 | 1.01367 | 282 | 0.99890 | 342 | 0.98506 |
| 223 | 1.01351 | 283 | 0.99861 | 343 | 0.98493 |
| 224 | 1.01334 | 284 | 0.99832 | 344 | 0.98481 |
| 225 | 1.01317 | 285 | 0.99804 | 345 | 0.98469 |
| 226 | 1.01299 | 286 | 0.99775 | 346 | 0.98457 |
| 227 | 1.01281 | 287 | 0.99747 | 347 | 0.98446 |
| 228 | 1.01263 | 288 | 0.99718 | 348 | 0.98436 |
| 229 | 1.01244 | 289 | 0.99690 | 349 | 0.98426 |
| 230 | 1.01225 | 290 | 0.99662 | 350 | 0.98416 |
| 231 | 1.01205 | 291 | 0.99634 | 351 | 0.98407 |
| 232 | 1.01186 | 292 | 0.99605 | 352 | 0.98399 |
| 233 | 1.01165 | 293 | 0.99577 | 353 | 0.98391 |
| 234 | 1.01145 | 294 | 0.99550 | 354 | 0.98383 |
| 235 | 1.01124 | 295 | 0.99522 | 355 | 0.98376 |
| 236 | 1.01103 | 296 | 0.99494 | 356 | 0.98370 |
| 237 | 1.01081 | 297 | 0.99467 | 357 | 0.98363 |
| 238 | 1.01060 | 298 | 0.99440 | 358 | 0.98358 |
| 239 | 1.01037 | 299 | 0.99412 | 359 | 0.98353 |
| 240 | 1.01015 | 300 | 0.99385 | 360 | 0.98348 |

Appendix-E

Values of $E_o\lambda$, the mean solar ToA Irradiance ($W\mu m^{-2}$) provided by USGS/NASA

| Band | $E_o\lambda$ watts/(meter squared * μm) |
|-------------|---|
| 1 | 1970 |
| 2 | 1842 |
| 3 | 1547 |
| 4 | 1044 |
| 5 | 225.7 |
| 7 | 82.06 |
| 8 | 1369 |

Appendix-F

List of all Landsat ETM+ images acquired for or used in this thesis

| No. | Landsat Scene ID |
|-----|-----------------------|
| 1. | LE71370442000235SGS00 |
| 2. | LE71370442000283SGS00 |
| 3. | LE71370442000299SGS00 |
| 4. | LE71370442000331SGS00 |
| 5. | LE71370442001173SGS00 |
| 6. | LE71370442001189SGS00 |
| 7. | LE71370442001221SGS00 |
| 8. | LE71370442001253SGS00 |
| 9. | LE71370442001269SGS00 |
| 10. | LE71370442001333SGS00 |
| 11. | LE71370442002256SGS00 |
| 12. | LE71370442002272BKT00 |
| 13. | LE71370442002288BKT00 |
| 14. | LE71370442002304SGS00 |
| 15. | LE71370442003227ASN01 |
| 16. | LE71370442003307ASN04 |
| 17. | LE71370442003323ASN01 |
| 18. | LE71370442004166BKT00 |
| 19. | LE71370442004182PFS01 |
| 20. | LE71370442004230PFS01 |
| 21. | LE71370442004246PFS02 |
| 22. | LE71370442004294PFS01 |
| 23. | LE71370442005152PFS00 |
| 24. | LE71370442005168PFS00 |
| 25. | LE71370442005216PFS00 |
| 26. | LE71370442005232PFS00 |
| 27. | LE71370442005248PFS00 |
| 28. | LE71370442005280PFS00 |
| 29. | LE71370442006139PFS00 |
| 30. | LE71370442006155PFS00 |
| 31. | LE71370442006219PFS01 |
| 32. | LE71370442006267PFS00 |
| 33. | LE71370442006283PFS00 |
| 34. | LE71370442006299PFS00 |
| 35. | LE71370442007222PFS00 |
| 36. | LE71370442007270PFS00 |
| 37. | LE71370442007286PFS00 |
| 38. | LE71370442007302PFS00 |
| 39. | LE71370442007334SGS00 |
| 40. | LE71370442008161PFS00 |

| No. | Landsat Scene ID |
|-----|-----------------------|
| 41. | LE71370442008177PFS00 |
| 42. | LE71370442008209SGS01 |
| 43. | LE71370442008273PFS00 |
| 44. | LE71370442008289PFS00 |
| 45. | LE71370442008305SGS00 |
| 46. | LE71370442009163SGS01 |
| 47. | LE71370442009291SGS00 |
| 48. | LE71370442009339SGS00 |
| 49. | LE71370442010182PFS00 |
| 50. | LE71370442010278SGS01 |
| 51. | LE71370442010294SGS00 |
| 52. | LE71370442011153PFS00 |
| 53. | LE71370442011265PFS00 |
| 54. | LE71370442011281PFS00 |
| 55. | LE71370442011297PFS00 |
| 56. | LE71370432012156PFS00 |
| 57. | LE71370442012172PFS00 |
| 58. | LE71370442012204EDC00 |
| 59. | LE71370442012220PFS00 |